ABSTRACT

Title of Dissertation: EFFECT OF VEGETATION STRUCTURE ON UNDERCANOPY SOLAR RADIATION USING LIDAR REMOTE SENSING

Anupam Anand, Doctor of Philosophy, 2017

Directed by: Dr. Ralph Dubayah, Geographical Sciences

Estimation of under-canopy radiation is crucial for characterizing vegetation–energy interactions and for a better understanding of its implications for ecosystem studies and forestry applications. Under-canopy radiation regimes are difficult to model due to the complex interaction of light with vegetation structure. Also, measuring radiation under the canopy over large areas is challenging using traditional field-based procedures. In this context, LiDAR remote sensing shows great potential for radiation estimation because it directly measures the three-dimensional canopy structure. The primary aim of this dissertation is to improve the understanding of under-canopy light regime using discrete return LiDAR and estimate solar radiation in forests with different structural characteristics. Based on the availability of LiDAR data, research sites were chosen in the coniferous forests of Sierra National Forest

(SNF), California, and a chronosequence of mixed deciduous forest plots located in the Smithsonian Environmental Research Center (SERC), Maryland. First, LiDAR-derived digital surface models with and without vegetation canopy were used to assess the first-order effect of vegetation on solar radiation in SNF. The results showed a significant difference (p value < 0.001) in insolation values between the two surface models, with the mean solar irradiation over the bare surface almost three times higher than vegetation canopy surface. Next, a ray-tracing method was used to estimate beam radiation using LiDAR point clouds, and estimates were compared with *in situ* pyranometer measurements across three forest plots in SERC and were found to be in good agreement (RMSE = 13.94 W/m^2). Lastly, LiDAR-derived vertical light transmittance values were compared with measurements from field-based PAR sensors, across five forest plots in SERC and were found to be in good agreement (R^2 = 0.84). These results suggest that LiDAR remote sensing can provide reliable fine-scale estimates of beam radiation and vertical transmittance values under the vegetation canopy without the need for extensive ground measurements. This information provides a better understanding of radiation variability under the canopy and can help potentially improve the estimates from a range of land surface models such as snowmelt and hydrological models, and possibly help downscale general circulation model (GCM) predictions.

EFFECT OF VEGETATION STRUCTURE ON UNDERCANOPY SOLAR RADIATION USING LIDAR REMOTE SENSING

by

Anupam Anand

Dissertation submitted to the Faculty of the Graduate School of the
University of Maryland, College Park, in partial fulfillment
of the requirements for the degree of
Doctor of Philosophy
2017

Advisory Committee:

Professor Ralph Dubayah, Chair
Professor Christopher Justice
Dr. Michelle Hofton
Dr. Jan Dempewolf
Dr. Joseph Sullivan

Dedication

To

My parents,

Arbind Kumar Singh & Gayatri Singh

and

all forces seen and unseen

Acknowledgements

I would first like to thank my advisor Prof. Ralph Dubayah, for all his support and guidance, and most importantly for not giving up on me. Thank you for the invaluable life lessons that you imparted not only in the classroom but also in the mountains of SNF, forests of the northeast, canyons of Arizona and the deltas of Mississippi.

I appreciate the support and encouragement of my committee members Prof. Christopher Justice, Dr. Michelle Hofton, Dr. Jan Dempewolf and Prof. Joseph Sullivan. It has been an honor to work with you all.

Special thanks to Dr. Geoffrey Parker and Dr. Patrick Neale at the Smithsonian Environmental Research Center (SERC) for providing the field data and valuable inputs to my research.

Thanks to my friends and colleagues at the Global Land Cover Facility. I benefited and learned so much from working with you over the years. To Dr. John Townsend, Joe, Saurabh, and Min thank you. Thank you, Hao, for your help and critical feedback. To Jyothy, for your time, valuable inputs, and for the countless brainstorming sessions. Members of the VCL lab including Sage, Anu, Amanda, Qiongyu for your help in the initial years of graduate school - the time spent hugging trees, laying transects, and measuring biomass with you during various field campaigns will be cherished forever.

To Pattie, Praveen, Do Hyung, Sumalika, Lee Ann for many pep talks. Thank you to all my ex-housemates Jitesh, Sabya, Atul, Rohit, Saket, Priya, Krishna, Nihal and Pavan for being the guinea pigs for my experiments in the kitchen, for listening, and sharing the challenges as well as our interests. Thank you, Rakesh, Varun, BK, Sandy, Aditya, and Priti for nagging, probing and encouraging me to finish and keeping the friendship intact even when I kept missing in action often during the high times, and defaulted on wishing you on your birthdays and anniversaries.

Thanks to NASA for funding the major part of my graduate school endeavors. Specifically through many PIs thanks are due to their Biodiversity program for the opportunity to work on the USGS led climate biological response project, the Carbon Cycle and Ecosystems Program for the opportunity to work in various campaigns, and NASA G-LiHT for providing the LiDAR data.

Thanks to CI for providing me an opportunity to work on the initial phase of the Vital Signs program, it helped me understand how science could help in evidence-based policy making. Many thanks to the University of Maryland- College Park, and the Department of Geographical Sciences for supporting my doctoral education and research through various fellowships, scholarships and research awards. Thanks to Dr. Sun, Rachael, Bob, Liz, and Wilhelmina for your continuous support.

Thanks to Geeta Batra, Aaron Zazuetta, and Juha Uitto at the Global Environment Facility's Independent Evaluation Office for your encouragement and necessary support to complete this undertaking. Thank you, Aaron, for reminding me not to lose focus from the Ph.D., Geeta for providing me enough room to work on it and to Juha for using his subtle humor to remind and motivate me at every opportunity.

Lastly, thanks to my family in India, for your enduring support, faith, and prayers, I cannot thank you enough.

Table of Contents

Contents

List of Tables

List of Figures

Chapter 1 Introduction

1.1 Motivation and Background

Solar radiation is the primary source of energy that drives all biological and physical processes on earth. It plays a critical role in plant growth, succession, hydrological processes (e.g., snowmelt and evaporation), and surface energy balance. Understanding the distribution and variability of solar radiation is key to understanding plant growth, habitats the hydrological cycle and global climate (Murphy, Freas, & Weiss, 1990; Rich & Weiss, 1991; Weiss, Rich, Murphy, Calvert, & Ehrlich, 1991). Solar radiation also controls the canopy structure, soil temperature, evaporation, understory species composition and microclimate conditions at the stand level (Gutschick, 1991; Parker, Lefsky, & Harding, 2001). The three-dimensional canopy structure is key to forest function because canopy elements determine the quantity, quality, and spatiotemporal distribution of under-canopy light conditions. The amount of light passing through a forest canopy is regulated by tree species, size and location, the amount of canopy elements, their organization and spectral characteristics, and the angle of solar incidence (Colbert et al., 1990; Pukkala, Becker, Kuuluvainen, & Oker-Blom, 1991; Jennings, Brown , & Sheil, 1999; MacFarlane et al., 2003). Studies have examined the interaction of vegetation structure and availability of under-canopy light, and its effect on plant growth and yield forecasting (Naesset, 1997;

Battaglia et al., 2002; Hardy et al., 2004), on energy exchange patterns above and below the canopy (Ni, 1997), for biodiversity estimation (Hyde et al., 2006), and for understanding hydrological and ecological processes in forest ecosystems (e.g., Pomeroy & Dion, 1996; Hardy et al., 2004; Essery et al., 2008).

Under-canopy radiation regimes determine a range of ecological and biological processes and components in forest ecosystems, such as species diversity, species distribution, community structure, and succession processes (MacArthur, 1964; Martens, Breshears, & Meyer, 2000; Svenning, 2002; Frelich, Machado, & Reich, 2003; von Arx, Dobbertin, & Rebetez, 2012). Understory light environment also influences growth and competition, net primary production, and vegetation types (Sakai & Akiyama, 2005; von Arx et al., 2012). Understanding under-canopy radiation profiles and regulating under-canopy light levels are often essential for agroforestry systems, commercial plantations, and for conservation purposes (Bellow & Nair, 2003; Frelich et al., 2003; Jennings et al., 1999). Canopy radiation schemes are also important to consider in dynamic global vegetation models (Loew et al., 2014).

The presence of vegetation affects radiation, energy balance, and snowmelt under the canopy. Interaction of vegetation with radiation impacts under-canopy snow processes by influencing the timing, quantity, and duration of snowmelt. Predicting snow accumulation and snowmelt in forested areas is complex because most snow models are not sensitive to canopy properties (Storck, Lettenmaier, & Bolton, 2002). Snow models' performance is also

inconsistent at forest sites in comparison with open sites because of the complex interactions among snow, energy transfer, and trees (Rutter et al., 2009). In most hydrological studies, estimation of solar energy over vegetation areas is either neglected or oversimplified by considering vegetation as a turbid medium or using leaf area index (LAI) as a proxy for the amount of vegetation (Mahat & Tarboton, 2012). Incorporating the three-dimensional effect of vegetation structure, canopy geometry and their spatial distribution, and accurate characterization of the under-canopy radiation regime is necessary for validation of hydrological cycle and snowmelt models, and will lead to better estimation of soil moisture, hydrological flow, and snowmelt (Fu & Rich, 2002; Hardy et al., 2004; Varhola, Coops, Weiler, & Moore, 2010; Mahat & Tarboton, 2012).

Measuring under-canopy light is essential for forest management and silvicultural practices. Forest managers alter the forest canopy through thinnings to modify the canopy transmittance, and thereby the under-canopy light levels (Messier, 1996), to achieve specific objectives such as habitat management or seedling growth (Hale, Edwards, Mason, Price, & Peace, 2009). Knowledge of under-canopy light distribution on the forest floor may potentially be useful for mapping and monitoring disturbances to forest ecosystems, such as diseases, invasive species, or logging (Rosam, 2015).

1.2 Deriving Canopy Structure and Estimating Under-Canopy Radiation

Most physical models that estimate solar radiation reaching the earth's surface tend to simplify the process by focusing primarily on the effect of terrain,

atmosphere, and solar geometry (Peng, Zhao, & Xu, 2014). Therefore, in comparison with atmosphere and topography, the effects of which have been widely studied, there are fewer studies on the association between vegetation structure and radiation regime (Dozier, 1980; Dubayah, 1994; Kumar, Skidmore, & Knowles, 1997; Reuter, Kersebaum, & Wendroth, 2005). Lack of canopy structure information at the stand level makes such studies difficult (Parker, Lefsky, & Harding, 2001). Vegetation effect is either simplified, assuming it to be a homogenous medium (Verseghy, McFarlane, & Lazare, 1993), or based on actual field data from forest (e.g., Parker et al., 2001; Stadt et al., 2005). Deriving three-dimensional vegetation structure using information gathered from forest survey is a tedious process. Traditional optical remote sensing was of limited use because of its inability to derive vertical canopy structure. Estimating under-canopy solar irradiance is another challenging process, which traditionally uses pyranometers, quantum sensors hemispherical photographs, and photosynthetically active range (PAR) sensors (e.g., Rich, 1990; Parker et al., 2001; Hardy et al., 2004).

In the last decade, light detection and ranging (LiDAR) remote sensing has been useful in providing vital and detailed information about the three-dimensional structure of vegetation (Lim, Treitz, Wulder, St-Onge, & Flood, 2003). Discrete return LiDAR is widely used in ecosystem studies and for resource management because of its availability and natural capacity to represent complex vegetation structures and ground features with accuracy (Lefsky, Cohen,

Parker, & Harding, 2002; Lim et al., 2003; Evans et al. 2009). Studies have begun to incorporate LiDAR-derived information on vertical canopy structure for biodiversity research and applications (e.g., Goetz et al. 2007; Turner et al. 2003). Using LiDAR as an active sensor not only provides information about canopy structure and forest biophysical parameters (Lefsky, Harding, Cohen, Parker, & Shugart, 1999; Morsdorf, Kötz, Meier, Itten, & Allgöwer, 2006; Korhonen, Korpela, Heiskanen, & Maltamo, 2011), but also helps us understand how light behaves as it travels through the vegetation canopy (Parker et al., 2001; Essery et al., 2008; Varhola et al., 2010). This information is vital for understanding the interplay of light and vegetation and can be further used to estimate the under-canopy solar radiation.

Therefore studying the spatio-temporal aspects of under-canopy light distribution is crucial for a sound understanding ecological processes and ecosystem functions within forests. However, characterization of forest canopies is challenging because of its structural complexity.

1.3 Dissertation Outline

The primary goal of this doctoral research was to improve characterization of under-canopy light regime in forest stands using discrete return LiDAR data.

This dissertation will address the following specific objectives:

- Assess the first order effect of vegetation canopy on solar radiation using digital surface models (DSM) derived from small footprint discrete LiDAR.

- Estimate and inter-compare under-canopy beam radiation using three-dimensional vegetation structure derived from LiDAR data across forest plots at different stages of succession.

- Estimate, inter-compare, and validate vertical light transmittance, LAI, and LAD derived from LiDAR across forest plots at different stages of succession.

The research sites are in the Teakettle Experimental Watershed in Sierra National Forest (SNF) in California (CA) and the Smithsonian Environmental Research Center (SERC) in Maryland. The SNF site has complex topography and mixed conifer forests. The SERC had relatively simple topography and mixed deciduous forest at different stages of succession. High-resolution discrete LiDAR data, the primary data source for this research, are available for these two sites along with the field data for model validation. These factors make the two sites suitable for studying under-canopy solar radiation using LiDAR.

The next sections give a brief overview of the dissertation.

1.4 Overview

This dissertation is divided into five chapters that includes an introduction (Chapter 1), followed by Chapters 2, 3, and 4, which present the main contributions of this dissertation and are formatted as articles. The fifth chapter concludes this dissertation.

In Chapter 2, the first-order effect of vegetation on solar radiation is assessed using DSM and digital elevation models (DEM) derived from small footprint discrete LiDAR. The data were acquired at the Teakettle Watershed in SNF in 2008. Solar radiation at both above and under tree canopies was then simulated to highlight the effect of trees on the underlying surface.

Chapter 3 estimates and compares the under-canopy direct beam radiation for forest plots at successional stages of growth—young (31 years old), intermediate (56 years old), and mature (116 years old) forest with different canopy characteristics. This involved characterization of three-dimensional vegetation structure from LiDAR data. A LiDAR-based custom ray-tracing model was then used to estimate under-canopy beam radiation. The validation of the model estimates was carried out using *in situ* measurements from above- and under-canopy pyranometers located at the SERC site. Finally, the estimates of under-canopy direct beam radiation at chronosequence were compared.

In Chapter 4, the light transmittance pattern and the vertical foliage profile were compared across forest plots at four successional stages of growth (old, mature, intermediate, and young), and at one plot with disturbance (logging).

Discrete LiDAR data were used to derive both vertical transmittance in the forest plots (canopy gap) and vertical foliage profiles. For validation, the PAR measurements collected by the quantum sensor were compared with the LiDAR-derived vertical transmittance values across three plots for which *in situ* PAR data were available.

Chapter 5 is the final chapter that summarizes the results, discusses the limitations, and provides insight into future research directions.

The overall goal of this research was to improve the characterization of under-canopy radiation regime and quantify radiation using discrete LiDAR remote sensing. The research is expected to improve the representation of radiation transmission through forest canopies and add to the knowledge on the impact of vegetation structure on under-canopy radiation. This knowledge gained here open new avenues for studying radiation using LiDAR, which may have a broad range of applications from forest management and timber resource planning, ecological modeling, energy balance studies to snowmelt, and hydrological simulations.

Chapter 2 Spatial Variability of Solar Insolation under a Mixed Coniferous Forest—A LiDAR-Based Study

2.1 Introduction

Spatiotemporal distribution of radiation beneath the vegetation canopy is a major component of surface energy balance and is of particular interest to forest managers, wildlife biologists, and hydrologists because it helps elucidate the biophysical processes operating at the landscape level. It determines the rate of snowmelt, the rate of under-canopy photosynthesis, and the suitability of microclimate for animal habitats (Murphy et al., 1990; Rich & Weiss, 1991; Weiss et al., 1991) at the community, landscape, and ecosystem level (Murphy & Weiss, 1992; Rich, Weiss, Debinski, & McLoughlin, 1992).

The effect of stand-level vegetation structure on the variability of solar radiation is crucial because the small-scale variability of solar radiation influences the surface energy balance considerably, and also contributes greatly to the mosaic patterns in melting snow cover and the timing and amount of melt-water release (Pomeroy et al., 2008). The effects of the two other important factors in solar irradiance variability—atmosphere and topography—have been studied widely (Dozier, 1980; Dubayah, 1994; Kumar et al., 1997; Reuter et al., 2005). However, most studies which incorporate vegetation effects on solar radiation using conventional satellite remote-sensing-derived parameters are conducted at

the landscape level and do not incorporate the effects of stand-level vegetation structure on the spatiotemporal variability of solar radiation (Peng et al., 2014). Influence of stand-level vegetation structure is overlooked because accessing solar radiation at stand scale is challenging because of extremely high spatial and temporal variability (Parker et al., 2001).

With the availability of LiDAR data, highly accurate vegetation structure and surface parameters can be derived at tree-level resolution and used to study the variability of solar radiation (Lai, Chou, & Lin, 2010). These fine-scale vegetation and topographic metrics are crucial for accurate characterization of canopy light transmittance (Nilson, 1971; Pukkala et al., 1991). Discrete return, as well as full waveform LiDAR sensors, has been used to study under-canopy radiation regime (Essery et al., 2008; Lee, Slatton, Roth, & Cropper, 2009; Ni-Meister, Yang, & Kiang, 2010; Tang et al., 2012, 2014, 2016). The major difference between both these LiDAR sensors is the way return signal is collected (Lim et al., 2003). Of the two, discrete return LiDAR has a better horizontal resolution, whereas full waveform LiDAR provides better information on the vertical distribution of canopy elements because of its high sampling rate (typically 1–5 ns). A waveform LiDAR records reflected energy above a noise threshold at predetermined time intervals. As a result, even a small change in the vegetation structure can influence the shape of the waveform (Means et al., 1999). Regarding data availability, discrete return LiDAR data are more readily available compared with the waveform LiDAR data.

Most studies using LiDAR data to examine radiation regime beneath forest canopy use models based on either radiative transfer or geometric-optical principles or a combination of the two (Ni, Li, Woodcock, Roujean, & Davis, 1997; Essery et al., 2008). Most of these models need high computational capacities (Musselman, Molotch, Margulis, Kirchner, & Bales, 2012; Peng et al., 2014) which limit their use for larger areas.

In the recent decades, studies on solar insolation using LiDAR products have utilized LiDAR-derived DEMs, and few studies have made direct use of point clouds. From a remote-sensing perspective, the main difference between LiDAR and solar radiation is that while the LiDAR is near the nadir, the sun could be at any solar angle (Hopkinson, Chasmer, Lim, Treitz, & Creed, 2006; Essery et al., 2008; Musselman et al., 2012). Based on the assumption of opaque leaves, Hopkinson and Chasmer (2007) demonstrated the use of the LiDAR cloud point and radiative transfer principle to derive the first-order information on solar radiation. However, this method is not viable for practical purposes because of its high computation demand and expertise needed to run the radiative transfer model. This limitation can be addressed by using a LiDAR-derived canopy height model (CHM) for studying the first-order effect of tree canopies. This quick and user-friendly technique can be easily integrated with current Geographic Information System (GIS) platforms. Today, nearly all commonly used GIS platforms have an integrated solar module, for example, Solar analyst, r.sun, and Sextante (Dozier, 1980; Dubayah, 1994; Dubayah & Rich, 1995; Kumar et al.,

1997; Šúri & Hofierka, 2004).These tools estimate solar shortwave energy, which is also the most crucial part of radiation, because solar shortwave energy adds the greatest amount to the energy balance, and directly or indirectly other parts are contingent on it (Kumar et al., 1997). These tools are increasingly used for ecological modeling (Austin & Van Niel, 2011) and potential solar energy estimation (Clifton & Boruff, 2010). Additionally, LiDAR-derived high-resolution terrain models have made it easier to model solar radiation at a finer scale.

Two types of solar radiation models are currently available to estimate spatial distribution of solar radiation over the earth's surface: (i) Vector based data models (Teller & Azar, 2001,Steemers, 1990), and (ii) Raster-based models (Frew & Dozier, 1986; Frew, 1991, Dubayah & Rich, 1995; Rich, Hetrick, & Saving, 1995; Fu & Rich, 2002, Kumar et al., 1997, Hofierka & Suri 1997). Raster-based models have been successfully used to study terrain effects on solar radiation at landscape levels, whereas the application of vector-based models is limited to vector data and urban studies (Yu, Liu , Wu, & Lin, 2009).

The primary objective of this study was to assess the first-order effect of vegetation on solar radiation using DSM derived from small footprint discrete LiDAR. This was accomplished through two main steps: First, forest structure and bare surface topography of the landscape were derived using LiDAR. Then, insolation with and without tree cover was modeled, and the difference between the two was analyzed. In the first step, we derive the surface and canopy structure

from LiDAR data by converting the point cloud into the DSM and DEM. We then derived the CHM by subtracting the DEM from DSM. In the second step, we used the LiDAR-derived elevation models as primary inputs to r.sun—a raster-based solar insolation model—to calculate both diurnal and seasonal insolation with and without tree cover. We then used conventional and spatial statistics to describe and compare the spatial and temporal variability of solar insolation.

In the next section, we describe the study site and methods followed by a section on the results. The discussion considers the potential implication of this study for remote sensing and ecological applications, as well as the limitations of this study.

2.2 Methods

2.2.1 Study area

Teakettle Watershed located in Sierra National Forest (SNF) is about 80 km east of Fresno, CA north fork of the Kings River drainage basin between Yosemite and King's Canyon National Parks (http://www.fs.fed.us/psw/ef/teakettle/). Elevation ranges from 1,980 m to 2,590 m with an average of 2,249 m (**Figure 2.1**). Teakettle is 1,300 ha of old-growth forest of which approximately two-thirds are mixed conifers. Mixed-conifer forests usually have characteristic patches with tree clusters with closed-canopy , persistent gaps, and shrub groves (North et al., 2002). They typically consists of a fine-scale assortment of four patch categories: patches with closed

canopy, patches primarily of mountain whitethorn, areas with rocks and very thin soils and open gaps. Within the mixed-conifer type, Jeffrey pine is prevalent on shallow soil conditions, whereas altitudes above 2,300 m are dominated by red fir while humid sites are occupied by lodgepole pine. The last disturbance was a widespread fire in 1865 (http://teakettle.ucdavis.edu). The heterogeneous spatial structure at Teakettle offers distinct microclimate and habitats possibly linked with high biodiversity consisting of diverse group of under canopy plants, invertebrates species and several types of fungi (North et al., 2002). The presence of complex topography and forest types made this area suitable for our study.

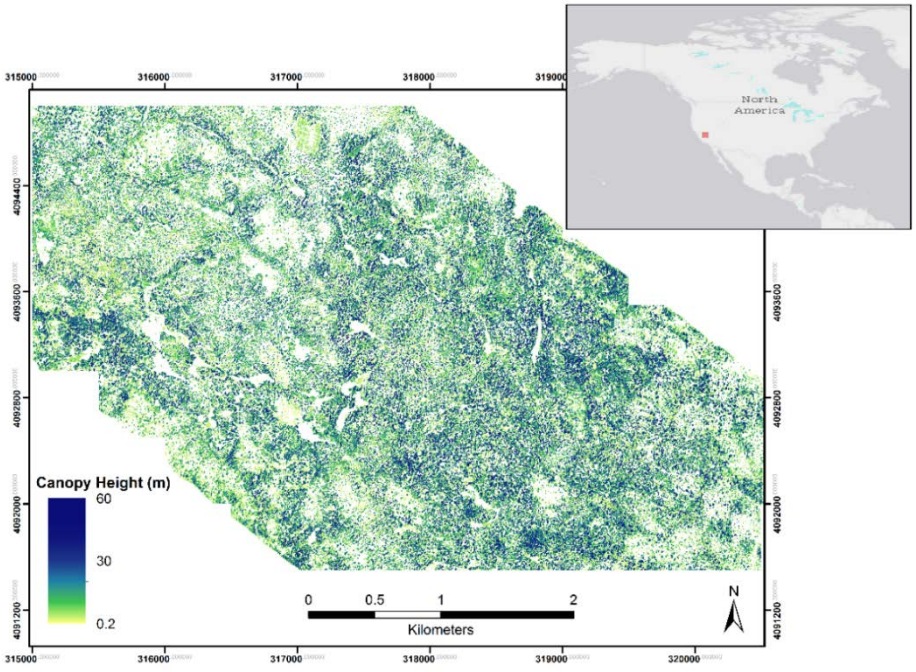

Figure 2.1 Location of Teakettle Watershed, Sierra National Forest, CA (inset). The main image shows canopy height model for the study area. Lighter color patches indicate rocky bare areas and darker patches indicate high vegetation areas.

2.2.2 Data

The primary source of data for this study is point clouds from discrete return LiDAR acquired for the Teakettle Watershed in Sierra National Forest, CA in summer 2008. The average point density of the LiDAR data is ~13 points/m^2 (**Figure 2.2**).

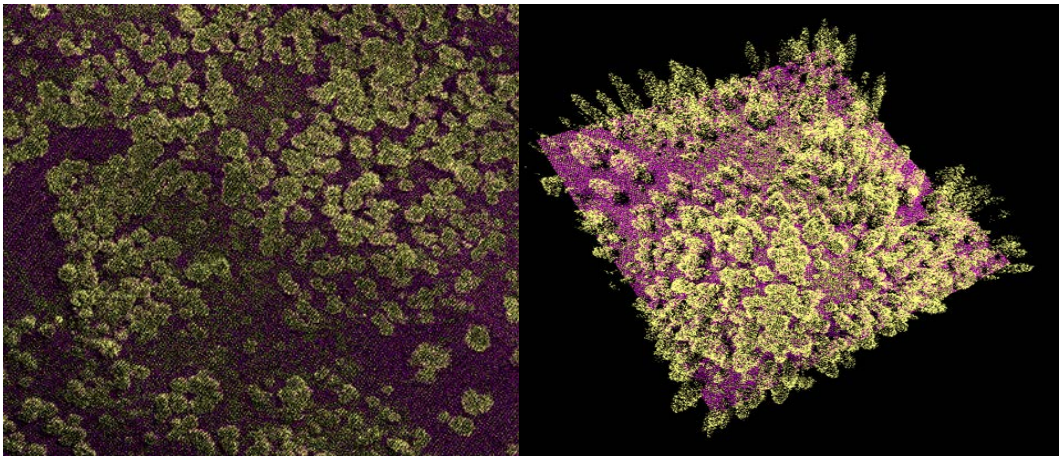

Figure 2.2 A subset of the classified LiDAR point clouds in nadir (left), oblique (right) perspectives. Data points, sampled with the intensity of approximately 13 points/m^2, were classified by height into two classes—vegetation (green) and ground (violet).

The LiDAR point cloud data was classified by the provider as per Society for Photogrammetry and Remote Sensing (ASPRS) standards and made available in LAS v1.1 format (http://www.lasformat.org). We used classes 1–6 for our analysis. Class 2, the ground return, was the most relevant for our study. Information about elevation, intensity, return number, flight-line, and scan angle for each return was also already available with the data.

2.2.3 Derivation of canopy structure from LiDAR point cloud

Surface and tree structure characteristics were derived from LiDAR data by converting the point cloud into a digital surface model (DSM) and a digital elevation model (DEM) at a grid resolution of 1 m. The DSM, which may include trees, buildings, and other such features, was created using the first return. The DEM, which represents the bare earth or ground surface, was created using the last return of the point cloud. This task was simplified by the availability of ground and non-ground classification of the point cloud and lack of any built features since the study area was located in a national forest. The Canopy Height Model (CHM) was derived by subtracting the DEM from DSM. We also classified the surface with and without trees based on the CHM. A 0.2 m height threshold was used to generate a tree/no-tree mask to accommodate minor surface model errors.

2.2.4 Solar insolation estimation

A raster-based potential solar insolation model, r.sun, was used for this study. It is a spatially explicit model and can use LiDAR-based elevation models as a primary input. The choice of this particular model was based on its usability; it needs a fewer number of parameters. It calculates potential direct, diffuse, and total incoming solar radiation for any period together with the solar illumination duration (**Figure 2.3**). It accounts for location, elevation, aspect, slope, shadow

effects of the surrounding topography, effects of the atmosphere, and diurnal and seasonal changes of the solar angle.

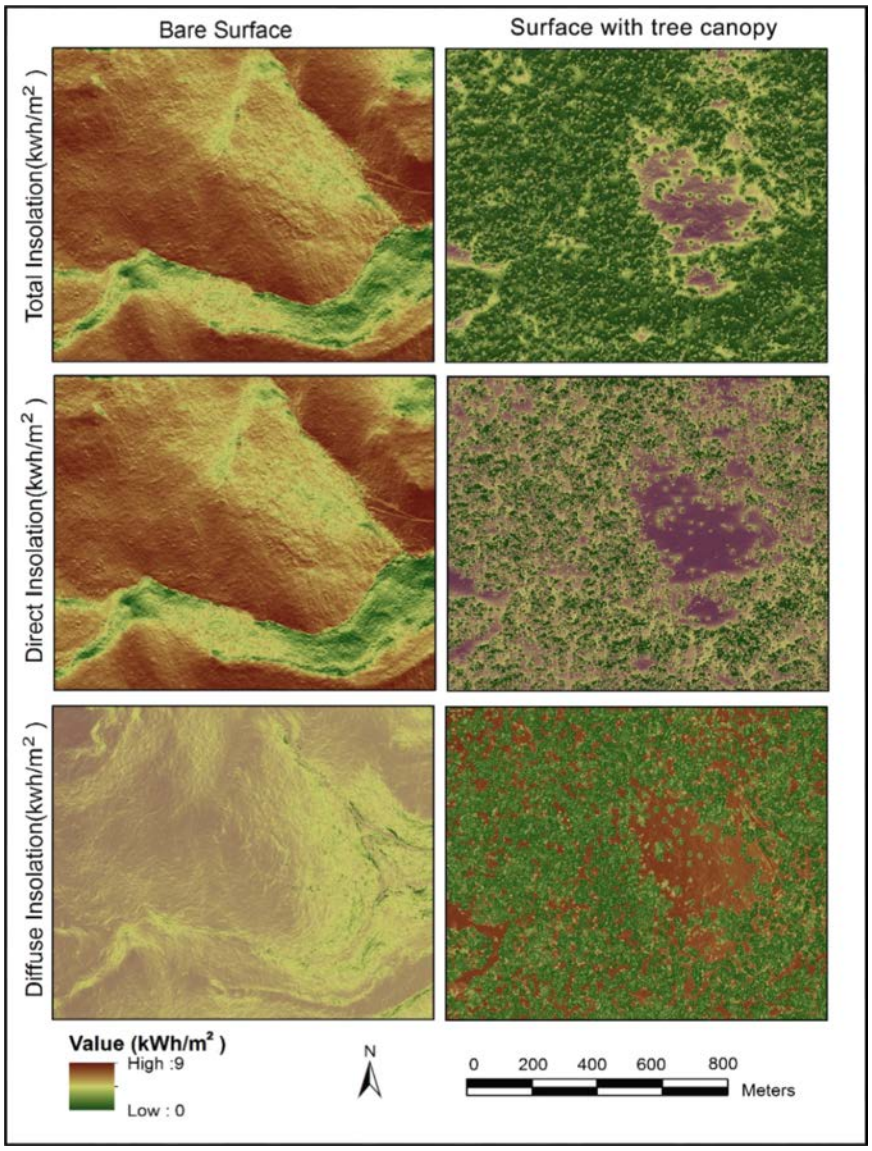

Figure 2.3 Total, direct, and diffuse radiation output from a solar radiation model. The panel on the left shows the radiation output for the bare surface, the right panel shows radiation output for the same site with trees. The average surface radiation values are always higher for the bare surface when compared

with the surface that includes trees. However, the radiation output shows higher variability when the surface includes trees.

Using the model, we calculated the total potential incoming shortwave radiation for the study area. The derived DEM and DSM were primary inputs to the model. The model simulates the solar insolation in watts hour per square meter (kWh/m^2), or mega joules per square meter (MJ/ m^2), given the time duration in Julian days, time step in minutes, the atmospheric transmittance and the number of sky directions for calculation of sky view factor.

Since solar radiation calculation takes a lot of computational time, we used multiple processors to run r.sun model, which was able to distribute the task to multiple processers. This reduced the computation cost by a factor of 10. This time difference was an important consideration when calculating solar radiation for longer time periods. We also calculated the total solar radiation for summer solstice, winter solstice, and equinox. Furthermore, we estimated the diurnal hourly radiation for summer solstice to study the effect of hourly radiation change.

2.2.5 Statistical analysis of solar insolation

We used both standard statistics as well as spatial statistics to describe and compare the spatial and temporal variability of solar insolation. Statistical difference between the radiation values for bare and canopy surface was investigated using the Wilcoxon signed-rank test, a non-parametric equivalent of

paired *t*-test with the null hypothesis that the paired data do not have significantly different means.

Local index of spatial association (LISA) methods—Geary's *C* and Moran's *I*—were used for spatial association in insolation values. Moran's *I* and Geary's *C* are two common measures used to study spatial autocorrelation. Higher Moran's *I* values indicate positive spatial autocorrelation. Clusters of high value are known as hot spots and low value are known as cold spots. The major limitation of Moran's *I* is that it is based on global averages and therefore can be easily biased by outliers. Geary's *C* deals with this restriction better because the interaction is not the cross-product of deviations from the mean like Moran's *I*, but rather of the deviations in intensities of each observation location with one another. The interpretation of both Moran's *I* and Geary's *C* is different. Unlike Moran's *I*, a low Geary's *C* value indicates high spatial correlation. Therefore, they both show inverse relation. Since Global LISA does not provide a detailed aspect, we also used correlograms to study the correlation at varying lag distances (Isaaks & Srivastava, 1989).

2.3 Results

2.3.1 Site topography and canopy surface characteristics

The Teakettle study site has a complex topography with mixed conifers typical of mid-elevation sites in the SNF (**Figure 2.1**). The surface models derived from LiDAR point cloud showed that the site was mostly covered with

trees except for a few prominent bare patches. These bare patches were the canopy gaps in rocky areas not suitable for vegetation growth (**Figure 2.2**).

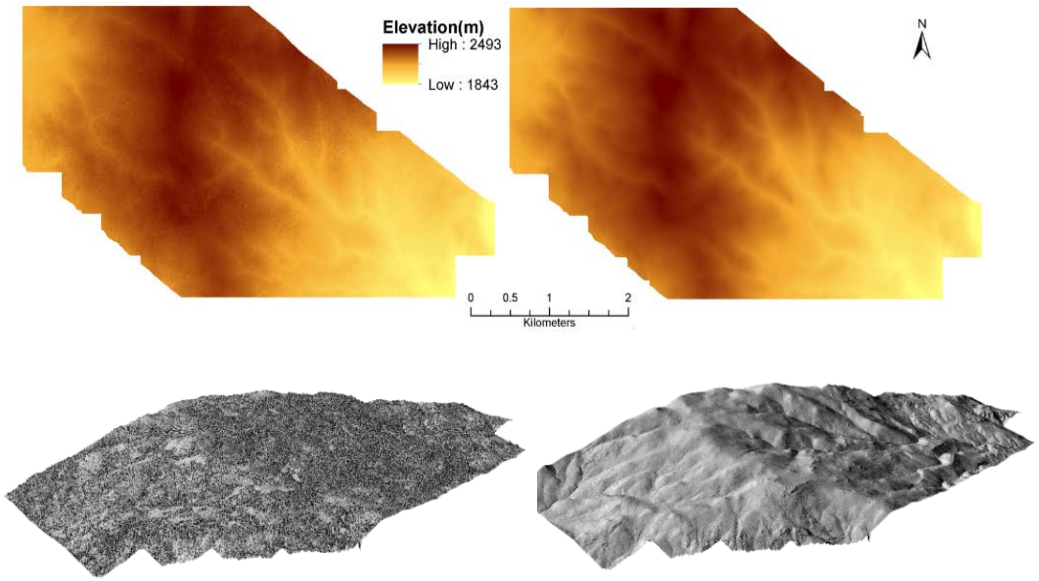

Figure 2.4 LiDAR-derived DSM and DEM, with and without trees. The upper panel shows two-dimensional images of the surface model derived from LiDAR. The lower panel shows the DSM, which includes tree (left) and the one without tree canopies (right).

The surface models derived from LiDAR point cloud showed that the site was mostly covered with trees except for a few prominent bare patches. These bare patches were the rocky areas unsuitable for vegetation growth (**Figure 2.4**). The two surface models created using LiDAR point cloud revealed different surface characteristics. The average elevation of the site with vegetation was 2,282.190 m, whereas the site without vegetation was 2,273.93 m. This difference in average height of the canopy surface compared with the bare surface can be

attributed to the presence of trees. Descriptive statistics comparing the two surface models showed the height difference due to the presence of trees (Table 2.1).

Table 2.1 The topographic characteristics of the canopy surface (DSM), bare surface (DEM), and canopy height model (CHM) for the Teakettle Watershed

	Min	**1st Q**	**Median**	**Mean**	**SD**	**3rd Q**	**Max**
DSM (m)	1,842.88	2,169.744	2,282.190	2,257.52	129.46	2,364.141	2,492.61
DEM (m)	1,828.09	2,162.036	2,273.931	2,249.07	129.60	2,355.996	2,462.76
CHM (m)	0.20	3.39	12.18	14.39	12.07	22.8	60.00

The CHM created from surface models of the Teakettle Watershed (**Figure 2.1**) showed a lot of variability in the spatial distribution of canopy height. The canopy height ranged from 0.2 m to 60 m, with an average height of 14.39 m and a standard deviation (SD) of 12 m (Table 2.1). The northwest section had relatively shorter trees compared to the rest of the study area.

2.3.2 Spatial and temporal pattern of solar insolation

To investigate how insolation patterns varied throughout the day and seasons, we simulated both hourly as well as daily total insolation (sum of direct and diffuse) at both above and beneath the tree canopy. Direct and diffuse radiation were also estimated however we only report the results based on analysis of total radiation.

Diurnal radiation pattern

Mean solar irradiation flux over the canopy surface model was 10.2 W/m^2 at 6 a.m. and 9.1 W/m^2 at 6 p.m.; with a value of 363.1 W/m^2, it was maximum at noon. For the bare surface, the mean insolation values were 30 W/m^2 at 6 a.m. and 29 W/m^2 at 6 p.m. The average value at noon was 959 W/m^2.

Compared to the canopy surface model, the bare surface model estimated higher irradiance flux (**Figure 2.5**).

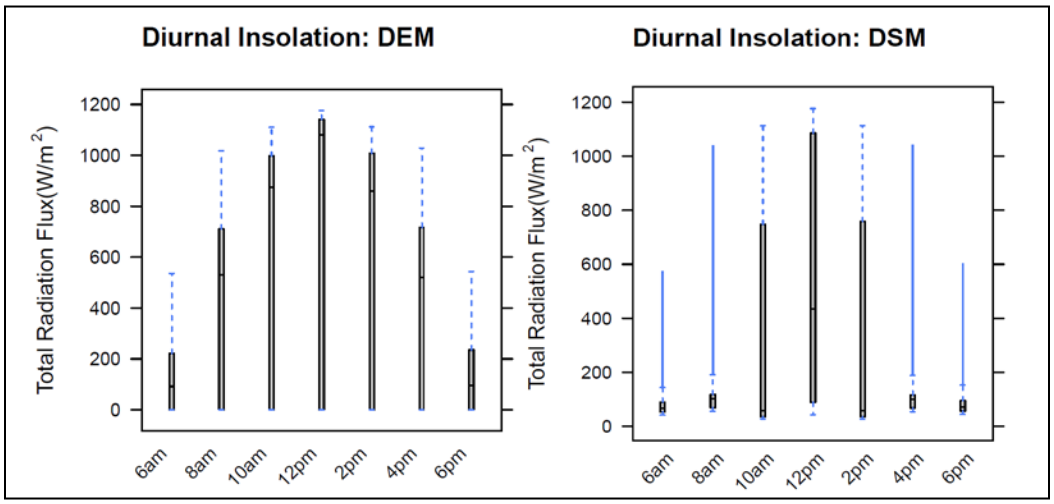

Figure 2.5 Diurnal distribution of solar insolation with tree (left) and bare surface (right). The data for all time steps show a cyclical pattern. Mean values of irradiation for the DEMs are much higher when compared with the DSM; however, the DSM shows higher variability.

The coefficient of variation (CV) for the canopy surface showed uniform pattern with the canopy surface showing more variance throughout the day. The CV for the bare surface model was close to 125 at 6 a.m. and 6 p.m. At noon, the CV was 13, the lowest during the day. The canopy surface CV was 255 at 6 a.m.

and 244 at 6 p.m. The CV was at a minimum 113 for the bare area around 12 noon (**Figure 2.6**).

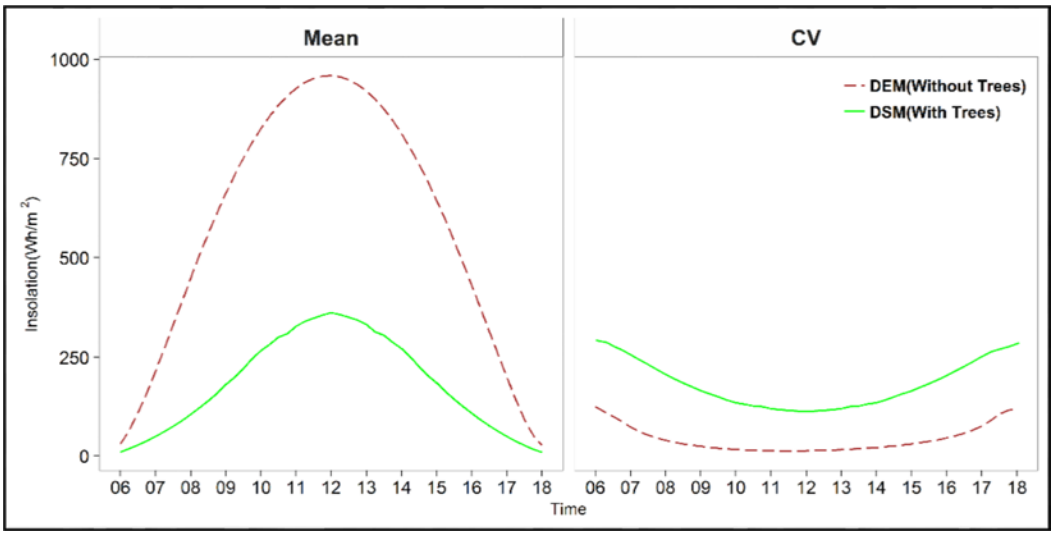

Figure 2.6 Comparisons of hourly mean (left) and coefficient of variation (right) for the surface with tree canopy, and bare surface insolation. The red dotted line represents bare surface, and the green line represents insolation value for the surface with trees. The bare surface hourly mean insolation values are always higher than the mean insolation of the surface with trees. The CV shows an opposite pattern. The CV for the insolation value is always higher for the surface with trees. The CV for both the surface model peaks during the dusk and dawn.

Solstice and equinox

The canopy surface model estimated a mean insolation of 3.76 kWh/m^2 during summer solstice, 2.4 kWh/m^2 during equinox, and 1.25 kWh/m^2 during winter solstice (see Supplementary Table 2). The mean insolation showed a decreasing trend from summer solstice to winter solstice, dropping almost three times from summer solstice to winter solstice. Radiation statistics showed a

similar pattern where insolation reduced from summer solstice to winter solstice. Bare surface insolation showed a similar trend. However, the insolation values were much higher than the canopy surface model (**Figures 2.7** and **2.8**). The mean insolation received by the surface without trees was 9.37 kWh/m^2 during summer solstice, 6.7 kWh/m^2 during equinox, and 3.43 kWh/m^2 during the winter solstice (see Supplementary Table 2). The SD of solar insolation for the canopy surface model was 2.34 kWh/m^2 during summer solstice, 1.68.41 kWh/m^2 during the equinox, and 0.89 kWh/m^2 during the winter solstice. It was less for the bare surface model with a SD of 0.42 kWh/m^2 during summer solstice, 0.74 kWh/m^2 during the equinox, and 0.77 kWh/m^2 during the winter solstice (see Supplementary Table 2).

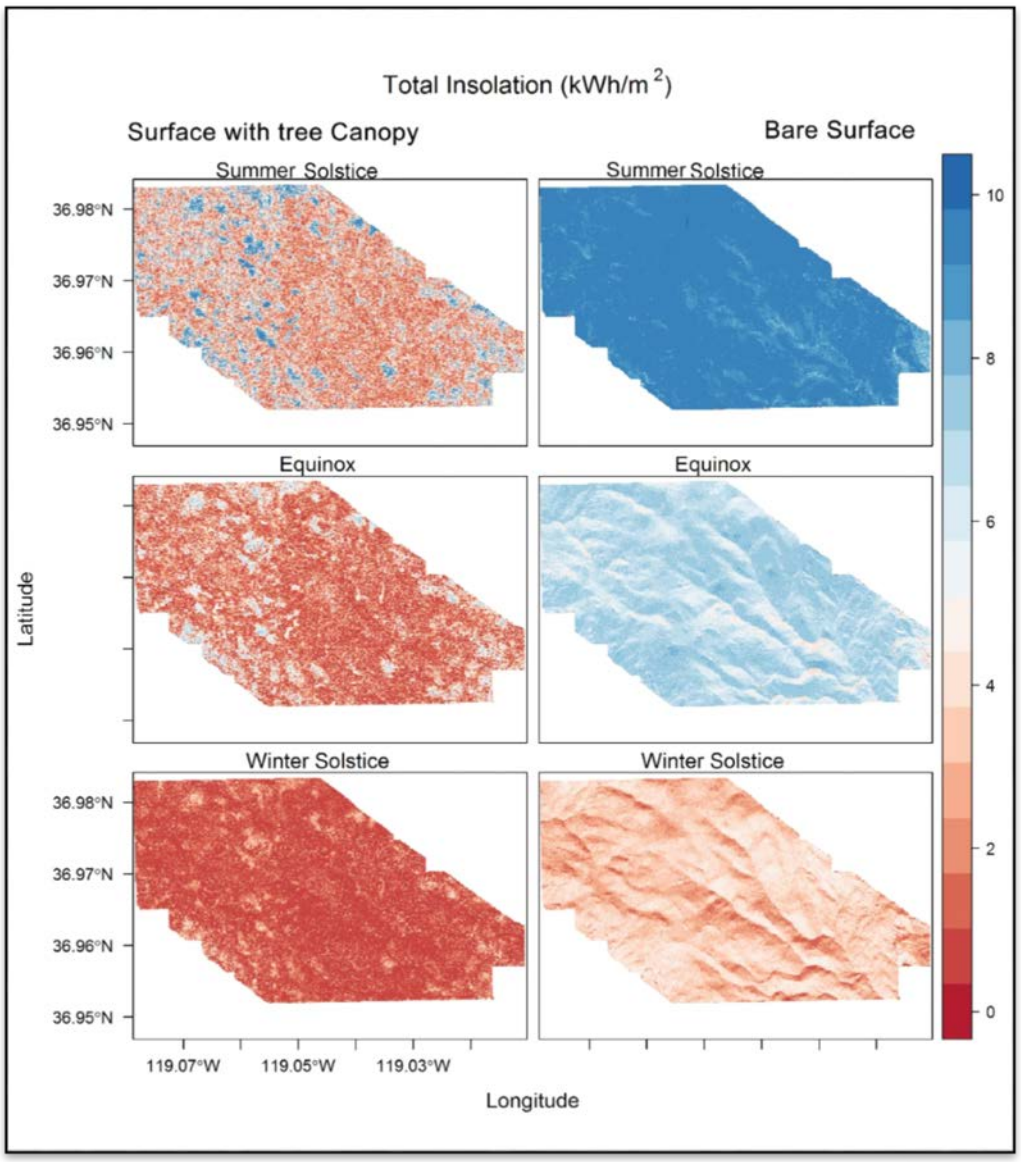

Figure 2.7 Map of insolation during summer solstice, equinox, and winter solstice, with and without trees. The shades of blue show high insolation values and the shades of red show low insolation values. The insolation on the surface with tree canopy is more heterogeneous compared to the bare surface insolation. The bare surface has higher insolation values for all the 3 days.

Overall three main observations were made by comparing the bare surface insolation to the insolation over the surface with tree canopy:

- The canopy surface insolation showed much more variability in solar insolation values. During the summer solstice, the coefficient of variability for the canopy surface was 66% and only 4% for the bare surface.
- The canopy surface insolation showed lower average insolation values.
- The distribution of insolation followed a normal or near normal distribution on the bare surface. However, it did not demonstrate a similar distribution on the canopy surface model.

Overall the heterogeneity of insolation was important during all times of the year, but most pronounced during the winter solstice.

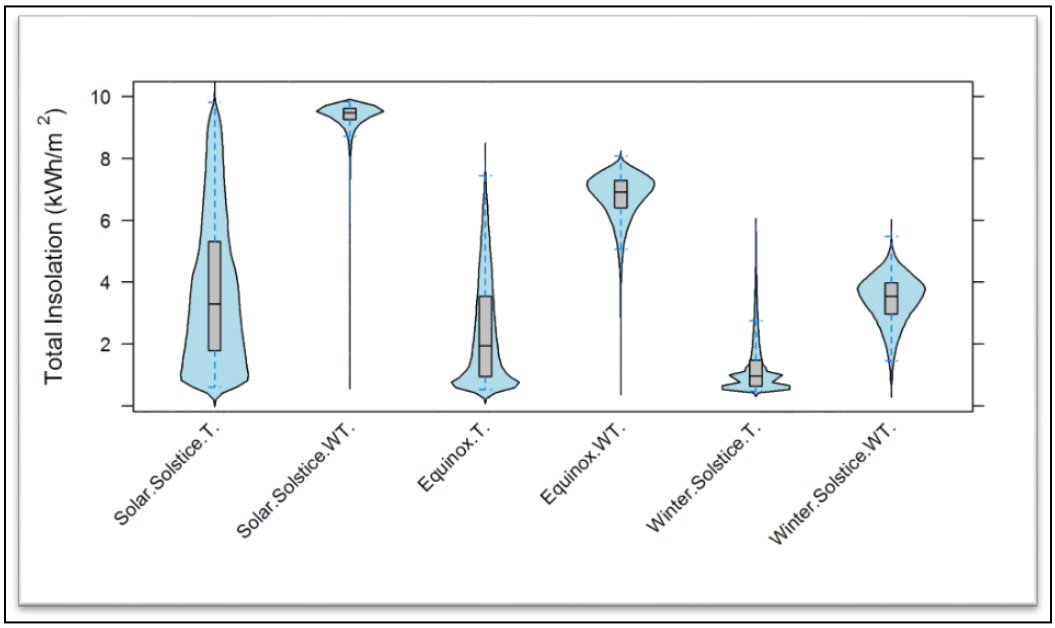

Figure 2.8 Solar insolation distribution across the summer solstice, equinox, and winter solstice. The boxplot shows that the insolation values for the bare surface

are higher than the surface with tree canopies for all the three days. The surface with tree canopy has more variability as depicted by larger inter quartile range.

We also compared the isolation for open areas where there are no trees in both the models. The isolation values progressively decreased from summer solstice to winter solstice. The DSM, which contained the canopy surface, showed much more variability, which may be attributed to the heterogeneity of the canopy surface model.

Statistical difference

Statistical significance of the difference between the insolation values for bare and canopy surfaces was investigated using the Wilcoxon signed-rank test with 5,000 randomly selected locations. The test showed that the insolation significantly differed between the canopy and bare-earth surface models (*p* value < 0.001). The pseudo-median was 3,583.22 kWh/m^2 for the summer solstice, 2,942.17 kWh/m^2 for the equinox, and 1,272.93 kWh/m^2 for the winter solstice (see Supplementary Table 1). Results showed that the solar insolation for the bare and canopy surfaces varied significantly by season.

Spatial correlation

Spatial autocorrelation analysis was based on local and global parameters, which emphasize the spatial correlation between the insolation values (see Supplementary Table 3). Moran's *I* value for the canopy surface insolation showed a decreasing trend with 0.84 during summer solstice to 0.79 during equinox and finally decreasing to 0.64 during the winter solstice (**Figure 2.9**). This

trend was not pronounced on the bare surface, which instead showed a minor decrease in the Moran's *I* value across the seasons. For the bare surface, the spatial autocorrelation did not vary much across the seasons. For canopy insolation, maximum autocorrelation was in the summer months during the solar solstice and minimum during the winter solstice. Geary's *C* also showed a similar pattern, indicating that the autocorrelation between levels of bare surface insolation do not vary with the seasons, whereas the canopy surface insolation showed a decreasing trend through the seasons (see Supplementary Table 3).

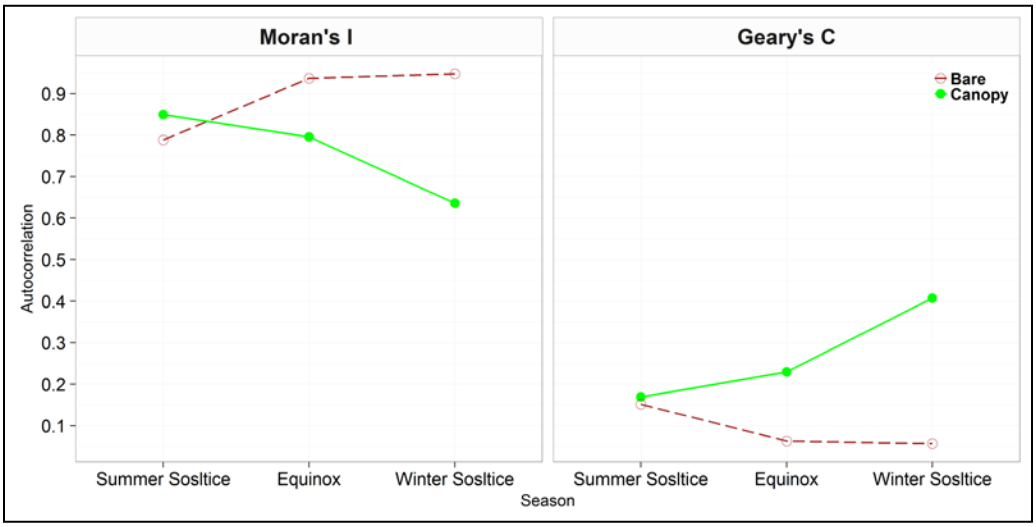

Figure 2.9 Comparison of Moran's *I* and Geary's *C* for the canopy insolation value of the surface with tree canopy (green line) and the bare surface (brown dotted line). Both measurements of spatial-autocorrelation show that the bare surface insolation values are more auto-correlated.

2.4 Discussion

In this chapter, we assessed the first-order effect of vegetation on solar radiation using DSM and DEM derived from small footprint discrete LiDAR.

The first part of this study shows how LiDAR point clouds can be used to better characterize site topography and canopy surface characteristics (**Figure 2.4**). The two surface models created using LiDAR data illustrated the different surface features of the study area with and without vegetation. Our approach is useful for radiation studies that have traditionally relied on coarser surface topographic models such as Shuttle Radar Topography Mission (SRTM) and satellite-derived vegetation metrics (Varhola & Coops, 2013). LiDAR-derived high-resolution surface models enable better studies of forest stand-level microclimate. While we choose to apply our method to coniferous forests, this approach can be utilized for other forest types. This approach is also useful for studying microclimatic patterns at the forest edge and forest gaps (Galo et al., 1992), in treefall gaps (Canham et al., 1990), and for hydrological modeling, snowmelt, and microclimate studies.

Next, we examined how insolation patterns varied throughout the day and seasons by simulating both hourly as well as daily total insolation at both above and beneath the tree canopy. We found that solar irradiation follows a cyclic diurnal pattern. Irradiation values were lowest at sunrise and sunset, and highest at noon. The diurnal pattern in solar radiation suggests solar geometry drives irradiation (**Figure 2.5**). Insolation both above and beneath canopy showed this

cyclic pattern. However, they differed in the intensity and variability of insolation values (**Figure 2.6**). The bare surface showed less variance and higher average values of solar insolation, whereas surfaces with trees showed lower values of mean insolation and larger variability. Mean solar irradiation flux over the surface with tree canopy is three times less in the morning (10 W/m^2 vs. 30 W/m^2) and 2.6 times at noon when compared to the bare surface radiation values. Although these values may seem to indicate that there is far less solar energy on the surface with trees, the total amount of solar energy in the system remains same. For the surface with trees, the "missing" energy actually absorbed and reflected that drives various biogeochemical processes, such as photosynthesis, evapotranspiration, and maintaining soil and atmospheric temperature.

The CV is highest during morning and evening. Dubayah, Dozier, and Davis (1990) explained that optical depth of the atmosphere controls these observed peaks, and the magnitude of this is controlled by the average slope of the area.

Over the seasons, the total insolation followed a cyclic pattern and showed a decreasing trend from summer solstice, to equinox, to winter solstice in that order (**Figure 2.7**). Solar geometry influences this cyclic pattern of radiation in both the surface models. During summer, there is high insolation as the sun's angle is small; and towards winter, the sun angle becomes oblique, thereby resulting in less radiation. So, by examining how insolation patterns vary spatially

and temporally, we show the effect of canopy structure in the heterogeneity of radiation distribution. This variability is related to the interaction of solar radiation with the canopy structure. Open canopies allow sunlight to illuminate the ground without major modifications and therefore show less variability. Closed heterogeneous canopy structure modifies the incoming light, creating strong spatial and temporal variations when compared to bare surface or above canopy (Lundquist, Dickerson-Lange, Luz, & Cristea, 2013). Heterogeneous canopies have a more variable microclimate. Therefore, LiDAR-derived canopy structure models can help us to estimate better the spatiotemporal distribution of microclimates corresponding with the diurnal and seasonal changes in solar angle.

Our last step was to see if the solar radiation values for each of the two surfaces were spatially auto correlated. We found that the canopy radiation levels were less auto correlated with each other between the seasons compared to the bare surface radiation levels (**Figure 2.9**). Moran's *I* value for the canopy surface insolation for the summer solstice was 0.84 compared to 0.96 for the bare surface. The Moran's *I* values for both the surfaces decreased over the equinox and winter solstice. However, the bare surface radiation values were consistently more auto correlated when compared with the surface with tree canopy (**Figure 2.9**), which suggests that canopy surface was more heterogeneous compared to the bare surface.

There is much scope for improving solar radiation models. Our work only took into consideration the effect of shadows and the canopy gaps. However, the real canopy structure is much more complex due to the different optical properties of other canopy elements such as leaves and branches. Canopy representation can be improved with the use of LiDAR point clouds with tree geometry. Solar radiation can further be modeled using LiDAR-derived gap probability, defined as the probability of a photon to make it through a point within the canopy (Ni et al., 1997). Radiative transfer models can also be used to model the multiplicative scattering of light by the canopy elements. In the next chapter, we introduce more canopy complexities by using a radiative transfer model and ray tracing to study how radiation interacts with vegetation structure.

2.5 Conclusion

Our approach of modeling canopy surface and estimating solar insolation provides a spatially explicit model relevant for studying many important ecological patterns and processes. First, it illustrates a basic model that can be integrated into GIS and used for ecological research. Second, it shows the central role that canopy structure plays on solar insolation and its effect on the variability of solar insolation and thus forging a path for integrating local effects to forest stand and landscape scales. Third, our approach demonstrates how high-resolution LiDAR data can be used to derive canopy structure and has the potential for applications to understand the link between ecological and microclimatic patterns and processes. Finally, this work improves our understanding of the direct

mechanistic link between canopy structure, variability of solar insolation, and heterogeneity in under-canopy microclimates. Understanding these linkages is central to the basic ecological processes and has the potential to improve hydrological models and snowmelt assessments.

Chapter 3 Impact of Forest Structure and Age on Under-Canopy Light Regime in a Temperate Deciduous Forest

3.1 Introduction

The three-dimensional canopy structure of the forest primarily determines the quantity, quality, and spatiotemporal distribution of under-canopy light conditions. The influx of radiation into a forest canopy is regulated by the amount and organization of canopy elements, their spectral properties, together with the illumination geometry (Pukkala et al., 1991; Jennings et al., 1999). In contrast, above-canopy solar radiation is affected principally by the position of sun and topography. Thus, under-canopy solar radiation regime is complex and variable when compared to the top of the canopy solar radiation.

Understanding under-canopy light conditions is crucial because it influences a broad range of biophysical components in forest ecosystems including: plant growth, net primary production, demography and population dynamics of individual species, community structure, competition, and succession (Latham, Zuuring, & Coble, 1998; Svenning, 2000; Frelich et al., 2003; Bellow & Nair, 2003). Under-canopy light conditions also determine the surface energy budget, which has significant implications on the hydrology and snowmelt in forested ecosystems. Several theoretical studies have proposed a strong link between forest structure, canopy elements and light attenuation (Campbell & Norman, 1989; Kuuluvainen & Pukkala, 1989). However, many other studies

demonstrate that understory light distribution pattern are much more complex and do not always show a clear relationship with the forest structure (Ross, Flanagan, & Roi, 1986; Brown & Parker, 1994; Denslow & Guzman, 2000). Therefore, mapping the forest understory light conditions is of interest to foresters, hydrologists, and ecologists (Jennings et al., 1999; Musselman, Margulis, & Molotch, 2013; Peng et al., 2014).

Light plays a fundamental role in driving forest succession (Oliver, 1980; Guariguata & Ostertag, 2001). The general presumption is that the amount of light reaching the forest floor decreases as a succession progresses, but empirical studies do not point to a single trend. Across a moist tropical chronosequence, Denslow and Guzman (2000) found no relationship between mean plot light levels or CV of light levels among forests with a different structure. Similarly, another study by Brown and Parker (1994) observed that allometric measurements of tree structure were not able to explain the variability in near canopy surface light availability in temperate deciduous forests at various levels of succession. They envisioned foliage density, LAI and other crown based measurements to be more representative and informative in understanding the relation between forest structure and light pattern. Another study by Kabakoff & Chazdon (1996) points out that the canopy structure may indirectly affect the light availability inside the forest canopy through impacts on under-canopy vegetation.

However, empirical studies have suggested that variation in light transmittance can be better explained by the structural parameters of forest

canopies (Küppers, 1989; Brown & Parker, 1994). Conducting an empirical study in lowland Costa Rica in select old-growth and second-growth forests, Montgomery and Chazdon (2001) challenged the belief that, canopy and under-canopy vegetation within a forest have a direct bearing on light attenuation near the floor . While comparing light transmittance and heterogeneity to forest structure, they concluded that forest structure might be a major predictor of availability of light only at large spatial scales. They also found that structure was not suitable for predicting the availability of light within plots, or across plots that are similar in their overall physical configuration. At finer scales such as at the plot level, less obvious parameters such as individual tree structure, species types and composition, and vertical distribution of foliage may be more crucial. In another study, in old-growth plots at La Selva in Costa Rica, Clark, Clark, Rich, Weiss, and Oberbauer (1996) found significant canopy height autocorrelation at 2.5-m intervals. However, the correlations between canopy height and under-canopy light availability were not strong even at that fine scale.

Variability of radiation under forest canopies has been studied using the either direct, diffuse, or photosynthetically active radiation components, or a combination of these elements. However, as diffuse radiation has a rather predictable diurnal pattern, direct radiation accounts for the most of the differences in incoming radiation. Hutchison and Matt (1977) observed that the horizontal variability of radiation in a temperate broadleaf forest was largely due to the attenuation pattern of direct beam radiation. Pukkala et al. (1991)

considered direct radiation suitable for comparing under-canopy radiation regimes of different forest plots (Brown & Parker, 1994; Lee et al., 2009; Musselman et al., 2013; Peng et al., 2014). Musselman et al. (2013) evaluated the utility of airborne LiDAR data and ray-tracing model to estimate the transmittance of the direct solar beam in a complex terrain with conifers. They were able to demonstrate the utility of the ray trace models to illustrate the effect of complex canopy structure on direct solar radiation transmissivity.

Estimation of radiation regime within a forest canopy needs a detailed description of the position, density, and angular distribution of various canopy elements (Oker-Blom, Pukkala, & Kuuluvainen, 1989). Traditionally, under-canopy solar radiation has been estimated using pyranometers, hemispherical photographs, and PAR sensors, but these have small spatial footprints and cannot capture the variability even at short distances. Recently, both ground and airborne LiDAR have frequently been used to estimate canopy parameters and study the interaction of solar radiation with canopy structure. Using airborne LiDAR for radiation studies has two main advantages: LiDAR data can provide spatially explicit estimates of forest biophysical variables such as canopy cover, canopy height, and LAI (Lefsky et al., 1999; Morsdorf et al., 2006; Korhonen et al., 2011; Tang et al., 2012). It can also provide estimates of light transmittance (Parker et al., 2001; Essery et al., 2008; Varhola et al., 2010). The main difference between the illumination geometry of solar radiation and LiDAR is that, while LiDAR is usually incident at nadir, solar illumination geometry has a diurnal and seasonal

cycle of variation (Chasmer & Hopkinson, 2007). LiDAR data are also used for directly estimating canopy transmittance.

Several studies have used LiDAR for characterization of canopy structure and estimation of solar radiation under the forest canopy. Parker et al. (2004) demonstrated the novelty of using a portable LiDAR systems, for rapid measurement of small-scale forest structure. Essery et al. (2008) used LiDAR data and a ray-tracing model for elliptical canopies. In another study Lee et al. (2009) used LiDAR data to simulate solar radiation on the forest floor. They defined a field of view function between a point on the forest floor and the sun. In a similar effort with LiDAR data, Kobayashi et al. (2012) modelled the radiation environment in an oak woodland using a spatially explicit LiDAR-based three-dimensional radiative transfer model. Musselman et al. (2013) also used LiDAR data and a three-dimensional model based on ray-tracing principles to estimate direct solar beam attenuation in a forest with structural complexity and compared those outputs to the estimates from a Beer's Law-type transmittance model. Recently, Peng et al. (2014) used LiDAR and a ray-tracing model to estimate the spatiotemporal distribution of under-canopy light on the forest floor as well as a vertical gradient of the forest stand. Frazer, Magnussen, Wulder, and Niemann (2011) provided a general description of how spatially explicit forest parameters could be obtained from LiDAR and ground-based measurements. In this paper, we evaluate the impact of canopy structure as well as age on the under-canopy

distribution of light on the forest floor using a chronosequence of temperate deciduous forest.

The objective of this study was to estimate and inter-compare under-canopy beam radiation using three-dimensional vegetation structure derived from LiDAR data across three forest plots at different stages of succession. Canopy structure information derived from LiDAR data and a custom geometric canopy radiative transfer model was used for this comparison. As discussed by Pickett (1989), we assumed that many sites at different stages of succession can represent the development of a single site through time and can be used to evaluate the impact of age on light under-canopy regime.

3.2 Methods

Our study began with the characterization of three-dimensional vegetation structure from LiDAR data. We then used a LiDAR-based ray-tracing model to estimate under-canopy beam radiation. The validation of the model estimates was carried out using *in situ* measurements recorded by above- and under-canopy pyranometers at the Smithsonian Environmental Research Center (SERC), Maryland. Finally, we compared the estimates of under-canopy direct beam radiation at chronosequence.

3.2.1 Study area

The study area is located within the Smithsonian Environmental Research Center (SERC) in Edgewater, Maryland, USA (38°53′N, 76°33′W) (**Figure 3.1**),

on the estuary of Rhode River (http://www.serc.si.edu/). The area is generally composed of two forest types: upland forests of “tulip poplar,” a common upland forest type in the mid-Atlantic coastal plain and piedmont (Brush, Lenk, & Smith, 1980), and floodplain forests of “river birch-sycamore.” SERC has several mixed-species deciduous forest plots at different successional stages. Agriculture or logging was practiced in the past with few areas that do not have any record of historical disturbance (Filley et al., 2008) but the SERC forests, for at least the last 120 years have been relatively undisturbed (Duncanson et al., 2014) .

The chronosequence forest plots referred in this study are mixed hardwood types consisting of tulip poplar forest associations (Parker, O’Neill, & Higman, 1989; Pukkala et al., 1991; Brown & Parker, 1994; Parker and Russ, 2004). The forest plots are young (31 years old), intermediate (56 years old), and mature (116 years old) with distinct canopy characteristics. Successional age is defined as the number of years since a forest was cut or abandoned after agricultural use, SERC uses aerial photographs and reviews the environmental history of local land use to determine the successional age of these forest plots (Brown & Parker, 1994).

Tulip poplar, beech, sweetgum, and red maple species are the most common in the young plot; in mature forests, the main species are oaks, hickories, beech with a variety of mid- and sub-canopy species, and the old forests are primarily tulip poplar, beech, and several oak and hickory species (Brown & Parker, 1994; Filley et al., 2008).

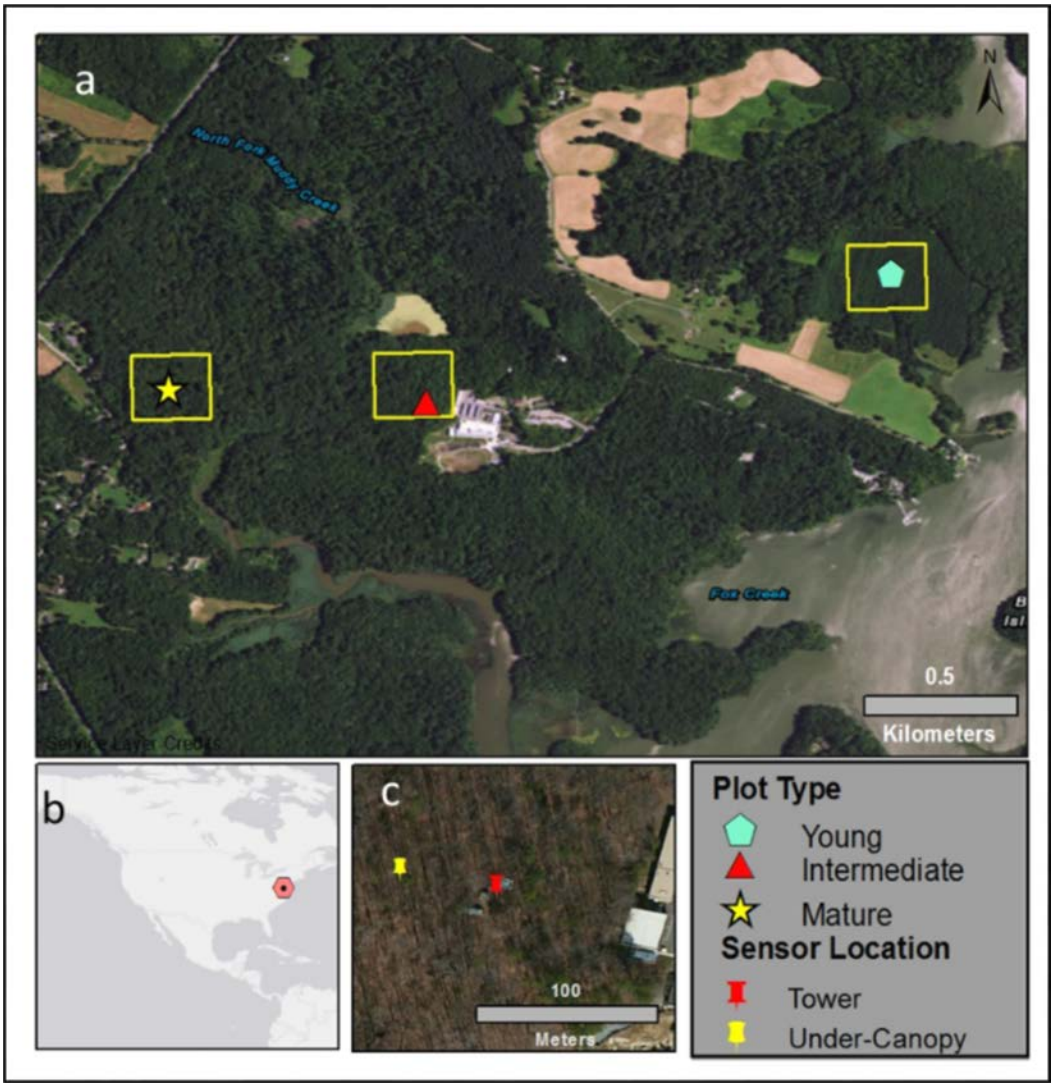

Figure 3.1 Map shows chronosequence sites at Smithsonian Environmental Research Center (SERC), Maryland. These vegetation chronosequences represent young, intermediate, and mature growth forest plots. The rectangular boxes represent the plot size 200 × 200 m used for the analysis. (c) The inset maps shows the location of the two pyranometer sensors, the first one located on an experimental tower and the second one is located under forest canopy.

3.2.2 LiDAR data and acquisition

The LiDAR data used for this study were acquired by the G-LiHT airborne scanning LiDAR (VQ-480, Riegl Laser) system on October 5, 2011, with an average point density of 50 m^2 during leaf-on and clear sky conditions. G-LIHT LiDAR data products are distributed as classified point cloud data and digital terrain and CHM together with other forest matrixes (Cook et al., 2013) available through G-LIHT webpage (http://gliht.gsfc.nasa.gov/ext/maps/index.html).

3.2.3 Pyranometer data

The solar radiation data were measured using Eppley model PSP precision spectral pyranometers at two sites in the Smithsonian Environmental Research Center (SERC) (**Figure 3.1**): (a) Meteorological tower site and (b) under canopy. The tower is 36.5 m, located at 38.89 N 76.56 W (NAD27); in the intermediate plot adjacent to the Mathias Laboratory and provides a stable platform and open sky view (https://serc.si.edu/). The under-canopy data were collected around 150 m west of the tower site in the same forest plot.

The Eppley model pyranometer measures radiation from 285 to 2,800 nm. It is a thermopile-type instrument that produces an electrical signal directly proportional to the solar radiation reaching the sensor. The instrument at SERC is connected to a data logger by weather proof copper wires. The data reported at the 1-min interval are the average of six readings each 10 s apart (https://serc.si.edu/).

Data from the tower site acquired on 5th October and coinciding with the date of LiDAR data acquisition were used as model input. Data from the under-canopy pyranometer were used for validation of the model.

3.2.4 Vegetation structure data for chronosequence plots

LiDAR returns within the canopy have been used for estimation of vegetation structure and composition (Hopkinson et al., 2006; Morsdorf et al., 2006; Hopkinson & Chasmer, 2007). We used a LiDAR-derived CHM, fractional vegetation cover, and rugosity as the measure of vegetation structure, and the R software package to analyze these vegetation metrics. We derived CHM by subtracting the surface elevation from the terrain model derived from classified LiDAR point cloud. The process involved filtering of spurious point clouds before grounds points were interpolated as terrain and the non-ground points as the surface model (Lim et al., 2003). Fractional vegetation cover is an important indicator reflecting the extent of horizontal coverage of vegetation. Fractional vegetation cover is calculated from LiDAR returns by dividing the number of returns above a standard height by the total number of returns within a specific radius (Korhonen et al., 2011). Rugosity, a measure of surface roughness, is the SD of canopy height (Parker & Russ, 2004). Increase in a forest's rugosity, in general, is related with increasing age and is correlated with various forest functions (Parker & Russ, 2004). These simple metrics were used to distinguish the vegetation structure of the three eastern mixed species deciduous plots at

chronosequence and the impact of age on the influx of direct beam radiation in the under canopy of these plots.

3.2.5 Estimating solar radiation on the forest floor

Solar radiation on the forest floor was estimated using a reverse ray-tracing model based on Mussleman (2013). In this model, a reverse ray tracing method is used i.e. the ray traced from the ground towards the sun to identify the LiDARs which fall along the ray direction (Groot, 2004; Musselman et al., 2013). Ray-tracing models can help precisely characterize the canopy light environment as a function of height within forest environment. Data from the pyranometer based on the meteorological tower was used as model input.

The procedure for estimation of the under-canopy direct beam radiation as adapted from Mussleman (2013) involved the following steps:

1. Voxel transformation of the point intermediate clouds at a grid resolution (1 × 1 × 1 m). Rays were traced from each grid cell on the ground towards the sun.

2. Rays were traced from each grid cell on the ground towards the sun (reverse). Solar angle was obtained from the Python routine “solarpy,” which given time, location, and time zone provided the solar altitude and azimuth.

3. The intersection of the ray with the voxels identifies the path of solar ray. LiDAR points for all those voxels were included to extract the total number of LiDAR points. Transmittance is proportional to the radiation of canopy versus total LiDAR point intermediates.

4. The process was repeated for multiple time step.

This ray-tracing model was then validated against the under-canopy pyranometer data as described in the next section.

3.2.6 Solar radiation model validation

The LiDAR solar radiation model estimates were evaluated against measurement from the under-canopy pyranometer located in the intermediate plot. We used uncertainty metrics based on average differences between the ray-tracing model and the under-canopy pyranometer data quantified by mean bias error (MBE), mean absolute error (MAE), and root-mean-squared error (RMSE). The RMSE error was split into systematic (RMSEs) and non-systematic (RMSEu) errors (Willmott, 1982).

3.2.7 Comparison of solar radiation data for different vegetation structure

Forest solar radiation estimated using the ray-tracing model was compared across the forest plots at young, intermediate, and old stages of growth. The forest structure for these plots was derived using LiDAR point cloud as described in *Section 2.4*. Diurnal variability in light transmission mainly results from variations in the altitudinal and azimuthal position of the sun. During the selected day, the direct beam radiation reaching the forest floor was estimated for three scenarios—hourly, noon, and total. Hourly direct beam solar radiation indicates the diurnal variation of radiation (in relation with solar angle), whereas beam radiation at noon is helpful in identifying peak radiation when the sun is at its

highest angle. Daily total direct beam radiation gives an estimate of the total energy accumulated over the day for a particular site, and unlike in hourly data, there was no variability.

The total daily solar radiation for these three plot types were compared using the Kruskal–Wallis (KW) rank sum test (Kruskal & Wallis, 1952). The KW, a nonparametric statistical test, was used to assess the differences in radiation values among the three plots. The null hypothesis is that the radiation values in all the three forest plots have the same average (median). The alternative hypothesis is that at least one forest plot is a distribution with a different average (median).

While KW was used to test the differences between the plots, it did not provide any specific *post hoc* pairwise comparisons between the plots. The Dunn test uses a Bonferroni-adjusted multiple *t*-tests to analyze the differences between the pre-treatment and post-treatment means within each treatment group (Dunn, 1964; Howell, 2012).It involves summing up jointly ranked data. These two tests were performed using the statistical software R using DescTools package.

3.2.8 Vegetation structure and solar radiation

The Random Forest (RF) method was used to understand the correlation between the structural parameters of vegetation and solar radiation. It is an useful nonparametric data mining method that can deal with both non-linear and multiplicative interactions. It was developed as an extension of classification tree and regression tree (CART) to improve the model prediction. A RF is a collection

of a large number of CART that uses two levels of randomization for creating each classification and regression tree (Breiman, 2001). In the RF model, a random subset of the original data is used to construct each CART using a bootstrap sample with spare or a random sample. Out-of-bag data (oob), which refers to the portion of data not used to create the tree, are used to assess the model's predictability. Therefore, in RF, each tree offers an algorithm for data classification, and an estimate of predictive capability.

Additionally, at each split within each tree, a random subset of the available predictor variables is used to partition the data set into two groups with minimal heterogeneity until homogeneity of the data in each terminal node is maximum and cannot be increased by subdivision. Because of these two processes, the RF model prediction is better than the CART model, and there is no overfitting (Breiman, 2001).

Besides the predictive capability, RF can also be used to estimate the significance of variables. This is done by determining the mean decrease in prediction accuracy before and after permuting a variable. RF has been used widely in remote sensing science (Belgiu & Drăguţ, 2016) and in forest ecology (Cutler et al., 2007; Grossmann, Ohmann, Kagan, May, & Gregory, 2010) to identify the variable importance. The two most important measures of variable importance used in the study were the mean decrease in accuracy, and the mean decrease in node impurity. The first measure, the mean decrease in accuracy, is calculated from permuting the data. After permuting each predictor variable, the

prediction error and the mean standard error (MSE) on the (oob) portion of the data are recorded for each tree. The difference between the prediction error and MSE is then averaged and normalized by the SD of the differences over all trees. This average is the second measure of variable importance stands for the total decrease in node impurities from splitting on the variable (Liaw & Wiener, 2002). Apart from the vegetation structure matrix derived from LiDAR, we included age as a categorical variable to see if the stand type affects the variable importance of the model. The RF variable importance analysis was done in the R package RF (Liaw & Wiener, 2002; https://cran.r-roject.org).

3.3 Results

3.3.1 Vegetation structure from LiDAR data

The chronosequence plots showed distinct variation in their vegetation structure corresponding to developmental trends. The young stand was the shortest with a mean CHM of 11.34 m, followed by the intermediate (29.31 m) and the mature plot (30.34 m). Under ideal growing conditions, old-growth tulip poplar trees may be nearly 61 m high, but more often they are from 30.5 to 45.7 m at maturity (www.na.fs.fed.us). The maximum CHM of the young plot was 29.15 m, the intermediate plot was 42.99 m, and the mature plot was 44.1 m (**Figure 3.2**). Height variation in terms of SD was about 2 m for the young plot and 6 m for both the intermediate and mature plots. Canopy rugosity followed a similar pattern with 1.48 m (young plot), to 3.89 m (intermediate), to 3.71 m (mature).

The mean value of rugosity for the young plot was 1.5 m, 3.9 m for the intermediate, and 3.7 m for the mature plot. However, the mean fractional vegetation cover varied by only 3% amongst the plots with the young plot having least at 96% and the mature plot having 99%.

The median CHM for the young forest plot was less than half of the median CHM for the mature forest plot with a much less interquartile range (**Figure 3.2**). The median rugosity and interquartile range for the young forest plot were the least and highest for the intermediate plot (**Figure 3.2**).

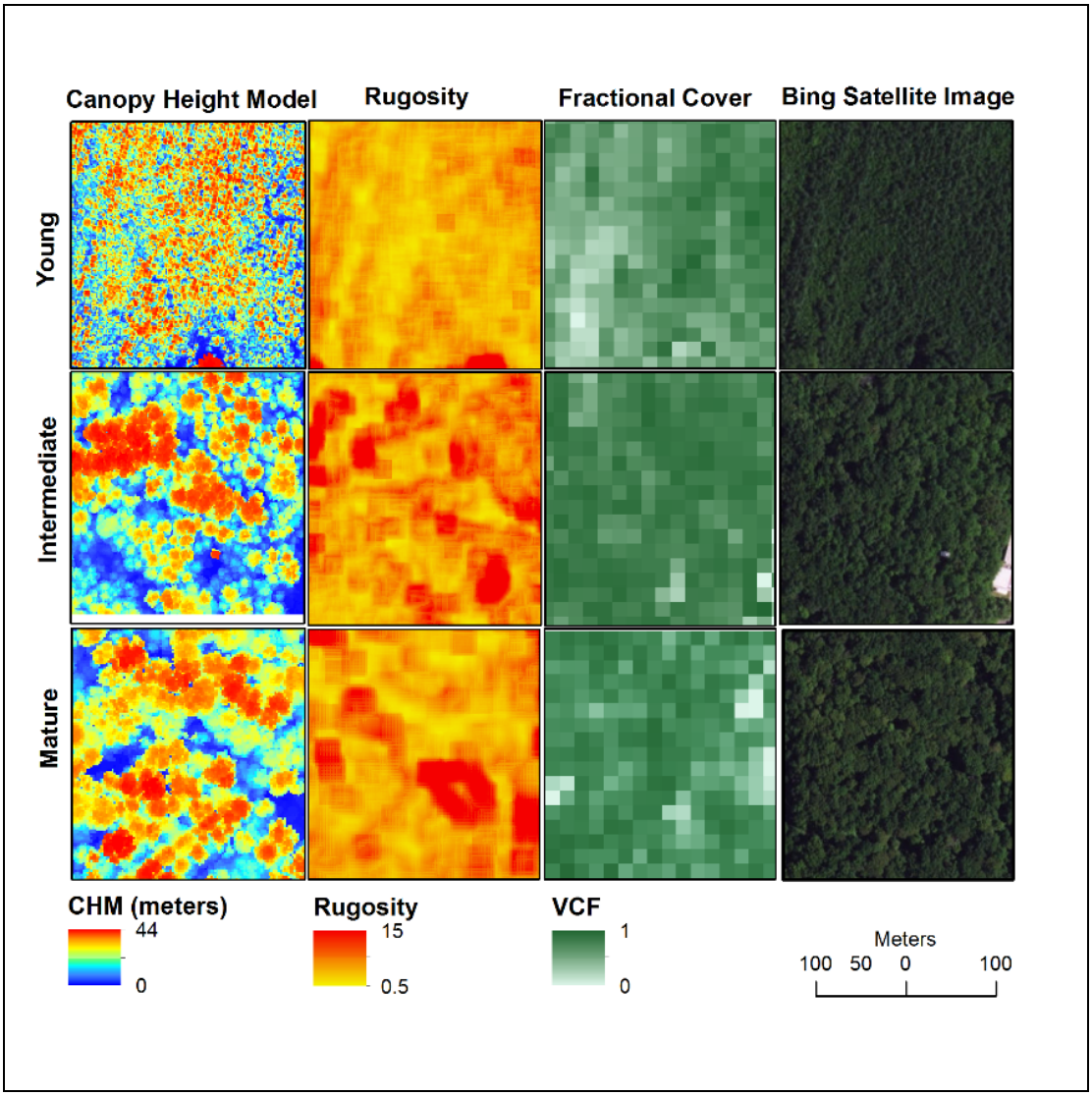

Figure 3.2 Spatial representation of canopy height model, rugosity, and vegetation fractional cover derived from LiDAR measurements in the three sites. The mature and intermediate forest plots have higher canopy height and fractional vegetation cover compared to the young plot. The canopy height and rugosity are more evenly distributed in the young plot. The rightmost panel shows satellite (RGB) images for all the sites. Each plot is 200 × 200 m in size.

3.3.2 Solar radiation on the forest floor

The hourly mean under-canopy radiation in the young plot differed significantly from the intermediate and mature plots. It had a Gaussian diurnal pattern with high canopy penetration at noon and low at dawn and dusk. In comparison, the intermediate and mature plots had significantly lower radiation penetration and did not follow a pure Gaussian pattern (**Figure 3.3**). Amongst the three plots, mean under-canopy radiation was lowest in the mature plot. All forest plots showed highest radiation peak at solar noon (**Figure 3.3**). Daily total under-canopy direct beam radiation showed a similar pattern (**Figure 3.4**). The median total daily beam radiation was 1.17 kWh/m^2 for the young plot, 0.27 kWh/m^2 for the intermediate plot, and 0.16 kWh/m^2 for the mature plot (**Figure 3.4**). The floor of the young forest plot received the highest mean total direct beam radiation (1.2 kWh/m^2), followed by the intermediate (0.35 kWh/m^2) and mature (0.21 kWh/m^2) plots. The variability also showed a similar pattern, with a SD of 0.38 kWh/m^2 for the young, 0.30 kWh/m^2 for the intermediate, 0.17 kWh/m^2 for the mature plot.

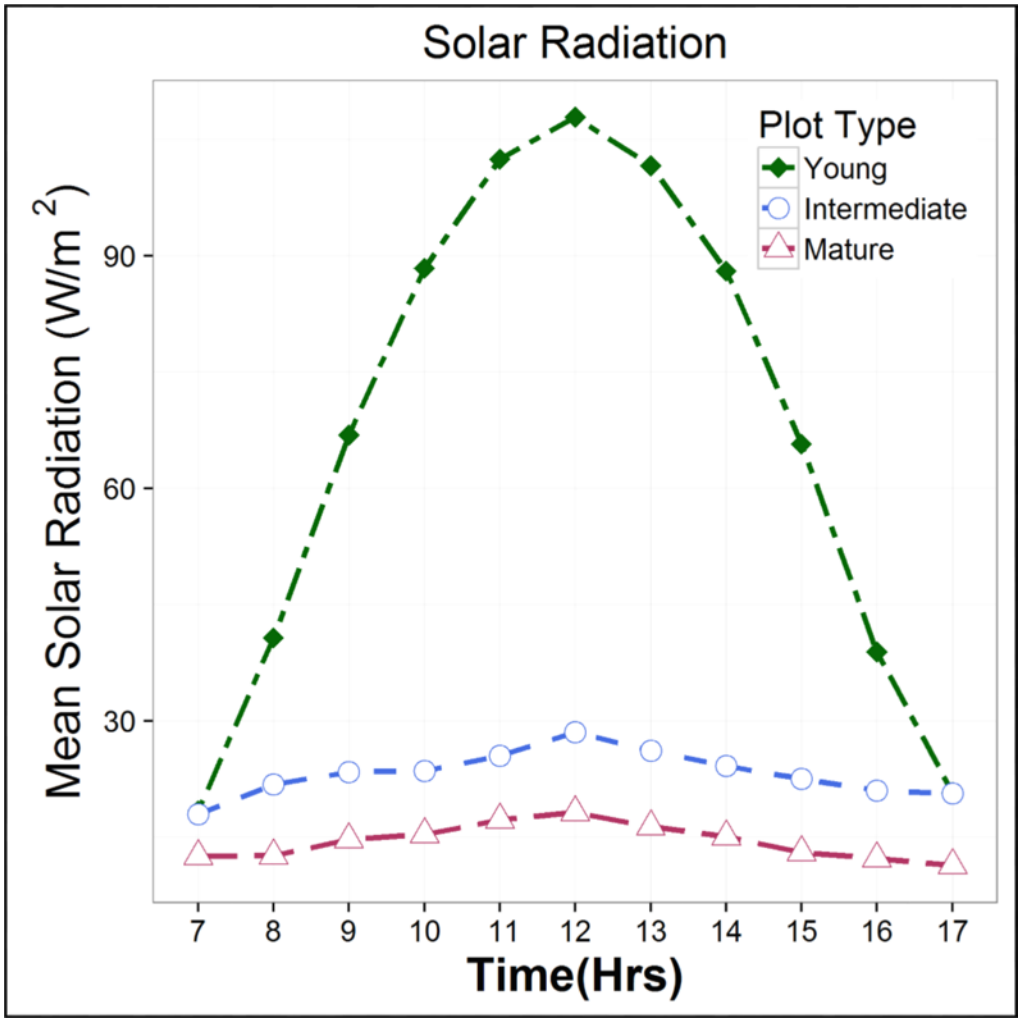

Figure 3.3 Hourly mean solar radiation flux for the three forest plots on October 5, 2011 shows differences in hourly mean solar beam radiation among young, intermediate, and mature forest plots. Mean solar radiation is comparatively higher for the young plot (1.17 kWh/m^2) when compared with the intermediate (0.27 kWh/m^2) and mature plots (0.16 kWh/m^2).

The Kruskal-Wallis rank sum test for the three forest plots showed that the median daily radiation values differed significantly (p value < 0). The results of the *post hoc* Dunn's test showed that mean rank sum difference was highest

between the mature and young forest (–16,694.526; *p* value < 0) plots, followed by the intermediate and young (–12,268.768; *p* value < 0) plots (see Supplementary Table 5). These inferential tests showed a significant difference in the beam radiation estimates between the three forest plots.

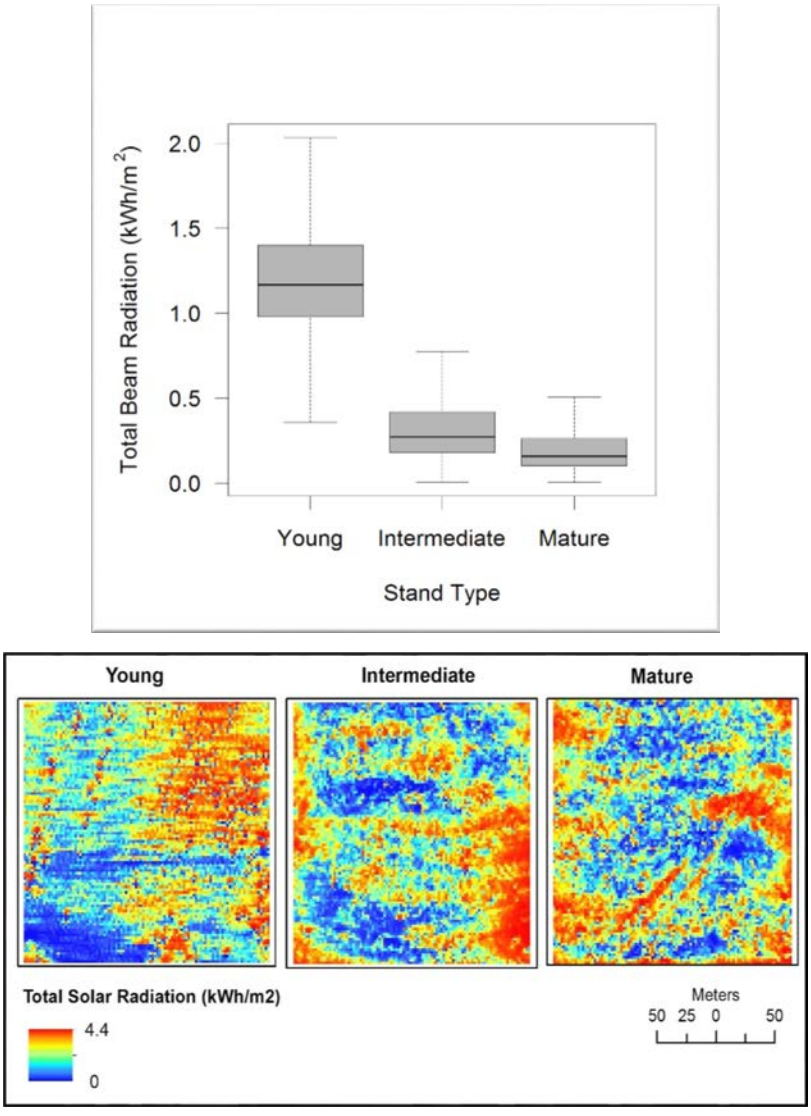

Figure 3.4 (Top) Box-plot of total daily beam radiation on October 5, 2011 differed significantly amongst different plot types. (Below) Total daily solar

radiation on October 5, 2011. Higher values are shown in darker shades of red; blue color represents lower radiation values.

3.3.3 Validation of under-canopy solar radiation model

The under-canopy solar radiation model was validated by comparing the model estimates to the *in situ* pyranometer measurements taken at the intermediate plot (**Figure 3.1**). The general pattern of diurnal variation in light transmittance was captured similarly by both the radiation model and the pyranometer. Canopy penetration peaked around 9 a.m. and 2 p.m., and was low at dawn and dusk. RMSE between the two was 13.94 W/m^2 with a MAE of 8.59 W/m^2 and a MBE of 5.40 W/m^2 (**Figure 3.5**) on October 5, 2011. The RMSE was equally partitioned between systematic (inaccuracy) and unsystematic (imprecision) components, with RMSEs of 9.19 W/m^2 and RMSEu equaling 10.48 W/m^2. The overall linear relationship between LiDAR estimates and pyranometers measurements was $R^2 = 0.5$.

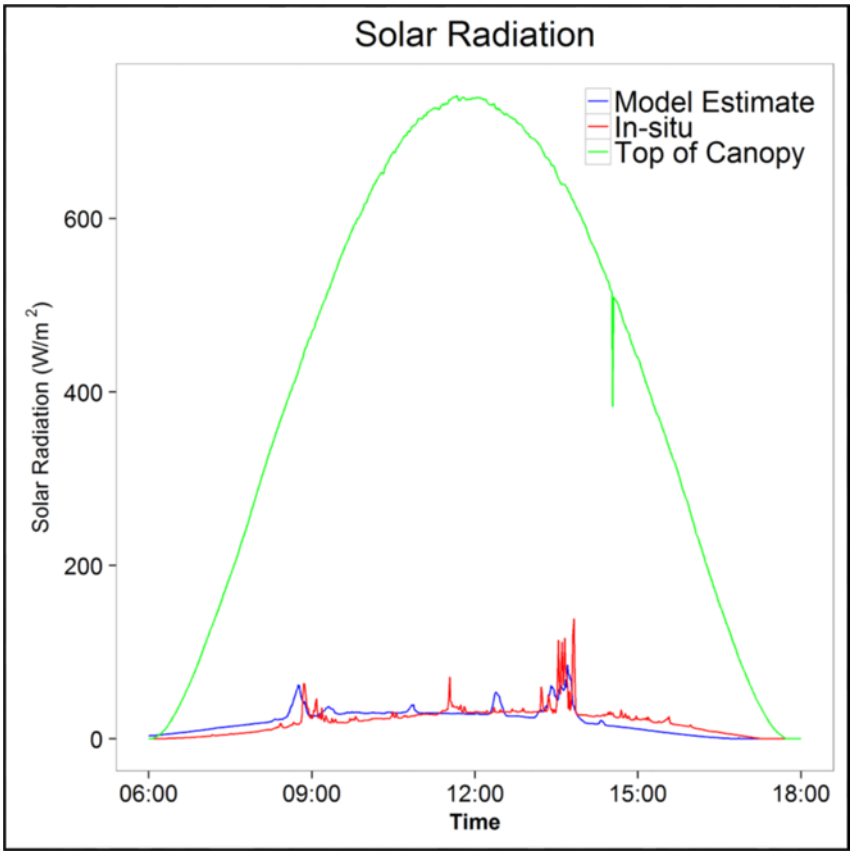

Figure 3.5 Ray-tracing model versus pyranometer data modeled at minute interval on October 5, 2011, coinciding with the date of LiDAR data acquisition. The green line shows top of the canopy solar radiation; blue line shows model estimate and *in situ* pyranometer data are shown in red color. There is a fair agreement between the radiation model and the pyranometer. Both the estimates show that canopy penetration peaked around 9 a.m. and 2 p.m., and was low at dawn and dusk. Notably there is a minor lag between the model-estimated and pyranometer values, improving which could lead to a better agreement between the two (R^2 = 0.5, MBE = 5.40 W/m^2).

3.3.4 Vegetation structure and solar radiation

Before running the RF model, it was made sure that the independent variables are not highly correlated. The results from the RF analysis showed that CHM was the most important variable and led to a 51.4% increase in MSE, and increase in nodal purity by 122, followed by the fractional cover which accounted for a 28% increase in MSE. In the alternate model, where we considered the plot age, our findings suggest that the age of the forest plot was the most significant variable accounting for a 39% increase in MSE, and an increase of 97 in nodal purity.

3.4 Discussion

In this chapter, we estimated and inter-compared under-canopy beam radiation across three deciduous forest plots—young (31 years old), intermediate (56 years old), and mature (116 years old) at SERC. We first characterized the three-dimensional vegetation structure from LiDAR data and then estimated the under-canopy beam radiation using a custom ray-tracing model. We validated the model estimates using *in situ* measurements from above- and under-canopy pyranometers located at the intermediate forest plot. We finally compared the estimates of under-canopy direct beam radiation across the three plots.

Earlier studies have established high correlation between field and LiDAR metrics and have supported the use of LiDAR measurements in different forest types such as deciduous and coniferous, to directly derive an understanding of

structural complexity and deduce age-related successional stage (Harding, Lefsky, Parker, & Blair, 2001; Parker & Russ, 2004; Lefsky, Hudak, Cohen, & Acker, 2005; Kane et al., 2010). As expected, the three plots exhibited variations in their vegetation structure through the mean CHM, rugosity, and fractional cover values. The young stand had the shortest (mean CHM of 11.34 m), whereas the mature plot had the highest (30.34 m). Canopy rugosity followed a similar pattern with 1.48 m (young plot), to 3.89 m (intermediate), and to 3.71 m (mature). However, the mean fractional vegetation cover varied by only 3% amongst the plots with the young plot having least at 96% and the mature plot having 99%.

The under-canopy radiation regimes between the young, and the intermediate and the mature forest plots (**Figure 3.3**) showed significant differences in values. Maximum radiation received at noon was around 107 W/m^2 for the young plot, 28 W/m^2 for intermediate plot, and 18 W/m^2 for mature plot, which is 14%, 4%, and 2.5 % of the top of the canopy radiation. Higher maximum transmittance in the young plot (14 %) suggests more gaps in the foliage. In deciduous forests, during the leaf-on season, only 1%–2% of incident light reaches the forest floor in comparison with 30%–40% in the leafless season (Parker, 1995, pp 88). Compared with the young plot, less direct beam radiation reached the forest floor in the intermediate (4%) and mature plots (2.5%). This was likely caused by the closed canopy of the intermediate and mature plots during the leaf-on season and a “bottom-heavy” structure. The forest plots at the SERC are primarily tulip poplar associations; for this forest type, the peak rates of

growth and mortality are reached by 30 years of age and their crown canopies are closed (Duncanson et al., 2014). We found that the mean rugosity value of the young plot (1.48) is almost half of the rugosity values of both the intermediate (3.89) and mature plots (3.71). A small rugosity value indicates that the canopy can be occupied with vegetation material at any level; however, high rugosity implies height restrictions at many spatial locations. After 50 years of growth, there is a likelihood of a distinct under-canopy growth that produces a bimodal foliage distribution (Parker et al., 1997). In later stages of succession, more shade-tolerant dominants develop and reach the mid-canopy, creating a ‘‘bottom-heavy’’ structure. The “bottom-heavy” structure and the appearance of canopy gaps of different ages produce a vegetation profile more vertically uniform in the old growth forest (Parker, 1997; Parker & Russ, 2004).

For assessing the validity of the LiDAR-based model estimates, validation data for all the three plots do not exist, we only could use pyranometer measurements from the intermediate plot coinciding with the date of LiDAR data acquisition. We found an overall close match between the LiDAR-derived model estimates of under-canopy direct beam radiation and the pyranometer measurements at the intermediate plot (R^2 = 0.5). Despite the differences between the two methods for estimating solar radiation, the validation results were positive. Both the radiation model and the pyranometer captured the general pattern of diurnal variation in light transmittance in a similar manner showing peak canopy penetration around 9 a.m. and 2 p.m., and low at dawn and dusk.

RMSE between the two was 13.94 W/m^2 with a Mean Absolute Error of 8.59 W/m^2 and a Mean Bias Error of 5.40 W/m^2 (**Figure 3.5**) on October 5, 2011. However, we observed some shift in radiation peaks, which may be have been caused by GPS location error due to attenuation of the GPS signal by the forest canopy.

The result from the RF analysis highlights two important points. First, when the categorical age is not considered, the CHM or the canopy height is the greatest determinant of solar radiation on the forest floor followed by canopy cover. However, when the chronosequence age is considered, canopy cover becomes the most significant determinant of solar radiation. This highlights the complexity of factors influencing the amount of solar radiation that moves through the canopy. Previous studies have suggested that neither canopy height, canopy and sub-canopy vegetation nor even age fully explains the light transmittance on the forest floor (Clark et al., 1996; Denslow & Guzman, 2000; Montgomery & Chazdon, 2001). A study in the old-growth forests of Costa Rica found that canopy and sub-canopy vegetation was a weak predictor of under-canopy light availability (Montgomery & Chazdon, 2001). Thus, it is important that we consider the complex interactions of canopy light with other vegetation structural parameters, species types, distribution of leaves, and leaf optical properties across multiple forest types (Küppers, 1989; Parker, 1995; Montgomery & Chazdon, 2001).

Our study focused only on the direct beam component of the under-canopy radiation, and the model estimates of under-canopy direct beam radiation closely matched the *in situ* pyranometer measurements. Validation results suggest, that at least in part, differences in under-canopy radiation are caused by the direct beam component, while diffuse radiation component has a rather uniform directional distribution (Pukkala et al., 1991). Hutchison and Matt (1977) observed that direct beam radiation had the greatest attenuation and largely controlled the variability of radiation in the horizontal, in a deciduous forest composed predominantly of tulip poplar forest. Pukkala et al. (1991) also supported the suitability of direct beam radiation for predicting the spatial distribution of light regime below simulated forest canopies at different latitudes. We have shown the use of a spatially explicit model for estimating the influx of direct beam radiation under the forest canopy at chronosequence using high-resolution LiDAR data. Our method demonstrates a means to study an under-canopy light environment in heterogeneous canopies characterized by high spatial variability.

3.5 Conclusion

Comparison of estimated under-canopy beam radiation across the deciduous forest plots suggests that age and structure of forest cause significant changes to the under-canopy beam radiation regime. The under-canopy radiation varied significantly between the chronosequence plots (p value < 0) explained by the differences in three-dimensional vegetation structure characterized by CHM,

fractional cover, and rugosity measures. We also demonstrated how LiDAR data in conjunction with a spatially explicit radiative transfer model could be utilized to capture this variation directly for large heterogeneous areas. Our study primarily focused on direct beam radiation for a horizontal surface. Future work could look at the spatiotemporal variation of diffused and PAR components, and transmittance along the vertical gradient. . Direct beam transmittance can also be estimated during different seasons to understand the impact of seasonal variability on the interaction of light and three-dimensional vegetation structure. More canopy structural measurements such as biomass and LAI in each plot can be included to understand the complexity of the canopy structure and its relationship with light transmittance.

In the next chapter, we look at transmittance along the vertical gradient and the PAR components for a better understanding of canopy light environments.

Chapter 4 Comparing Vertical Light Transmittance and Vertical Forest Structure in Forest Succession

4.1 Introduction

Canopy and canopy structure is key to forest function. The knowledge of light transmittance in canopies is crucial for understanding forest function because the radiation–vegetation interactions above, within, and below the forest canopy play a determining role in energy balance, leaf and soil temperature, evapotranspiration, stand microclimate and growth potential (Field & Mooney, 1986; Gutschick, 1991; Parker, 1995) and other important biophysical and ecological processes. The movement of light in a plant canopy is influenced by many factors, including solar position, distribution of light, biomass distribution, canopy structure and elements, and their optical properties (e.g., reflectance and transmittance).

Under-canopy radiation regime determines a range of ecological and biological processes and components in forest ecosystems, such as species diversity, species distribution, community structure, and succession processes (McArthur, 1964; Martens et al., 2000; Svenning, 2002; Frelich et al., 2003; von Arx et al., 2012). Under-canopy light environment also influences growth and competition, net primary production, and vegetation types (Sakai & Akiyama, 2005; von Arx et al., 2012). Understanding under-canopy radiation profiles and influencing below-canopy light levels is often essential to maintain agroforestry

systems or commercial plantations or for forest conservation purposes (Jennings et al., 1999; Bellow & Nair, 2003; Frelich et al., 2003). Radiation regimes within canopies are important for understanding the under-canopy microenvironment as well as processes such as photosynthesis, transpiration, and carbon sequestration. For instance, careful parameterization of the radiation regime in the ecosystem—quantifying the exchange of water vapor, gases, and heat between the biosphere and atmosphere—is essential. Canopy structure affects the radiative and convective exchanges within vegetation canopies and primarily determines the proportion of incident PAR absorbed within a canopy (Russell et al., 1989). Factors that influence the intercepted PAR also include age of vegetation, disturbances, and radiation climate (Kucharik et al., 1999). Studies that model vegetation and radiation interactions, water and heat regimes, and vegetation productivity also require adequate definition of canopy architecture and canopy radiation regime therefore becomes important for modelling both vegetation growth and functions (van Leeuwen et al., 2013).

The concept of canopy has several meanings. Carroll (1980) described the canopy as a region as well as collection of objects, whereas other definitions offer a much restricted meaning of referring to only the uppermost layers of the forest. Parker (1995) suggests height, species, leaves, branches, and position, size, and orientation of each canopy element all constitute the canopy. Researchers use simple descriptors of canopy structure such as height and cover of the canopy surface as well as more detailed metrics such as foliage-height profiles and light

gaps (Watt 1947; MacArthur & Horn, 1969; Aber, 1979; Canham et al., 1990; Spies, Franklin, & Klopsch, 1990). Empirical studies suggest that the structural parameters of forest canopies provide a better explanation of the variation in light transmittance (Küppers, 1989; Brown & Parker, 1994).

Techniques for modeling canopy architecture fall into three broad categories: direct measurement methods, allometric methods, and indirect measurement methods. LiDAR is an indirect method increasingly used to model radiation vegetation interactions because small footprint LiDAR has become more accessible for use in vegetation studies.

A complete description of the canopy at all scales of organization of canopy elements remains a complex and impractical endeavor. It is challenging to estimate light conditions within a canopy because of accessibility issues and the influence of terrain and solar position. Researchers have undertaken the task by ground-based sampling from individual trees; aerial measurements from masts, towers, balloons, and cranes (Yoda 1974; Ellsworth & Reich, 1993; Vose, Sullivan, Clinton, & Bolstad, 1995; Parker et al., 1996); and digital and hemispherical (fisheye) canopy photography (Rich, 1990; Frazer et al., 2011). Increasingly models are used to simulate the movement of light through canopies using statistically derived matrices such as the LAI, leaf area density (LAD) as well as the spatial arrangement of canopy elements.

Monsi and Saeki (1953) were the first to use canopy gap probability to describe beam penetration. Gap fraction or probability is the standard parameter

for studying radiation extinction through vegetation canopies (Ross, 1981). It refers to the probability that a ray will pass through randomly distributed canopy element and hits a reference point, usually the ground level, or the quantity of the integrated value of the gap frequency over a given area or volume that can be estimated. Therefore, measuring gap fraction is equivalent to measuring transmittance at ground level, at wavelengths for which the assumption of black vegetative elements is valid (Weiss et al., 2004).

The vertical profile of the foliage is characterized by the LAD. LAD is defined as the leaf area per unit volume (m^2/m^3) and is one of the most important variables for scaling up many biophysical processes from the leaf to the ecosystem level (Jarvis & McNaughton, 1986). Measurement of LAD is challenging in large and complex forest types (Bréda, 2003). Conventional methods for measuring LAD include direct measurement using plumb line and tripod (MacArthur & Horn, 1969), destructive sampling, and optical point quadrats (Parker, 1989); all are cumbersome and not spatially explicit.

Studies have examined the relationship between light transmittance and forest age. Examining the observed values of PAR transmittance with stand age and measures of canopy structure, Parker and Brown (1994) found that light transmittance varied as the three-dimensional canopy structures changed with time, and that transmittance was not significantly correlated with simple measures of forest structure such as height, above ground biomass, and LAI.

LiDAR data have made it possible to derive three-dimensional structural information to improve the characterization of under-canopy light regimes. Previous research has shown the uses of LiDAR-derived three-dimensional canopy architecture, including estimating timber yield and forest volume (Naesset, 1997; Means et al., 1999), wildfire management (Morsdorf et al., 2004), characterizing and identifying habitat (Hofton et al. 2006), and estimating forest carbon stocks (Stephens, 2007; Saatchi et al., 2011).

The objective of this study was to estimate, inter-compare, and validate vertical light transmittance, LAI, and LAD derived from LiDAR across forest plots at different successional stages of growth and at a plot with disturbance (logging).

4.2 Methods

Comparison of light transmittance across the forest plots at different successional stages of growth, and one with disturbance (logging) was a three-step process. The first involved derivation of vertical gap transmittance as a function of height from LiDAR. The second involved characterization of vegetation structure by deriving vertical foliage profile based on vertical gap as a function of height. The third, the validation step, involved evaluating LiDAR-derived vertical gap transmittance against measurement from the PAR sensor data across three plots where data was available.

4.2.1 Study area

The study area is located within the Smithsonian Environmental Research Center (SERC), Edgewater, Maryland, USA (38°53′N, 76°33′W) (**Figure 4.1**), on the Rhode River estuary (http: //www.serc.si.edu/). The area is generally composed of two forest types: upland forests of "tulip poplar," a common upland forest type in the mid-Atlantic coastal plain and piedmont (Brush et al., 1980), and floodplain forests of "river birch-sycamore." SERC has several mixed-species deciduous forest plots at various successional stages. Agriculture or logging was practiced in the past with few areas that have no record of ever being cleared (Filley et al., 2008) but the SERC forests, for at least the last 120 years have been relatively undisturbed (Duncanson et al., 2014) .

The five plots used in this study are old (200+ years), mature (116 years), intermediate (56 years), young (31 years old), and logged, consisting primarily of tulip poplar forest associations (Parker et al., 1989; Pukkala et al., 1991; Brown & Parker, 1994; Parker & Russ, 2004). Successional age, defined as the number of years since a forest was cutover or abandoned following agriculture—was determined at SERC using aerial photographs and by consulting environmental history of local land use (Brown & Parker, 1994).

The young forests are dominated by tulip poplar, red maple, sweetgum, and beech; in the mature stages, the forest plot consists composed of oaks, hickories, beech with a diverse mid- and sub-canopy species; and the old forests

are mostly populated by tulip poplar, beech, and several oak and hickory species (Brown & Parker, 1994; Filley et al., 2008).

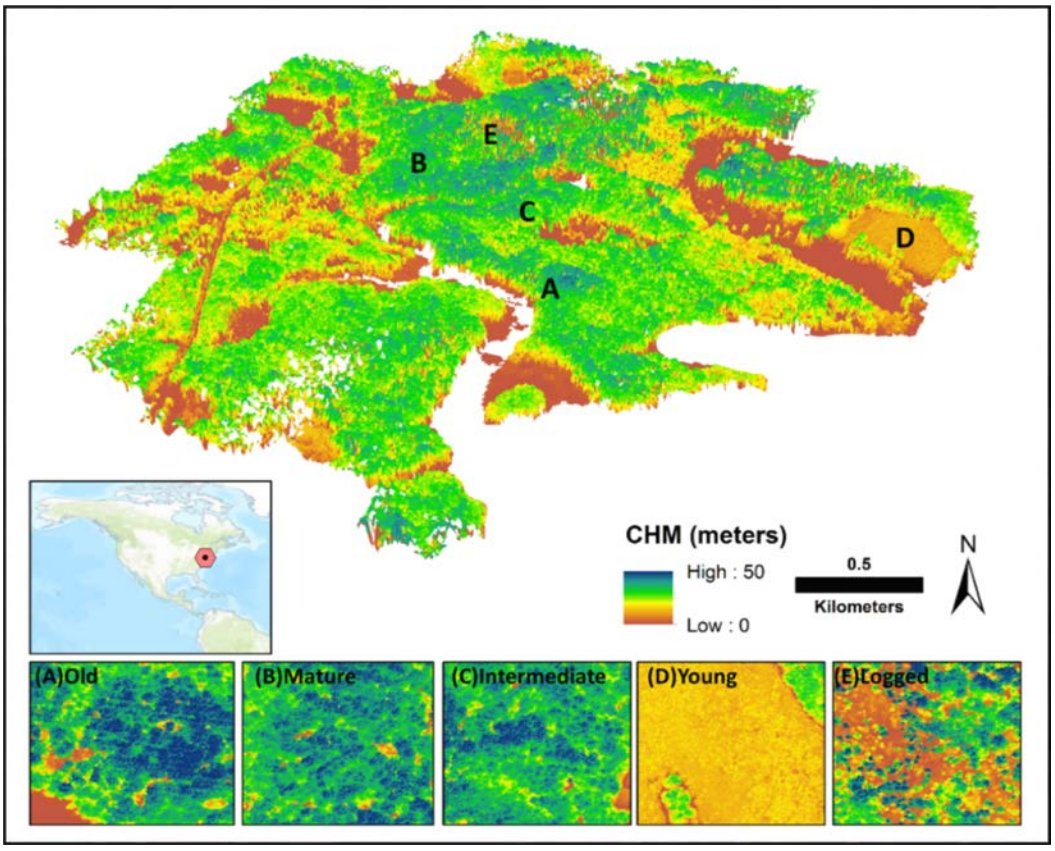

Figure 4.1 Map shows CHM for the chronosequence sites at Smithsonian Environmental Research Center (SERC), Maryland. These vegetation chronosequence represents old, mature, intermediate, young, and logged forest plots. The rectangular boxes represent the plot size 200 × 200 m used for the analysis.

4.2.2 LiDAR data and field data acquisition

The LiDAR data used for this study were acquired by the G-LiHT airborne laser scanner on October 5, 2011 and downloaded from the G-LIHT interactive webpage (http://gliht.gsfc.nasa.gov/ext/maps/index.html). The data products were available in a classified point cloud format with digital terrain (**Figure 4.2)** CHM, and other forest matrixes (Cook et al., 2013).

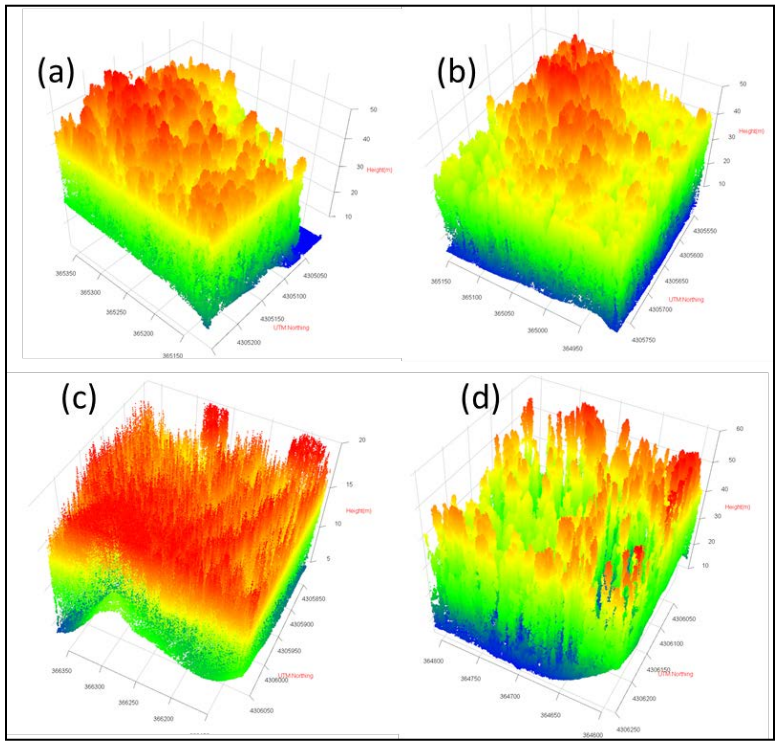

Figure 4.2 Subsets of the classified LiDAR point clouds (a) old plot, (b) intermediate, (c) young, and (d) logged representing different stages of forest growth. Data points, which were sampled with the intensity of approximately 50 points/m^2, are classified by height into two classes—vegetation and ground.

In situ PAR data acquisition

In all the chronosequence sites, vertical measurement of quantum flux were taken using a LiCor quantum sensor (LI 190; Li-Cor, Lincoln, NE) at several uniformly sampled points. The sensor records the light energy in the PAR of 400–700 nm. The sensor was mounted on a vertical pole and data were collected at a uniform height interval. Each measurement was cosine-corrected to take sun angle into account.

4.2.3 Derivation of canopy structure from LiDAR point cloud

Surface and tree structure characteristics were derived from LiDAR data by converting the point cloud into a DSM and a DEM at a grid resolution of 1 m. The DSM, which may include trees, buildings, and other such features, was created using the first return. The DEM, which represents the bare earth or ground surface, was created using the last return of the point cloud. The availability of ground and non-ground classification of the point cloud and the lack of any built features within the national forest made this task simple. The CHM was derived by subtracting the DEM from DSM. We also classified the surface with and without trees based on the CHM. A 0.2 m height threshold was used to generate a tree/no-tree mask to accommodate minor surface model errors.

4.2.4 Estimating vertical transmittance in the forest plots

Numerous studies have demonstrated success in retrieval of gap fraction using LiDAR, both ground and aerial (Ni-Meister et al., 2001; Chasmer & Hopkinson, 2007; Zhao et al., 2011). In recent years, researchers have used both discrete return and waveform LiDAR data to derive canopy gap (Ni-Meister et al., 2001; Morsdorf, et al., 2006; Essery et al., 2008; Hopkinson & Chasmer, 2009). A number of studies have studied the utility of LiDAR for estimating gap fraction (e.g., Parker et al., 2001; Todd et al., 2003; Morsdorf et al., 2006; Thomas et al., 2006; Hopkinson & Chasmer, 2007). Essery et al. (2008) modified Nilson's (1971) equation to calculate gap probability. Canopy gap, *p*, and LAI from LiDAR data are often derived assuming that gap fraction is corresponds to canopy transmittance. For this study, *p* was estimated as the ratio of the sum of all ground return intensities divided by the sum of all return intensities. The ground level was changed to height increments of 1 m to obtain the gap fraction at specific height intervals. The ground was assumed to be at 1 m above the LiDAR-detected ground to avoid any interference from vegetation on the forest floor.

4.2.5 Estimating of vertical foliage profile of the forest plots

Lefsky et al. (1999) pointed out that LiDAR has greater potential for deriving the foliage profile than other methods due to its ability to characterize canopy three-dimensional structure. Several studies have demonstrated LiDAR's utility for characterizing three-dimensional canopy structure for estimating under-canopy light conditions. For example, studies have used terrestrial LiDAR (Parker

& Russ, 2004), waveform LiDAR (Lefsky et al., 1999), and airborne discrete return LiDAR (Alexander, Moeslund, Bøcher, Arge, & Svenning, 2013), to characterize the vertical foliage profile. Tang et al. (2016) demonstrated the utility of spaceborne waveform LiDAR data to derive and validate the LAI and vertical foliage profiles product over the contiguous United States.

Following Nilson (1971), we considered probability that a beam will pass through the canopy without interception based on the following relationship between canopy gap (*p*) and LAD:

$$p_{t=} e^{-G(\theta)\sum \lambda l_t}$$

Here, *G* is the foliage area orientation function, λ is the effective foliage area volume density, and the summation includes all crown that the beam intersects. Assuming random orientations the $G = 0.5$. Using *p* values derived in the previous step (*Section 4.2.4*), we estimated the LAD.

To exclude the under-canopy vegetation, we considered the height at 1 m above the surface identified by the height of last return of LiDAR point. We derived LAI by cumulating the LAD values, as previous studies have done (Tang et al., 2012).

4.2.6 Comparison of foliage profile and vertical gap transmission

LiDAR-derived foliage profile and vertical gap transmittance were compared by plot type using two nonparametric inferential statistical tests to compare the foliage distribution and the vertical transmission in the forest plot. The first, the Kruskal–Wallis (1952) rank sum test (KW) assesses the differences among three or more independently sampled groups on a single, non-normally distributed continuous variable. The null hypothesis is that the transmittance values in all of the forest plots have the same median. The alternative hypothesis is that at least one forest plot type has a different average (median).

KW was useful only to identify the differences between the plots, but the Dunn (1964) test analyses differences between the pre-treatment(control) and post-treatment means within each treatment group using Bonferroni adjusted multiple *t*-tests (Howell, 2012). It involves summing up jointly ranked data. We used it for *post hoc* pair wise comparisons between the plots. KW and the Dunn test were performed using the statistical software R using the DescTools package.

Following Parker (2001), we used several matrices based on each plot's potential functional importance to characterize its transmittance profile. The height at which the transmittance value reaches 98% (h_{98}) was considered the top of the canopy "radiation-effective" height. This will avoid errors due to signal noise and to indicate that light has been level presumably intercepted. The bin-to-bin difference in mean transmittance was calculated to derive the vertical profile of the transmittance slope. Then we leveled this out using a moving window of

six vertical bins. Here lumicline refers to the maximum slope of the profile and lumicline height (H_{lum}) is its height in the canopy (following Parker, 1997). "H_{var}^{max}" is the height of the maximum variance in transmittance and the half-height (h_{50}) is the height where transmittance falls to half the outside value. The height where transmittance is at 25% (h_{25}) was also considered for characterization. T_{bulk}, the transmittance at the ground level, is generally considered at 0 m, but we considered it at 1 m to avoid interference from understory vegetation. The vertical foliage profile was compared across the forest plots using LiDAR-derived summary statistics of LAD. Inferential statistics were used to test if the vertical foliage profile varied significantly amongst successional stages of forest growth. Thereafter, the effective LAD was compared for each of the forest stand.

4.2.7 Validation of LiDAR-derived and field-based measurement of vertical transmittance

The estimates of the PAR transmittance collected from the quantum sensor were compared with the LiDAR-derived vertical transmittance across the three plots for which data were available. The uncertainty metric used here was based on average differences between the ray-tracing model and the under-canopy pyranometer data quantified by MBE, MAE, and RMSE. The RMSE error was further split into RMSEs and RMSEu errors (Willmott, 1982).

4.3 Results

4.3.1 Comparison of LiDAR-derived canopy height across plots

The cumulative distribution of the canopy height suggests that the forest plots exhibit distinctive forest structural characteristics. Parker and Russ (2004) suggest that calibrated hypsography can be used to characterize the developmental stage and the surface complexity of forest stands by illustrating outer canopy shape. The youngest plot showed the most uniform shape, with hundred percent of the canopy within 20 m and 50% of the trees within 10 m; the curve varied from intermediate to mature and to the old (**Figure 4.3**).

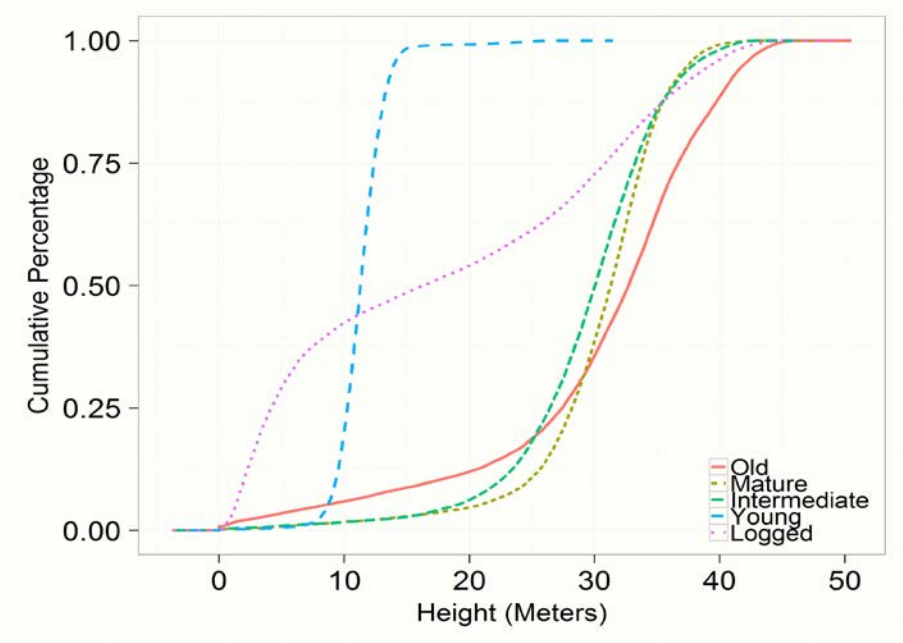

Figure 4.3 Comparison of canopy height hypsograph for the chronosequence forest plots (200 × 200 m) derived from airborne LiDAR. The forest plots are distinguished by individual color and line type. The old, mature, and intermediate plots show a concave curve, often associated with ageing plots, whereas the

young plot is characterized by a convex curve, which represents forest undergoing active growth.

The logged plot showed a unique curve, with more than half of the canopy height within 20 m. The tail end of the curve shows the percentage of canopy gap within the forest plot, which was maximum in the logged plot (**Figure 4.3**).The mean and maximum height, the slope of the curve, and the proportion of height close to the ground usually changes with age. The mean heights of the old (30 m), young (11 m), and logged plots (18 m) exhibited this trend. The logged plot had the largest canopy height deviation at 13 m, followed by the old growth plot at 9.4 m. The young plot had the smallest height deviation, at 2 m. The maximum height of the canopy was within the range of 42–46 m for the old, mature, intermediate, and logged plots, and 29 m for the young plot.

4.3.2 Comparison of vertical transmission for different vegetation structure

The vertical distribution of transmittance was asymmetrical in all the plots. The vertical distribution of canopy transmittance for different plots varied by the maximum height and successional stage of growth. For example, at 30 m, the old plot showed less transmittance compared with the younger and logged plots. Even though the average height for the old, mature, and intermediate plots were similar, we see a distinct pattern of transmittance at different height level, illustrated by the spatial distribution of transmittance (**Figure 4.5**). The frequency distribution of mean gap transmittance varied by plot age. The mean gap

transmittance differed significantly (p value < 0.001) across the forest plots. The *post hoc* Dunn's test revealed no significant difference ($p < 0.001$) in gap transmittance value between the old, mature, and intermediate plots. All the plots showed high transmittance in the upper part of their canopies and displayed a decreasing trend in transmittance closer to the ground (**Figure 4.4**).The skewness was negative in the upper part of canopy, but as canopy height decreased, the skewness became positive, indicating high transmittance in the upper part of the canopy and low transmittance closer to the forest floor (**Figure 4.4**). Each plot displayed distinct transmittance curves. The old, mature, and intermediate plots showed similar transmittance curves, whereas the transmittance curves of the young and the logged plots had steep slopes (**Figure 4.6**). The CV displayed an increasing trend with decreasing height (**Figure 4.4**). Overall, the old plot had the largest CV, followed by the intermediate and mature plots, which had very similar CV patterns across all heights. The logged and young plots displayed the least CV at all heights.

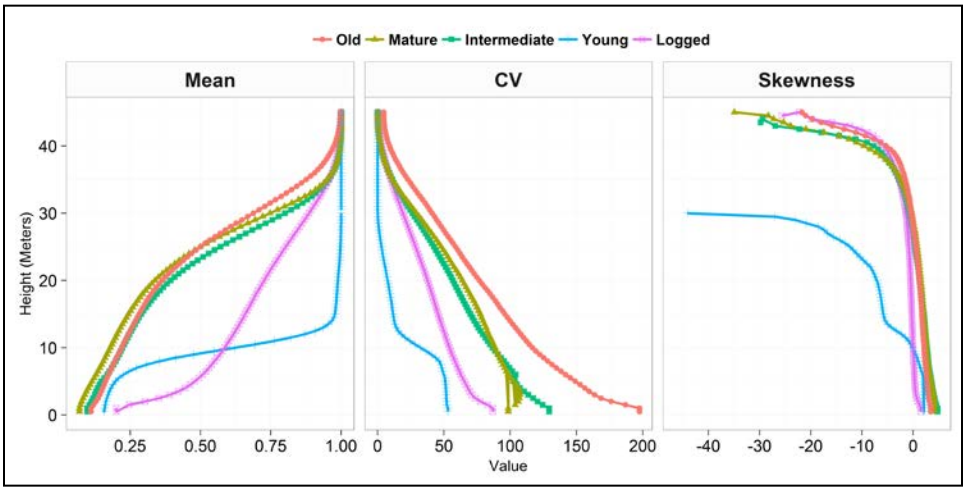

Figure 4.4 Comparison of vertical transmittance profiles of the five forest plots. The forest plots are distinguished by colored lines. The left panel present the mean, the center panel shows the coefficient of variation (CV), and the right panel shows skewness of vertical gap transmittance distribution as a function of height. All the plots show high transmittance in the upper part and a decreasing trend in transmittance closer to the ground. The coefficient of variation (CV) displays an increasing trend with decreasing height. The skewness is negative in the upper canopy, indicating high transmittance in the upper part of the canopy.

The maximum rate of change in transmittance values as a function of height (slope) was between 0.02 and 0.07 in all the plots (Table 4.1). The young and logged plot showed the maximum slope, whereas the old and intermediate plots showed the minimum. The height of maximum slope (H_{lum}) was between 29 and 31 m for the old, mature, and intermediate plots, 11 m for the young plot, and 3 m for the logged plot.

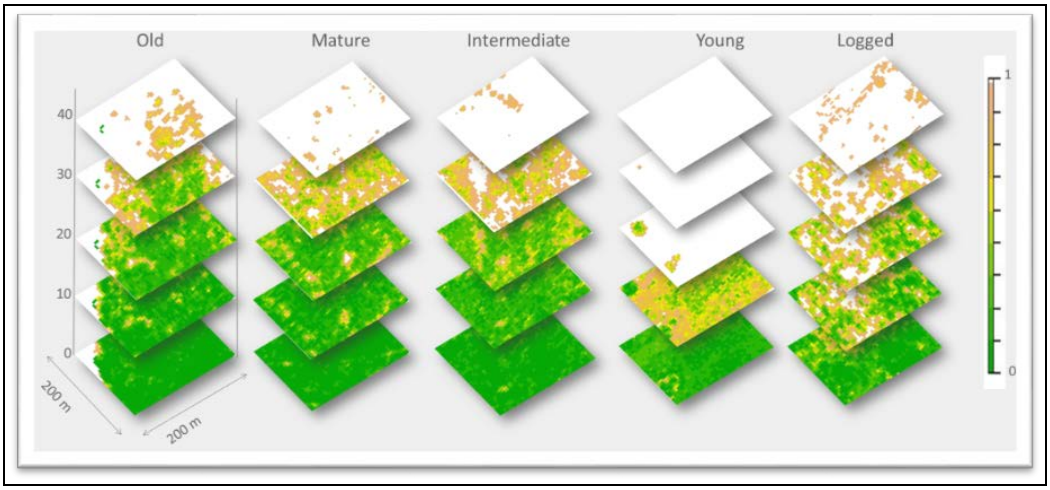

Figure 4.5 Three-dimensional transmittance for the chronosequence plots. Darker shades of green indicate low transmittance values, whereas the lighter shades of green and brown, and the white represent higher transmittance values. Transmittance values are stacked at vertical interval of 10 m. Histogram equalization was applied to all the stacked images to emphasize the shades.

The horizontal variation in gap transmittance for different heights showed that the height of the greatest variability ($H_{\text{var}}^{\max}$) for the old, mature, and intermediate plots was around 26 m, whereas it was at 10 m for the young plot and 7 m for the logged plot (Table 4.1). Heights of median transmittance, h_{50}, were within the range of 23–25 m for the old, mature, and intermediate plots; heights of median transmittance was 9 m for the young plot and 6 m for the logged plot. The radiation-effective height, at which the transmittance drops by 2% (h_{98}), was 41 m for the old plot, 37 m for both the mature and intermediate plots, and 38 m for the logged plot, whereas it was 15 m for the young plot. The h_{25} for the old, mature, and young plots was within the range of 12–15.5 m but

was almost half for the young (6.5 m) and logged (1.5 m) plots. T_{bulk}, the bulk canopy transmittances, differed across the plots. In the old plot, it was 11%, 10% in the intermediate plot, and only 7% in the mature plot. At 20%, T_{bulk} was maximum in the logged plot, followed by the young plot.

Table 4.1 Important Vertical Transmittance Characteristics Based on LiDAR-Derived Estimates

	Old	**Mature**	**Intermediate**	**Young**	**Logged**
Maximum slope	0.02	0.03	0.02	0.07	0.05
H_{lum} (m)	31.0	30.0	29.0	11.0	3.0
H_{var}^{max} (m)	26.0	26.0	25.5	10.0	7.0
h_{98} (m)	41.0	37.0	37.0	15.0	38.0
h_{50} (m)	25.0	25.0	23.0	9.0	6.0
h_{25} (m)	12.0	15.5	12.5	6.5	1.5
T_{bulk} @1 m (%)	0.11	0.07	0.10	0.16	0.20

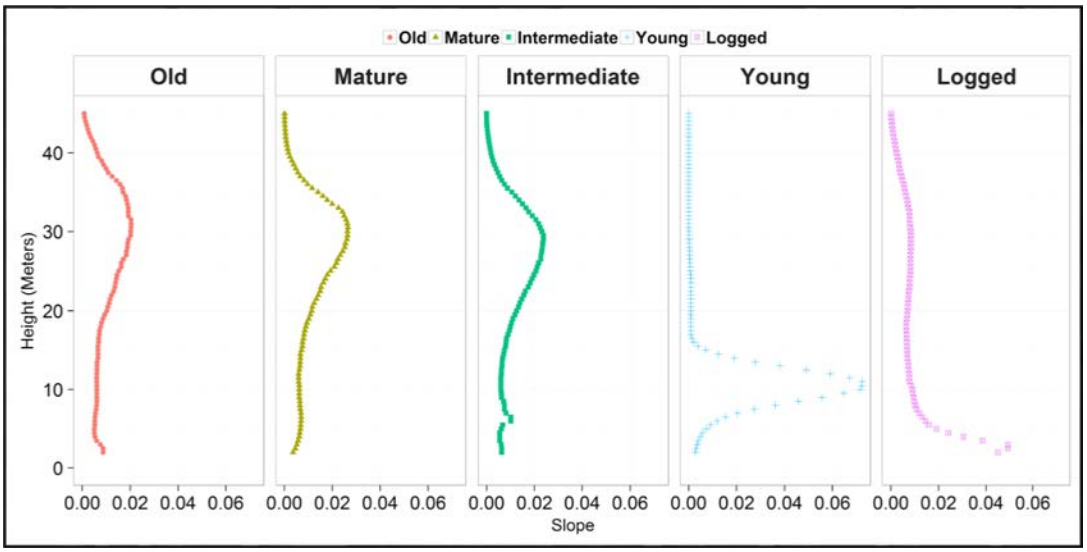

Figure 4.6 Vertical gap transmittance slope across forest plots. The images show slope of transmittance as a function of height for each plot in the chronosequence and the disturbed plot. Higher values signify higher rate of change. The old, mature, and the intermediate plots show similar transmittance curves, whereas the transmittance curves of the young and the logged plots have steeper slopes at a lower height.

4.3.3 Comparison of vertical foliage profiles

The mean LAD value varied across the forest plots. The old and mature plots had a mean LAD value of 0.12 $m^2 m^{-3}$, the intermediate plot had a mean LAD value of 0.10 $m^2 m^{-3}$, whereas the young forest plot had the highest mean LAD value of 0.37 $m^2 m^{-3}$. The logged plot had the lowest LAD value of 0.08 $m^2 m^{-3}$. The logged plot also had the largest variation of mean LAD value, and the old forest plot had the least. The maximum value of LAD was 0.73 $m^2 m^{-3}$ for the logged plot. The young plot's LAD value was 0.60 $m^2 m^{-3}$, the old plot's LAD value was 0.38 $m^2 m^{-3}$, the mature plot's value was 0.26 $m^2 m^{-3}$, and intermediate were at 0.24 $m^2 m^{-3}$ (Table 4.2). The height of maximum LAD value was 2 m for old, intermediate, and logged plots, and 4 m for the mature plot. The young plot had the highest maximum LAD value at 9 m (**Figure 4.7**).

Table 4.2 Summary of LAD Statistics across the Chronosequence Forest Plots. LAD Values were Derived using LiDAR Data

	Old	Mature	Intermediate	Young	Logged
Mean LAD (m^2 m^{-3}), CV	0.12 (63%)	0.12 (70%)	0.10 (69 %)	0.37 (87%)	0.08 (158%)
Max LAD (m^2 m^{-3})	0.38	0.26	0.24	0.60	0.73
LAD (height max (m)	2	4	2	9	2

The effective LAI, the cumulative LAD, also varied across the successional forest plots (KW test, $p < 0.001$). The *post hoc* Dunn's test revealed that the old–mature pair did not display a significant difference. The mean LAI was highest for the old plot at 2.5 m, followed by the mature at 2.4 m and intermediate at 2.1 m (**Figure 4.8**). The young and the logged plots have the lowest mean LAI (1.5 m^2 m^{-2}).

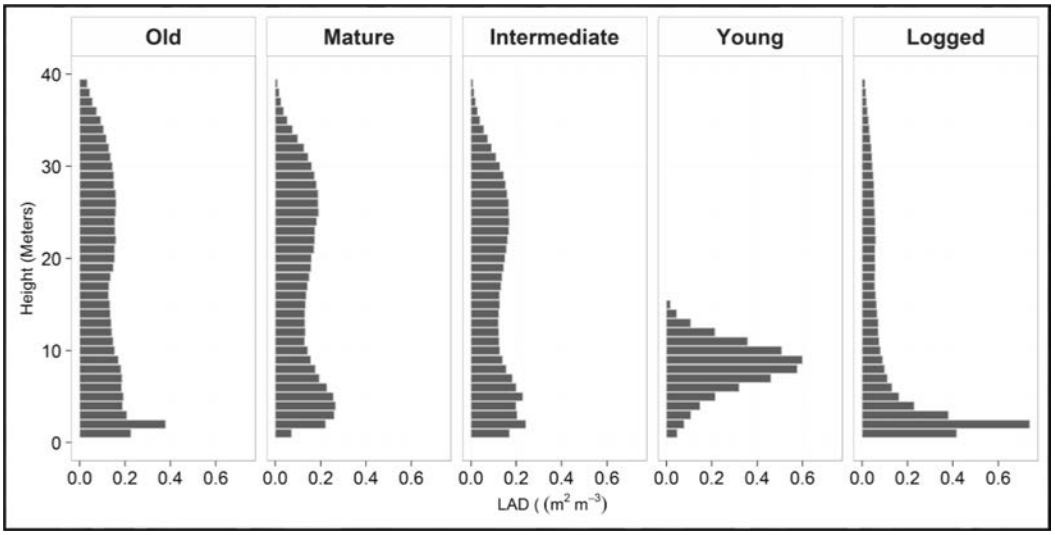

Figure 4.7 Vertical distribution of foliage area in the canopies of the successional forest plots based on airborne LiDAR estimates. The foliage area has been calculated at 1 m height interval. The graphs represent mean value of foliage area of the successional plots (200 × 200 m). Old, mature, and intermediate plots

have similar foliage distribution when compared with the young and logged plots.

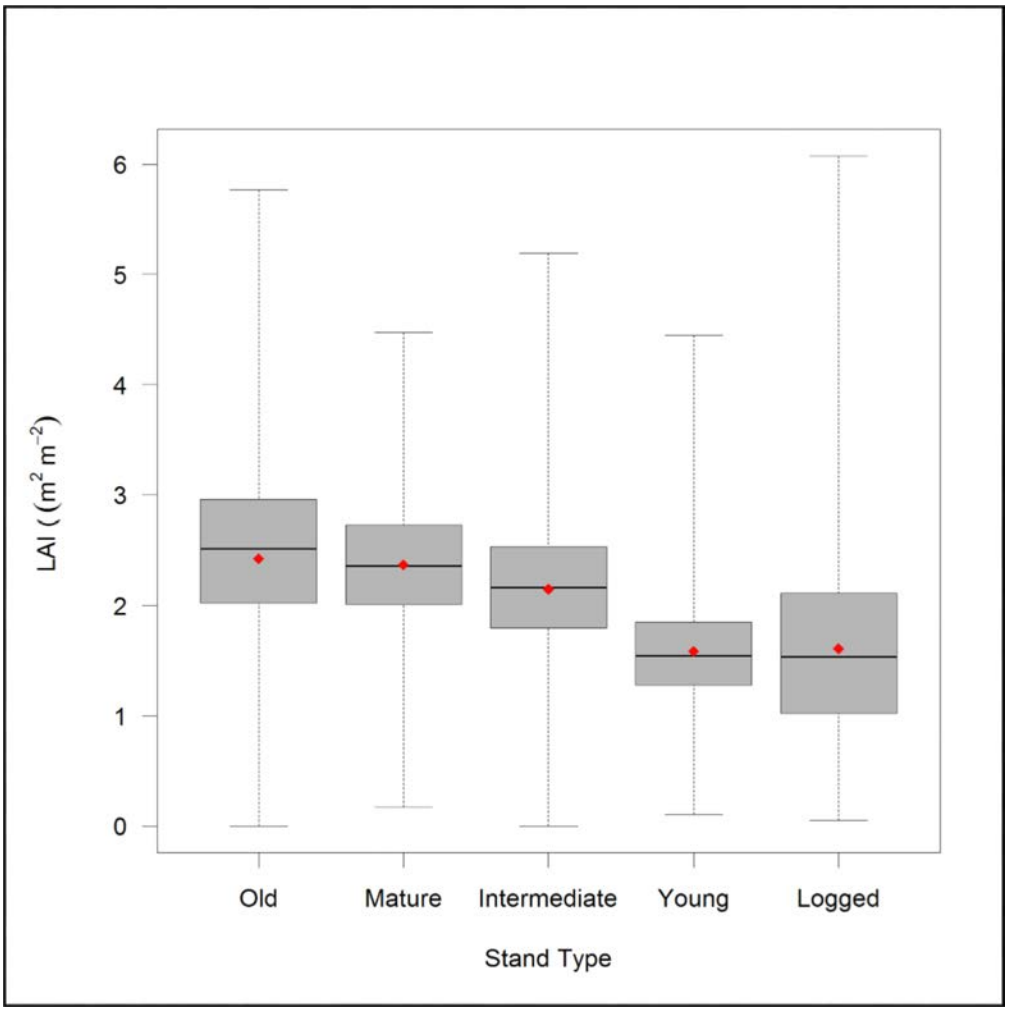

Figure 4.8 Comparison of LAI across forest plots shows a decreasing trend from old to the young stages of growth. The right most boxplot shows LAI for logged (disturbed) plot. The logged plot has a higher variability in LAI values when compared with the other plots. The LAI values are aggregated over 200 × 200 m plots. Red dot shows the mean LAI value for each forest plot.

The maximum value of LAI ranged from 4.5 m^2 m^{-2} in the mature plot to 6.07 m^2 m^{-2} in the logged plot. In terms of variability of LAI values, the logged forest plot displayed the maximum variability, followed by the old plot (**Figures 4.8** and **4.9**).

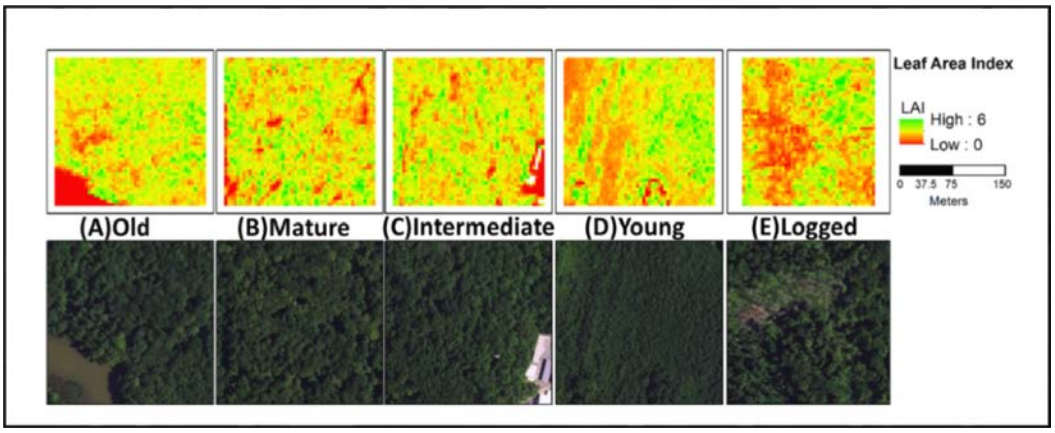

Figure 4.9 Comparison of Leaf Area Index (LAI) across forest plots at different stages of growth. The upper panel shows the LAI distribution, the lower plots show the satellite (RGB) images of the plots. Higher values of LAI are shown in shades of green and the lower values are shown in red. Lower values of LAI are associated with the areas of low vegetation density, water bodies, and canopy gaps. Built-up areas have zero LAI.

4.2.4 Comparison of LiDAR-derived and field-based measurement of vertical transmittance

LiDAR-derived vertical transmittance was compared with *in situ* data from PAR sensor for the three plots—young, intermediate, and old—for which data were available (**Figure 4.10**).

Within a particular plot, the PAR- and LiDAR-estimated transmittance curve showed notable similarities for all the three chronosequence plots. The shapes were similar but the intensity varied by plot. For the young plot, the PAR transmittance remained high up to 5 m and then the values dropped below the LiDAR estimates. Similarly, for the intermediate plot, the value of PAR transmittance values was higher than the LiDAR estimates up to 27 m. For the old plot, the PAR transmittance values were always lower than the LiDAR transmittance values (**Figure 4.10**).

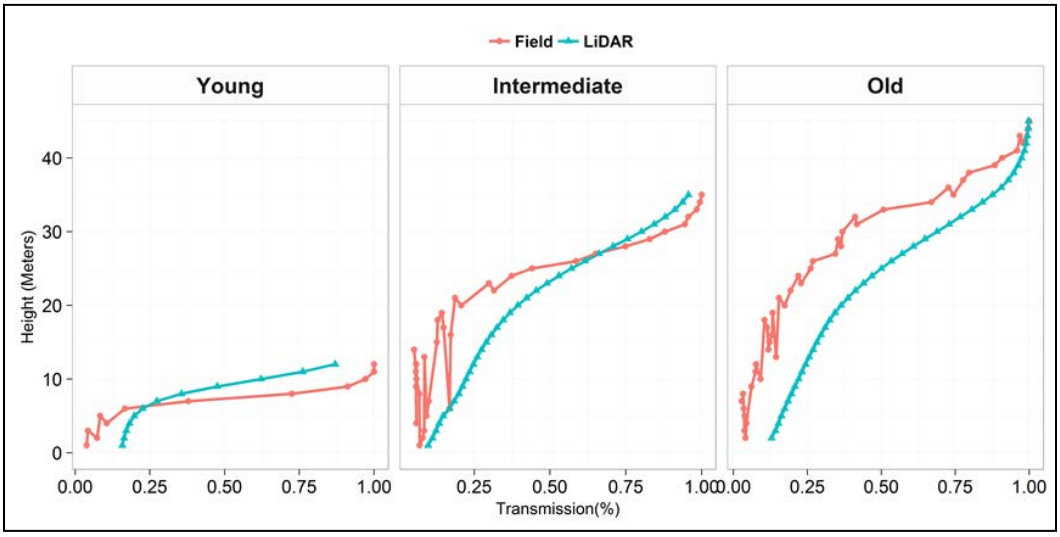

Figure 4.10 Comparison of field, PAR (red) and LiDAR (blue) estimates of transmittance for young, intermediate, and old chronosequence plots (Left to Right). The difference between the PAR and LiDAR transmittance can be attributed to multiple factors such as the difference in wavelength, sampling design. The LiDAR data show smooth line, whereas the coarse *in situ* line can be attributed to sampling pattern and effect of sunflecks.

Results indicate that the RMSE between the two data sets is 17%, with a MAE of 11% and MBE of −10%. The RMSE was equally partitioned between systematic (inaccuracy) and unsystematic (imprecision) components, with a RMSEs of 13% and RMSEu equaling 11%. The overall linear relationship between LiDAR vertical transmittance estimates and vertical PAR transmittance measurements is $R^2 = 0.84$. The coefficient of linear model is 0.76 with an intercept of 0.18 (**Figure 4.11**).

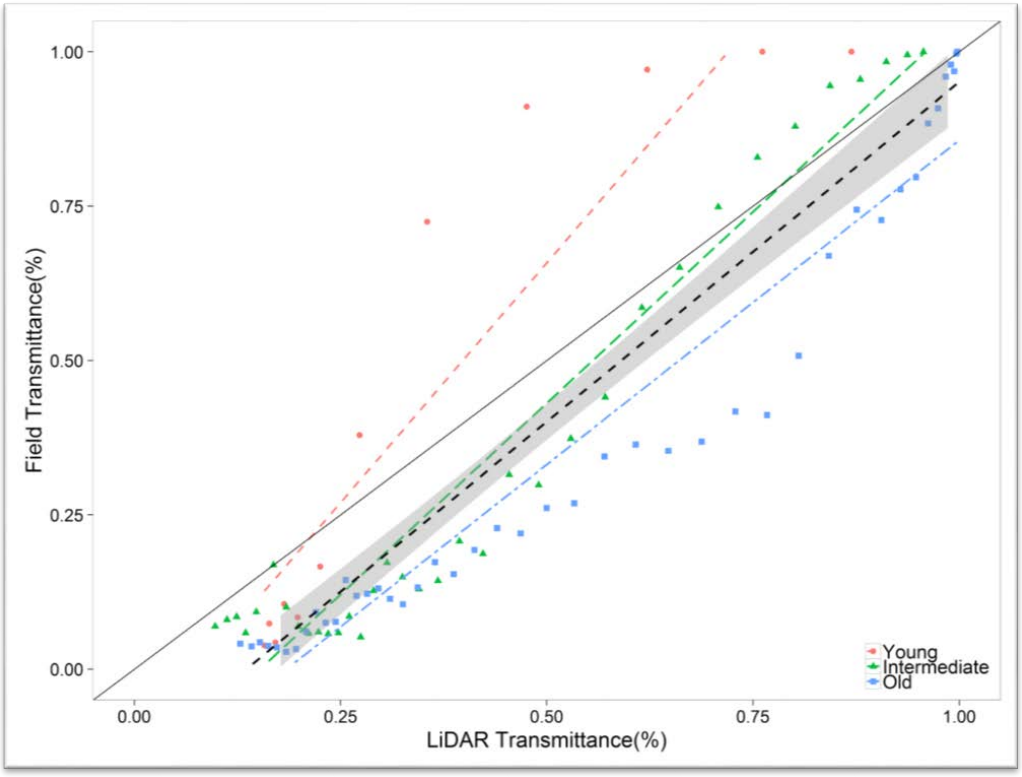

Figure 4.11 Scatterplots of estimated versus LiDAR-derived vertical transmittance. Points and dashed regression lines are identified with sites by color, the overall (across-site) regression is depicted by black dotted line, and the 1:1 line is solid black. The shaded area around the overall regression line shows 95% confidence interval. The site-specific regression lines show consistent

pattern in the slope, which increases with the successional stage. Overall the *in situ* and LiDAR-based estimates are in good agreement (R^2 = 0.84, MBE = 10%).

4.4 Discussion

The results demonstrate the utility of LiDAR data for estimating vertical light transmission across forest canopies in chronosequence and with disturbance in a temperate broadleaf forest type.

Vertical light transmittance varied across the forest plots. We observed similarities in light transmittance of old, mature, and intermediate plots (**Figure 4.4**), whereas the transmittance curves of the young and the logged plots showed a steep slope (**Figure 4.6**). This variation suggest that the vertical organization of vegetation in the young and the logged forest plots differed from the old, mature, and intermediate plots. Vertical gap transmittance was likely influenced by canopy structural parameters, and in the older undisturbed forest plots (**Figure 4.3**), light was intercepted gradually by their closed complex canopies than the younger and logged plots. In a tropical rainforest, Yamada, Yoshioka, Hashim, Liang, and Okuda (2014) compared forest light environments between a primary forest and a forest that was selectively logged. They found the former had more open canopies and a less heterogeneous light environment compared to primary forests. The steep transmittance profile of the selectively logged plot in comparison to the undisturbed forest plots, therefore, is likely due to its more open canopy.

The skewness was negative in the upper part of canopy, indicating high light transmittance, but positive at lower heights (<10 m) indicating less transmittance (**Figure 4.4**). The height of the greatest variability ($H_{\text{var}}^{\max}$) was the same for the old, mature, and intermediate plots (Table 4.2), suggesting variability in radiation interception was similar in these plots while $H_{\text{var}}^{\max}$ was at a much lower height for the young plot (10 m) and the logged plots (7 m), a likely influence of shorter canopy height and difference in distribution of canopy material.

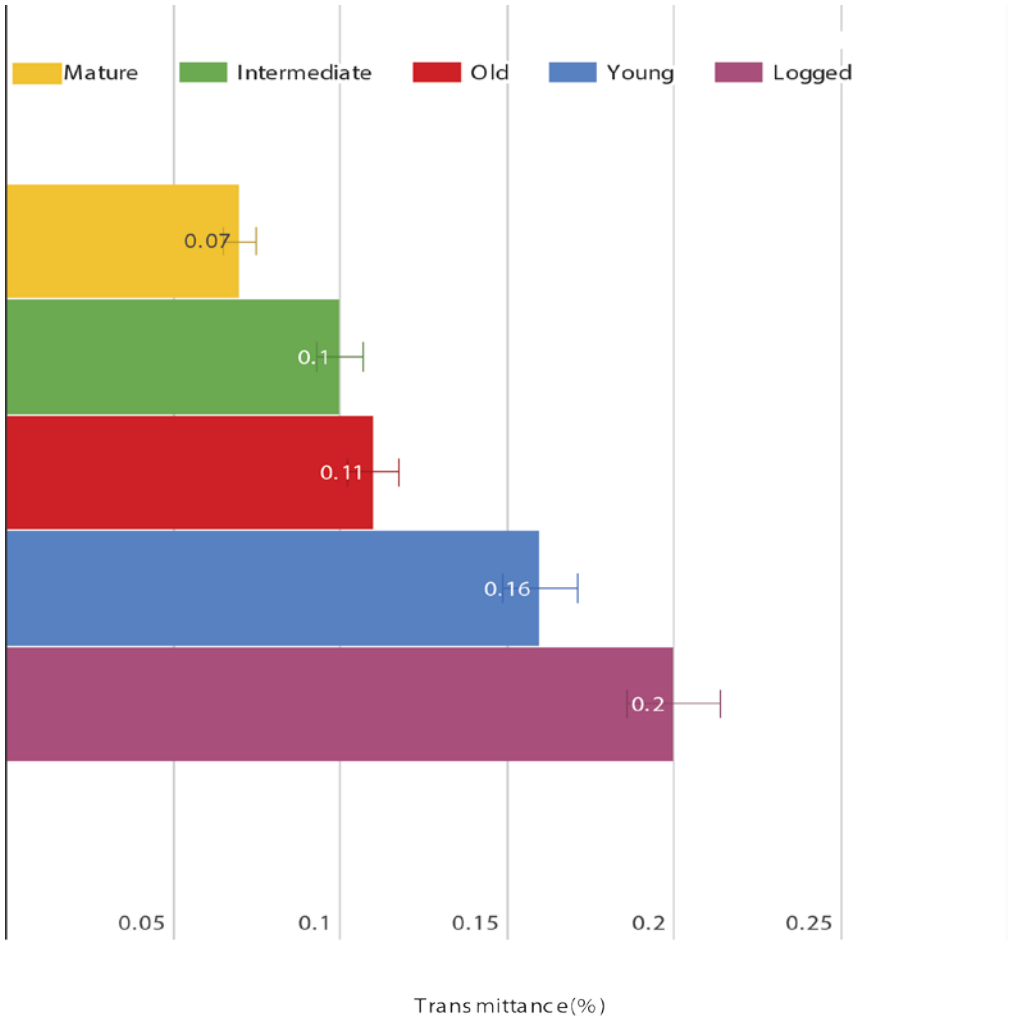

Figure 4.12 Comparison of vertical transmittance at the forest floor. Transmittance values were estimated 1 m above the ground surface to avoid the effect of understory vegetation and litter.

The results show that the transmittance at the ground level (1 m) was maximum for the logged plot (20%) and minimum for the mature plot (7%), suggesting light reached the forest more efficiently because of gaps in the canopy

due to selective logging (**Figure 4.12**). The results show that most radiation was intercepted in the upper parts of the canopy of the old, intermediate, and mature plots and less light penetrated deeply into the canopy of these three plots (**Figure 4.5**).

The mean LAD value was lowest for the logged plot (0.08 $m^2 m^{-3}$) and highest for the young plot (0.3 $m^2 m^{-3}$). The LAI displayed an inverse trend, with the youngest plot having the least LAI and older plots having increasing value (**Figure 4.8**). These findings are consistent with earlier documented ground-based in-canopy measurements and can be explained by patterns of forest development typical to the forest type in the study area (Parker & Russ, 2004). The effective LAI, which is the cumulative of the LAD, also varied across the successional forest plots (KW test, $p < 0.001$). The *post hoc* Dunn's test showed no significant difference between the old and mature plots. The mean LAI was maximum for the old plot (2.5) followed by the mature (2.4) and intermediate (2.1) plots (**Figure 4.8**). The young and the logged plots showed the lowest mean LAI (1.5 $m^2 m^{-2}$). This suggests that although vertical distribution of leaf material might be different across forest plots, cumulative LAI derived from satellite data might not be a suitable indicator for vertical transmittance of light, which is required to accurately understand the patterns of photosynthetic pathways and canopy growth (Ellsworth & Reich, 1993; Drewry et al., 2010).

When compared with the *in situ* data from the PAR sensor, LiDAR-derived vertical transmittance data agree with the field-based measurements. We observed that the LiDAR estimates were smoother, whereas the PAR data fluctuates at different height intervals, sometimes even exceeding the values at a lower height. This anomaly can be attributed to the effect of sun fleck or the other canopy opening at time of data acquisition. The LiDAR model overestimates the transmittance in the intermediate and old plots, whereas underestimates transmittance in the young plot (**Figure 4.10**). Disagreement between the LiDAR estimates and *in situ* data was likely due to a slight negative bias (MBE 10%) of the PAR data relative to LiDAR values. Overall a low systematic error (RMSE) of 13% suggests that LiDAR data can be used to derive vertical transmittance and the estimates can be further calibrated using *in situ* data. Inter-plot difference in the *in situ* and LiDAR measured vertical transmittance was likely due to difference in LiDAR return from different canopies. In very dense canopies, it is likely that few or none of the LiDAR points can reach the ground surface (Lefsky et al., 2002; Clark, Clark, & Roberts, 2004; Takahashi, Yamamoto, Miyachi, Senda, & Tsuzuku, 2006). We also observed that the line of best fit between the *in situ* and LiDAR-based transmittance follows a consistent pattern corresponding with the age of the plot. For example, the transmittance in the mature plot was under predicted followed by the intermediate plot, which was closer to the 1:1 line. In the young plot, LiDAR overestimates the transmittance when compared to the *in situ* data (**Figure 4.11**).

The difference between the PAR and LiDAR transmittance could be attributed to multiple factors. The PAR sensor operates at a different wavelength compared to the LiDAR, which operates in monochromatic wavelength. The sampling design of the PAR data collected spread grid sample, whereas the LiDAR information is based on much dense sample. Our results are consistent with the other studies (Lefsky, 1999 et al; Parker, 2001).

Our results demonstrate the utility of discrete return LiDAR to characterize canopy metrics and study the impact of canopy structure on vertical light transmittance. Given the way canopy functions are related to the spatiotemporal variability of light, this application of LiDAR has significance for broader applications for generating knowledge on habitat and forest functions. For example, vertical variability of light is one of the important parameters influencing photosynthesis at different height levels. Knaepen, Janssens, and Verryckt (2016) concluded that vertical profiles of photosynthesis should be taken into account when estimating carbon uptake by a tropical forest ecosystem. Therefore, the ability to measure vertical light transmittance also has implications for measuring carbon uptake by forests.

Our study also has implications on canopy stand management. Light travels through forest canopies, and therefore the light levels below the canopy can be influenced by manipulating canopy elements. Techniques such as thinning and positioning are used often by forest managers(Messier, 1996). The ability to estimate below canopy light levels at different vertical gradients along with the

knowledge of species or vegetation specific light requirements can guide the amount and frequency of canopy manipulation required to achieve specific objectives such as habitat management or seedling growth (Hale et al., 2009). The method illustrated here could be used to understand transmittance and foliage profiles at larger spatial scales and in different forest types.

4.5 Conclusion

This study demonstrated a non-tedious and simplistic use of airborne discrete return LiDAR to study the vertical light transmittance of forest canopies at different stages of growth without requiring extensive ground data collection. The light transmittance varied among the forest plots at chronosequence. However, the difference was noticeable between stands with dissimilar canopy characteristics such as stand age and canopy complexity. Several other studies have used large footprint waveform LiDAR data to derive vertical LAI profile estimates in tropical rain forests, demonstrating LiDAR data's explanatory power for the light transmittance within forest canopies (Tang et al., 2012, 2014, and 2016).

Our study focused on vertical transmittance. However, with three-dimensional modeling of LiDAR point clouds, future work can look at the transmittance at an oblique angle for better understanding of canopy light transmittance. More canopy structural metrics, such as canopy relief ratio and leaf angle distribution, can be included to understand the complexity of the canopy structure and its relationship with vertical light transmittance (Montgomery & Chazdon, 2001). The current study focused on mixed deciduous forest plots;

future research might apply the methodology to other forest types to obtain a broader understanding of radiation patterns under successional forest growth stages.

Chapter 5 Conclusion

This dissertation aimed to better characterize the under-canopy radiation regime using three-dimensional vegetation structure derived from LiDAR remote sensing in forest plots with different canopy characteristics. Overall, this research demonstrated the utility of small foot print LiDAR to illustrate vegetation structure and to provide reliable estimates of radiation and transmittance values under the canopy. The methods developed in this dissertation can be useful for characterizing forest successional stage using LiDAR-based vegetation metrics where field measurements are not available. It can also be useful for ecologists, foresters, and other conservation scientists interested in estimation of radiation at finer scales interested in snowmelt and hydrological simulations for forest ecosystems monitoring and management.

The main findings of this dissertation that were presented in the earlier chapters have been compiled into specific themes and presented as follows. First, this research demonstrated a way to estimate under-canopy solar radiation and vertical light transmittance values from discrete return LiDAR data without the need for labor-intensive field work, field sensors, and passive remote sensing. This study therefore adds to previous efforts to estimate radiation values from LiDAR rather than through traditional instrument-based empirical methods. In Chapter 2, I applied a spatially explicit model to assess the first-order effect of vegetation on solar radiation using LiDAR-derived surfaces with and without vegetation. I found that the presence of vegetation impacted both the magnitude

and variability of solar radiation, and showed how bare surfaces received almost three times the mean solar irradiance at noon and morning, compared to surfaces with vegetation cover. I also estimated the direct beam radiation on the forest floor using a ray-tracing model in Chapter 3 and estimated the vertical light transmittance values in Chapter 4 using LiDAR data.

Second, LiDAR-based estimates of solar radiation and canopy vertical light transmittance were in good agreement with different field-based radiation measurements. By comparing the modeled results with commonly used field-based measurements from pyranometer and PAR sensors, I showed that LiDAR can provide good estimates of direct beam radiation (RMSE = 13.94 W/m^2), and vertical light transmittance values (R^2 = 0.84) in mixed deciduous forests at different stages of succession, as shown in Chapters 3 and 4. These applications suggested that LiDAR data alone can provide accurate fine-scale measurements of both under-canopy beam radiation and vertical light transmittance in forest plots with different structural characteristics.

In addition, I found few differences between the PAR- and LiDAR-estimated transmittance values. In Chapter 4, I observed that the LiDAR estimates were smoother, whereas the PAR measurements fluctuated at different height intervals, with a magnitude exceeding the values at a lower height occasionally. This anomaly could be possibly explained by the impact of sun fleck or other canopy openings at time of data acquisition (Zavitkovski, 1981). I also found that when compared to the PAR data, the LiDAR model overestimated the transmittance in

the intermediate and old plots, but underestimated in the young plot (**Figure 4.10**). This could be due to the sensor type and sampling design. The PAR sensor was operated at a different wavelength compared to the LiDAR (visible vs. near-infrared bands). Also the sampling design of the PAR was based on a sampling grid, whereas the LiDAR information was acquired at a much higher spatial resolution. However, it was not possible to address these factors using current techniques. One possible solution could be to use multiband LiDAR system (Morsdorf et al., 2009). The consistency of acquisition spectrum should provide higher agreement and more realistic observations of PAR.

Third, LiDAR-derived metrics can well characterize the vegetation structure across forest types and help understand its effect on the under-canopy light regime. In Chapter 3, I found how the amount of radiation on the forest floor changed with the age of the forest plots. For example, I estimated that the amount of direct beam radiation at noon reaching the floor of the young plot was 14% of the top of the canopy radiation, compared to only 2.5% in the mature plot. In Chapter 4, I found how vertical light transmittance varied among the forest plots corresponding to differences in the vertical organization of canopy material determined by age, structure, and disturbance history. I found that vertical transmittance at the effective ground level (1 m above the surface) in the young plot was more than twice compared to the mature plot (16% vs. 7%), suggesting more light was intercepted within the mature plot. The relative difference between the intermediate and the old plot was only 1%, which can be attributed to large

gaps within the old plot created by the mortality of older trees. These findings suggest that to better model the solar regime and quantify radiation amounts under the canopy, we need the three-dimensional vegetation structure that can be reliably derived from LiDAR data.

Lastly, the RF analysis highlighted the complexity of factors influencing the amount of solar radiation that moves through the canopy. In Chapter 3, I found that when the categorical age was not considered, the CHM or the canopy height was the greatest determinant of solar radiation on the forest floor followed by canopy cover. However, when the chronosequence age was considered, canopy cover becomes the most significant determinant of solar radiation. This finding is in accordance with what previous studies have suggested, that neither canopy height, canopy and sub-canopy vegetation, or age can fully explain the sub canopy light regimes (Clark et al., 1996; Denslow & Guzman, 2000; Montgomery & Chazdon, 2001; Brown & Parker, 2004) and therefore, highlights the importance of integrating other vegetation structural parameters, optical properties, species types, and distribution of canopy elements, and their interaction with light.

Despite demonstrating the overall utility of LiDAR to provide detailed information on vegetation structure, and radiation values under the canopy, limitations of this study still remain and need to be addressed through future work. First, I considered only the direct beam component in the ray-tracing model in Chapter 3. I did not consider the diffuse radiation component to keep the model

simple, and also because previous studies and *in situ* measurements at the study site had indicated that the differences in understory radiation were mainly caused by the direct component of light (Hutchison & Matt, 1977; Pukkala et al., 1991). Second, I did not consider the multiple scattering and spectral properties of various canopy elements such as leaves and branches because it would have required site-specific field measurements. Future work could integrate these properties for better characterization of radiation regimes. Third, the ray-tracing model used in this study captured a high level of variability at a fine spatial scale, which is necessary to estimate stand-scale solar irradiance, which may potentially improve models such as snowmelt, hydrological, and energy balance models. This increased accuracy comes with high computational costs inhibiting its application at larger spatial scales. However, with increasing computational power and algorithm efficiency, ray-tracing models have potential for widespread use in near future.

The method elaborated and the findings presented in this research have the potential to improve a range of land surface model estimations. For example, current snow models use LAI as a proxy for vegetation and use Beer–Lambert's law to model exponential light extinction assuming a randomly distributed canopy. LAI has two major limitations—it does not capture canopy heterogeneity at finer scales, and LAI values derived from passive remote sensing are prone to saturation (Tang et al., 2014). Heterogeneous canopy with non-random distribution increases the uncertainty of these models (Pinty et al., 2004). Gray

and Male (1981) have pointed that the Beer's law-based approach may have limited utility for snowmelt processes when the assumption of a homogeneous and non-random canopy distribution is not satisfied. These issues have been mostly addressed using data from *in situ* pyranometers or hemispherical photographs (Musselman et al., 2012). However, unavailability of such ground-based measurements for larger areas limits their usage.

Solar radiation can be derived using ray-tracing or hybrid models that use 3D vegetation structure derived from LiDAR as the primary input. The methods illustrated in this research based on LiDAR-derived three-dimensional canopy structure were able to capture fine-scale variability in solar radiation at stand level. Through utilization of these methods there is a potential to incorporate, heterogeneous, non-random canopies, with smaller gaps, forest clearing and clumping within canopies, making it a good choice for modeling snowmelt and other hydrological processes.

Similarly, application of this work can possibly improve the characterization of vegetation–radiation interactions in land surface models such as Ecosystem Demography (ED) and Dynamic Vegetation Models (DVMs), which are widely coupled with Global Climate Models (GCM) (Quillet et al., 2010). These models are useful for modelling ecosystem structure, below-ground biomass, vegetation height and basal area, soil carbon stocks along with ecosystem fluxes. Like most of the current snow models, these models too use two stream approximation that rely on LAI and does not account for canopy structural parameters such as canopy

height, tree density, and crown parameters. The methods developed in this study can therefore fill these existing gaps in better representing the canopy–energy interactions and help in downscaling the GCM predictions.

Appendices

Supplementary Table 1: Wilcox-Rank Sum Test for Radiation Differences

Season	95% confidence interval	(Pseudo)median	Significance level
Summer solstice	3,558.104–3,608.264	3,583.223	99%
Equinox	2,923.147–2,961.247	2,942.179	99%
Winter solstice	1,266.292–1,279.551	1,272.937	99%

Supplementary Table 2: Data Summary of the DSM and DEM Radiation (kWh/m^2)

	Min	1st Q	Median	Mean	SD	3rd Q	Max
Summer solstice							
DSM (tree)	0.56	1.79	3.3	3.76	2.34	5.31	9.83
DEM (no trees)	0.03	9.25	9.47	9.37	0.42	9.61	9.83
Equinox							
DSM (tree)	0.49	0.94	1.93	2.4	1.68	3.5	8.10
DEM (no trees)	0.5	6.39	6.91	6.7	0.74	7.28	8.07
Winter solstice							
DSM (tree)	0.45	0.62	0.95	1.25	0.89	1.46	5.95
DEM (no trees)	0.45	2.97	3.53	3.43	0.77	3.9	5.8

Supplementary Table 3: Spatial Autocorrelation

	Moran' *I* (DSM)	Moran' *I* (DEM)	Geary' *C* (DSM)	Geary' *C* (DEM)
Solar solstice	0.84	0.96	0.15	0.05
Equinox	0.79	0.96	0.20	0.03
Winter solstice	0.64	0.94	0.35	0.03

Supplementary Table 4: Descriptive Statistics of the SERC plots

	Stand Type	Min	1st Q	Median	Mean	3rd Q	SD	Max
CHM	Young	0	10.25	11.29	11.34	12.36	2.02	29.15
	Intermediate	0	26.42	30.03	29.31	33.22	6.18	42.99
	Mature	0	28.19	31.29	30.34	33.75	5.73	44.1
Fractional cover	Young	0.74	0.95	0.97	0.96	0.98	0.03	0.99
	Intermediate	0.56	0.98	0.99	0.98	0.99	0.04	0.99
	Mature	0.85	0.99	0.99	0.99	0.99	0.02	1
Rugosity	Young	0.63	1.13	1.33	1.48	1.54	0.89	9.72
	Intermediate	0.781	2.56	3.48	3.89	4.6	1.91	13.1
	Mature	0.58	2.17	3.03	3.71	4.42	2.30	14.87

Supplementary Table 5: Dunn's test of multiple comparisons using rank sums(holm): Pairwise Comparison

Plots	mean.rank.diff	*p*val
Intermediate–young	−12,268.768	<2e−16***
Mature–young	−16,694.526	<2e−16***
Mature–intermediate	−4,425.759	<2e−16***

Bibliography

Aber, J. D. (1979). A Method for Estimating Foliage-Height Profiles in Broad-Leaved Forests. *The Journal of Ecology*, *67*(1), 35. doi.10.2307/2259335

Anderson, M. C. (1966). Stand structure and light penetration. II. A theoretical analysis. *Journal of Applied Ecology, 3*, 41–54.

Alexander, C., Moeslund, J. E., Bøcher, P. K., Arge, L., & Svenning, J.-C. (2013). Airborne laser scanner (LiDAR) proxies for understory light conditions. *Remote Sensing of Environment*, *134*, 152–161. doi.10.1016/j.rse.2013.02.028

Austin, M. P., & Van Niel, K. P. (2011). Improving species distribution models for climate change studies: variable selection and scale. *Journal of Biogeography*, *38*(1), 1–8. doi.10.1111/j.1365-2699.2010.02416.x

Battaglia, M. A., Mou, P., Palik, B., & Mitchell, R. J. (2002). The effect of spatially variable overstory on the understory light environment of an open-canopied longleaf pine forest. *Canadian Journal of Forest Research*, *32*(11), 1984–1991. doi.10.1139/x02-087

Belgiu, M., & Drăguţ, L. (2016). Random forest in remote sensing: A review of applications and future directions. ISPRS *Journal of Photogrammetry and Remote Sensing*, *114*, 24–31. doi.10.1016/j.isprsjprs.2016.01.011

Bellow, J. G., & Nair, P. K. R. (2003). Comparing common methods for assessing understory light availability in shaded-perennial agroforestry systems.

Agricultural and Forest Meteorology, *114*(3–4), 197–211. doi.10.1016/S0168-1923(02)00173-9

Breiman, L. (2001). Random forests. *Machine Learning*, *45*(1), 5–32.

Brown, M. J., & Parker, G. G. (1994). Canopy light transmittance in a chronosequence of mixed-species deciduous forests. *Canadian Journal of Forest Research*, *24*(8), 1694–1703. doi.10.1139/x94-219

Brush, G., Lenk, C., & Smith, J. (1980).The natural forests of Maryland: An explanation of the vegetation map of Maryland. *Ecological Monographs, 50*, 77–92.

Campbell, G. S., & Norman, J. M. (1989). The description and measurement of plant canopy structure. In G. Russell, B. Marshall, & P. G. Jarvis (Ed.), *Plant canopies: Their growth, form, and function* (pp. 3–19). Cambridge, UK: Cambridge University Press.

Canham, C., Denslow, J. S., Platt, W. J., Runkle, J., Spies, T. A., & White, P. S. (1990). Light regimes beneath closed canopies and tree-fall gaps in temperate and tropical forests. *Canadian Journal of Forest Research*, *20*, 620–631.

Carroll, G. L. (1980). Forest canopies: Complex and independent subsystems. In R. H. Waring (Ed.), *Forests: Fresh perspectives from ecosystem analysis* (pp. 87–107). Corvallis, OR: Oregon State University Press.

Chasmer, L. E., & Hopkinson, C. (2007). Modelling canopy gap fraction from Lidar intensity. *ISPRS Workshop on Laser Scanning*, 190–194.

Clark, D. B., Clark, D. A., Rich, P. M., Weiss, S., & Oberbauer, S. F. (1996). Landscape-scale evaluation of understory light and canopy structures: methods and application in a neotropical lowland rain forest. *Canadian Journal of Forest Research*, *26*(5), 747–757. doi.10.1139/x26-084

Clark, M. L., Clark, D. B., & Roberts, D. A. (2004). Small-footprint lidar estimation of sub-canopy elevation and tree height in a tropical rain forest landscape. *Remote Sensing of Environment*, *91*(1), 68–89. doi.10.1016/j.rse.2004.02.008

Clifton, J., & Boruff, B. J. (2010). Assessing the potential for concentrated solar power development in rural Australia. *Energy Policy*, *38*(9), 5272–5280. doi.10.1016/j.enpol.2010.05.036

Colbert, S. R., Jokela, E. J., & Neary, D. G. (1990). Effects of Annual Fertilization and Sustained Weed Control on Dry Matter Partitioning, Leaf Area, and Growth Efficiency of Juvenile Loblolly and Slash Pine. *Forest Science*, *36*(4), 995–1014.

Cook, B. D., Corp, L. A., Nelson, R. F., Middleton, E. M., Morton, D. C., McCorkel, J. T., … Montesano, P. M. (2013). NASA Goddard's LiDAR, hyperspectral and thermal (G-LiHT) airborne imager. *Remote Sensing*, *5*(8), 4045–4066. doi.10.3390/rs5084045

Cutler, D. R., Edwards, T. C., Beard, K. H., Cutler, A., Hess, K. T., Gibson, J., & Lawler, J. J. (2007). Random forests for classification in ecology. *Ecology*, *88*(11), 2783–2792. doi.10.1890/07-0539.1

Denslow, J. S., & Guzman G., S. (2000). Variation in stand structure, light and seedling abundance across a tropical moist forest chronosequence, Panama. *Journal of Vegetation Science*, *11*(2), 201–212. doi.10.2307/3236800

Dozier, J. (1980). A clear-sky spectral solar radiation model for snow-covered mountainous terrain. *Water Resources Research*, *16*(4), PP. 709-718. doi.198010.1029/WR016i004p00709

Drewry, D. T., Kumar, P., Long, S., Bernacchi, C., Liang, X.-Z., & Sivapalan, M. (2010). Ecohydrological responses of dense canopies to environmental variability: 1. Interplay between vertical structure and photosynthetic pathway. *Journal of Geophysical Research: Biogeosciences*, *115*(G4), G04022. doi.10.1029/2010JG001340

Dubayah. R. Dozier, J., & Davis, F. W. (1990). Topographic distribution of clear-sky radiation over the Konza Prairie, Kansas. *Water Resources Research*, *26*, 679–690.

Dubayah, R. (1994). Modeling a solar radiation topoclimatology for the Rio Grande river basin. *Journal of Vegetation Science*, *5*(5), 627–640. doi.10.2307/3235879

Dubayah, R., & Rich, P. M. (1995). Topographic solar radiation models for GIS. *International Journal of Geographical Information Systems*, *9*(4), 405–419. doi.10.1080/02693799508902046

Duncanson, L. I., Cook, B. D., Hurtt, G. C., & Dubayah, R. O. (2014). An efficient, multi-layered crown delineation algorithm for mapping individual tree

structure across multiple ecosystems. *Remote Sensing of Environment*, *154*, 378–386. doi.10.1016/j.rse.2013.07.044

Dunn, O. J. (1964). Multiple comparisons using rank sums. *Technometrics* *6*(3), 241–52. doi:10.1080/00401706.1964.10490181

Ellsworth, D. S., & Reich, P. B. (1993). Canopy structure and vertical patterns of photosynthesis and related leaf traits in a deciduous forest. *Oecologia*, *96*(2), 169–178. doi.10.1007/BF00317729

Essery, R., Bunting, P., Hardy, J., Link, T., Marks, D., Melloh, R., & Rutter, N. (2008). Radiative transfer modeling of a coniferous canopy characterized by airborne remote sensing. *Journal of Hydrometeorology*, *9*(2), 228–241.

Evans, J. S., Hudak, A. T., Faux, R., & Smith, A. M. S. (2009). Discrete Return Lidar in Natural Resources: Recommendations for Project Planning, Data Processing, and Deliverables. *Remote Sensing*, *1*(4), 776–794. doi.10.3390/rs1040776

Field, C. & Mooney, H.A. (1986). The photosynthesis –nitrogen relationship in wild plants. In T. J. Givnish (Ed.), *On the economy of plant form and function* (pp. 25–55). Cambridge, UK: Cambridge University Press.

Filley, T. R., McCormick, M. K., Crow, S. E., Szlavecz, K., Whigham, D. F., Johnston, C. T., & van den Heuvel, R. N. (2008). Comparison of the chemical alteration trajectory of *Liriodendron tulipifera* L. leaf litter among forests with different earthworm abundance. *Journal of Geophysical Research: Biogeosciences, 113*(G1), G01027. doi.10.1029/2007JG000542

Frazer, G. W., Magnussen, S., Wulder, M. A., & Niemann, K. O. (2011). Simulated impact of sample plot size and co-registration error on the accuracy and uncertainty of LiDAR-derived estimates of forest stand biomass. *Remote Sensing of Environment*, *115*(2), 636–649. doi.10.1016/j.rse.2010.10.008

Frelich, L. E., Machado, J.-L., & Reich, P. B. (2003). Fine-scale environmental variation and structure of understorey plant communities in two old-growth pine forests. *Journal of Ecology*, *91*(2), 283–293. doi.10.1046/j.1365-2745.2003.00765.x

Frew Jr, J. E. (1991). The image processing workbench. University of California at Santa Barbara Santa Barbara, CA, USA

Frew, J., & Dozier, J. (1986). The Image Processing Workbench—portable software for remote sensing instruction and research. In *International geoscience and remote sensing symposium* (pp. 271–276).

Fu, P., & Rich, P. M. (2002). A geometric solar radiation model with applications in agriculture and forestry. *Computers and Electronics in Agriculture*, *37*(1–3), 25–35. doi.10.1016/S0168-1699(02)00115-1

Galo, A. T., Rich, P. M., & Ewel, J. J. (1992). Effects of forest edges on the solar radiation regime in a series of reconstructed tropical ecosystems. *American Society for Photogrammetry and Remote Sensing Technical Papers*, 98–108.

Gay, L. W., Knoerr, K. R., & Braaten, M.O. (1971). Solar radiation variability on the floor of a pine plantation. *Agricultural Meteorology*, *8*, 39–50.

Gleeson, S. K., & Tilman, D. (1990). Allocation and the transient dynamics of succession on poor soils. *Ecology*, *71*(3), 1144–1155. doi.10.2307/1937382

Goetz, S., Steinberg, D., Dubayah, R., & Blair, B. (2007). Laser remote sensing of canopy habitat heterogeneity as a predictor of bird species richness in an eastern temperate forest, USA. Remote Sensing of Environment, 108(3), 254–263. doi. 10.1016/j.rse.2006.11.016

Gray and Male, 1981, Gray, D. M., & Male, D. H. (Eds.). (1981). Handbook of snow: principles, processes, management & use. Pergamon Press.

Grossmann, E., Ohmann, J., Kagan, J., May, H., & Gregory, M. (2010). Mapping ecological systems with a random foret model: Tradeoffs between errors and bias. Retrieved from http://www.treesearch.fs.fed.us/pubs/39540.

Groot, A. (2004). A model to estimate light interception by tree crowns, applied to black spruce. *Canadian Journal of Forest Research*, *34*(4), 788–799. doi.10.1139/x03-242

Guariguata, M. R., & Ostertag, R. (2001). Neotropical secondary forest succession: changes in structural and functional characteristics. *Forest Ecology and Management*, *148*(1), 185–206.

Gutschick, V. P. (1991). Joining leaf photosynthesis models and canopy photo-transport models. In *In: R.B. Myneni, & J. Ross (Eds). Photon-vegetation interactions: applications in optical remore sensing and plant ecology* (p. XVII, 565). Berlin: Springer-Verlag Berlin Heidelberg.

Hale, S. E., Edwards, C., Mason, W. L., Price, M., & Peace, A. (2009). Relationships between canopy transmittance and stand parameters in Sitka spruce and Scots pine stands in Britain. *Forestry*, *82*(5), 503–513. doi.10.1093/forestry/cpp020

Harding, D. J., Lefsky, M. A., Parker, G. G., & Blair, J. B. 2001. Laser altimeter canopy height profiles—Methods and validation for closed-canopy, broadleaf forests. *Remote Sensing of Environment, 76*(3), 283–297. doi:10.1016/S0034-4257(00)00210-8.

Hardy, J. P., Melloh, R., Koenig, G., Marks, D., Winstral, A., Pomeroy, J. W., & Link, T. (2004). Solar radiation transmission through conifer canopies. *Agricultural and Forest Meteorology*, *126*(3–4), 257–270. https://doi.org/10.1016/j.agrformet.2004.06.012

Hopkinson, C., Chasmer, L., Lim, K., Treitz, P., & Creed, I. (2006). Towards a universal lidar canopy height indicator. *Canadian Journal of Remote Sensing*, *32*(2), 139–152. doi.10.5589/m06-006

Hopkinson, C., & Chasmer, L. E. (2007). Modelling canopy gap fraction from lidar intensity. In *ISPRS Workshop on Laser Scanning 2007 and SilviLaser 2007* (pp. 190–194). IAPRS Espoo, Finland. Retrieved from http://www.academia.edu/download/39852439/MODELLING_CANOPY_GAP_FRACTION_FROM_LIDAR20151109-14046-101wiut.pdf

Hopkinson, C., & Chasmer, L. (2009). Testing LiDAR models of fractional cover across multiple forest ecozones. *Remote Sensing of Environment*, *113*(1), 275–288.doi.10.1016/j.rse.2008.09.012

Horn, H. S. (1971). *The Adaptive Geometry of Trees*. Princeton, N.J.: Princeton University Press. Retrieved from https://www.researchgate.net/publication/247746927_The_Adaptive_Geometry_of_Trees

Howell, D. (2012). *Statistical methods for psychology*. : Wadsworth Cengage Learning. Belmont, CA. USA

Hutchison, B. A., & Matt, D. R. (1977). The distribution of solar radiation within a deciduous forest. *Ecological Monographs*, *47*(2), 185–207. doi.10.2307/1942616

Hyde, P., Dubayah, R., Walker, W., Blair, J. B., Hofton, M., & Hunsaker, C. (2006). Mapping forest structure for wildlife habitat analysis using multi-sensor (LiDAR, SAR/InSAR, ETM+, Quickbird) synergy. *Remote Sensing of Environment*, *102*(1–2), 63–73. doi.10.1016/j.rse.2006.01.021

Isaaks, E. H., & Srivastava, R. M. (1989). *An Introduction to Applied Geostatistics*. Oxford University Press.

Jarvis, P. G., & McNaughton, K. G. (1986). Stomatal control of transpiration: Scaling up from leaf to region. *Advances in Ecological Research, 15*, 1–49.

Jennings, S., Brown, N., & Sheil, D. (1999). Assessing forest canopies and understorey illumination: Canopy closure, canopy cover and other measures. *Forestry, 72*(1), 59–74. doi.10.1093/forestry/72.1.59

Kabakoff, R. P., & Chazdon, R. L. (1996). Effects of canopy species dominance on understorey light availability in low-elevation secondary forest stands in Costa Rica. *Journal of Tropical Ecology*, *12*(6), 779–788.

Kane, V. R., McGaughey, R. J., Bakker, J. D., Gersonde, R. F., Lutz, J. A., & Franklin, J. F. (2010).Comparisons between field- and LiDAR-based measures of stand structural complexity. *Canadian Journal of Forest Research*, *40*(4), 761–73. doi:10.1139/X10-024.

Knaepen, W., Janssens, I. A., & Verryckt, L. (2016). Vertical variation in photosynthetic parameters in two different tropical forest ecosystems. Retrieved from http://ddd.uab.cat/record/164263.

Kobayashi, H., Baldocchi, D. D., Ryu, Y., Chen, Q., Ma, S., Osuna, J. L., & Ustin, S. L. (2012). Modeling energy and carbon fluxes in a heterogeneous oak woodland: A three-dimensional approach. *Agricultural and Forest Meteorology*, *152*, 83–100. doi.10.1016/j.agrformet.2011.09.008

Korhonen, L., Korpela, I., Heiskanen, J., & Maltamo, M. (2011). Airborne discrete-return LIDAR data in the estimation of vertical canopy cover, angular canopy closure and leaf area index. *Remote Sensing of Environment, 115*(4), 1065–1080. doi.10.1016/j.rse.2010.12.011

Kruskal, W. H., & Wallis, W. A. (1952). Use of ranks in one-criterion variance analysis. *Journal of the American Statistical Association, 47*(260), 583–621. doi.10.2307/2280779

Kucharik, C. J., Norman, J. M., & Gower, S. T. (1999). Characterization of radiation regimes in nonrandom forest canopies: theory, measurements, and a simplified modeling approach. *Tree Physiology*, *19*(11), 695–706.

Kuuluvainen, T., & Pukkala, T. (1989). Simulation of within-tree and between-tree shading of direct radiation in a forest canopy: Effect of crown shape and sun elevation. *Ecological Modelling*, *49*(1–2), 89–100. doi.10.1016/0304-3800(89)90045-8

Kumar, L., Skidmore, A. K., & Knowles, E. (1997). Modelling topographic variation in solar radiation in a GIS - environment. *International Journal of Geographical Information Science, 11*(5), 475. doi.10.1080/136588197242266

Küppers, M. (1989). Ecological significance of above-ground architectural patterns in woody plants: A question of cost-benefit relationships. *Trends in Ecology & Evolution*, *4*(12), 375–379. doi.10.1016/0169-5347(89)90103-1

Lai, Y.-J., Chou, M.-D., & Lin, P.-H. (2010). Parameterization of topographic effect on surface solar radiation. *Journal of Geophysical Research: Atmospheres*, *115*(D1), D01104. doi.10.1029/2009JD012305

Lee, H., Slatton, K. C., Roth, B. E., & Cropper, W. P. (2009) Prediction of forest canopy light interception using three-dimensional airborne LiDAR data. *International Journal of Remote Sensing*, *30*(1), 189–207. doi:10.1080/01431160802261171

Lefsky, M. A., Cohen, W. B., Parker, G. G., & Harding, D. J. (2002). Lidar Remote Sensing for Ecosystem Studies. *BioScience*, *52*(1), 19–30. doi.10.1641/0006-3568(2002)052[0019:LRSFES]2.0.CO;2

Lefsky, M. A., Hudak, A. T., Cohen, W. B., & Acker, S.A. (2005). Patterns of covariance between forest stand and canopy structure in the Pacific Northwest. *Remote Sensing of Environment*, *95*(4), 517–531. doi:10.1016/j.rse.2005.01.004

Lim, K., Treitz, P., Wulder, M., St-Onge, B., & Flood, M. (2003). LiDAR remote sensing of forest structure. *Progress in Physical Geography*, *27*(1), 88–106. doi.10.1191/0309133303pp360ra

Liaw, A., & Wiener, M. (2002). Classification and regression by random forest. *R News*, *2*(3), 18–22.

Latham, P. A., Zuuring, H. R, & Coble, D. W. (1998). A method for quantifying vertical forest structure. *Forest Ecology and Management, 104*(1–3), 157–170. doi:10.1016/S0378-1127(97)00254-5.

Lefsky, M. A., Harding, D., Cohen, W. B., Parker, G., & Shugart, H. H. (1999). Surface Lidar remote sensing of basal area and biomass in deciduous forests of Eastern Maryland, USA. *Remote Sensing of Environment*, *67*(1), 83–98. doi.10.1016/S0034-4257 (98)00071-6.

Loew, A., van Bodegom, P. M., Widlowski, J.-L., Otto, J., Quaife, T., Pinty, B., & Raddatz, T. (2014). Do we (need to) care about canopy radiation schemes in DGVMs? Caveats and potential impacts. *Biogeosciences*, *11*(7), 1873–1897. doi.10.5194/bg-11-1873-2014

Lundquist, J. D., Dickerson-Lange, S. E., Lutz, J. A., & Cristea, N. C. (2013). Lower forest density enhances snow retention in regions with warmer winters: A global framework developed from plot-scale observations and modeling. *Water Resources Research*, *49*(10), 6356–6370. doi.10.1002/wrcr.20504

MacArthur, R. H. (1964). Environmental Factors Affecting Bird Species Diversity. *The American Naturalist*, *98*(903), 387–397. doi.10.1086/282334

MacArthur, R.H., and Horn, H. S. (1969). Foliage profiles by vertical measurements. *Ecology, 50*, 802–804.

MacFarlane, D. W., Green, E. J., Brunner, A., & Amateis, R. L. (2003). Modeling loblolly pine canopy dynamics for a light capture model. *Forest Ecology and Management*, *173*(1–3), 145–168. doi.10.1016/S0378-1127 (02)00011-7

Mahat, V., & Tarboton, D. G. (2012). Canopy radiation transmission for an energy balance snowmelt model. *Water Resources Research*, *48*(1), W01534. doi.10.1029/2011WR010438

Martens, S. N., Breshears, D. D., & Meyer, C. W. (2000). Spatial distributions of understory light along the grassland/forest continuum: effects of cover, height, and spatial pattern of tree canopies. *Ecological Modelling*, *126*(1), 79–93. doi.doi: DOI: 10.1016/S0304-3800(99)00188-X

Means, J. E., Acker, S. A., Harding, D. J., Blair, J. B., Lefsky, M. A., Cohen, W. B., … McKee, W. A. (1999). Use of large-footprint scanning airborne

Lidar to estimate forest stand characteristics in the Western Cascades of Oregon. *Remote Sensing of Environment*, *67*(3), 298–308. doi.10.1016/S0034-4257(98)00091-1

Messier, C. (1996). Managing light and understorey vegetation in boreal and temperate broadleaf-conifer forests. In P.G. Comeau, & K.D. Thomas (Eds.), *Silviculture of temperate and boreal broadleaf-conifer mixtures* (pp. 59–81). Victoria, BC: BC Ministry of Forests; Land Management Handbook No. 36

Monsi, M., & Saeki, T. (1953). U¨ ber den Lichtfaktor in den Pflanzengesellschaften und seine Bedeutung fu¨ r die Stoffproduktion, *14*, 22–52.

Montgomery, R. A., & Chazdon, R. L. (2001). Forest structure, canopy architecture, and light transmittance in tropical wet forests. *Ecology*, *82*(10), 2707–2718. doi.10.1890/0012-9658(2001)082[2707:FSCAAL]2.0.CO;2

Morsdorf, F., Meier, E., Kötz, B., Itten, K. I., Dobbertin, M., & Allgöwer, B. (2004). LIDAR-based geometric reconstruction of boreal type forest stands at single tree level for forest and wildland fire management. *Remote Sensing of Environment*, *92*(3), 353–362. doi.10.1016/j.rse.2004.05.013

Morsdorf, F., Kötz, B., Meier, E., Itten, K. I., & Allgöwer, B. (2006). Estimation of LAI and fractional cover from small footprint airborne laser scanning data based on gap fraction. *Remote Sensing of Environment*, *104*(1), 50–61. doi.10.1016/j.rse.2006.04.019

Morsdorf, F., Nichol, C., Malthus, T., & Woodhouse, I. H. (2009). Assessing forest structural and physiological information content of multi-spectral

LiDAR waveforms by radiative transfer modelling. *Remote Sensing of Environment*, *113*(10), 2152–2163. doi.10.1016/j.rse.2009.05.019

Musselman, K. N., Margulis, S. A., & Molotch, N. P. (2013). Estimation of solar direct beam transmittance of conifer canopies from airborne LiDAR. *Remote Sensing of Environment*, *136*, 402–415. doi.10.1016/j.rse.2013.05.021

Murphy, D. D., Freas, K. E., & Weiss, S. B. (1990). An environment-metapopulation approach to population viability analysis for a threatened invertebrate. *Conservation Biology*, *4*(1), 41–51. doi.10.1111/j.1523-1739.1990.tb00266.x

Murphy, D. D., & Weiss, S. B. (1992). The effects of climate change on biological diversity in western North America: Species losses and mechanisms. In R. Peters, & T. Lovejoy (Eds.), *Global warming and biodiversity* (pp. 355–368). New Haven, CT: Yale University Press.

Musselman, K. N., Molotch, N. P., Margulis, S. A., Kirchner, P. B., & Bales, R. C. (2012). Influence of canopy structure and direct beam solar irradiance on snowmelt rates in a mixed conifer forest. *Agricultural and Forest Meteorology*, *161*, 46–56. doi.10.1016/j.agrformet.2012.03.011

Musselman, K. N., Margulis, S. A., & Molotch, N. P. (2013). Estimation of solar direct beam transmittance of conifer canopies from airborne LiDAR. *Remote Sensing of Environment*, *136*, 402–415.doi.10.1016/j.rse.2013.05.021

Naesset E. (1997). Estimating timber volume of forest stands us in airborne laser scanner data. *Remote Sensing of Environment, 61*, 246–253

Ni, W., Li, X., Woodcock, C. E., Roujean, J.-L., & Davis, R. E. (1997). Transmission of solar radiation in boreal conifer forests: Measurements and models. *Journal of Geophysical Research: Atmospheres*, *102*(D24), 29555–29566. doi.10.1029/97JD00198

Ni, W. (1997). A coupled transilience model for turbulent air flow within plant canopies and the planetary boundary layer. *Agricultural and Forest Meteorology*, *86*(1), 77–105. doi.10.1016/S0168-1923(96)02403-3

Nilson, T., (1971). A theoretical analysis of the frequency of gaps in plant stands. *Agricultural and Forest Meteorology*, *8*, 25–38.

Ni-Meister, W., Jupp, D. L. B., & Dubayah, R. (2001). Modeling lidar waveforms in heterogeneous and discrete canopies. *Geoscience and Remote Sensing, IEEE Transactions on*, *39*(9), 1943–1958

Ni-Meister, W., Yang, W., & Kiang, N. Y. (2010). A clumped-foliage canopy radiative transfer model for a global dynamic terrestrial ecosystem model. I: Theory. *Agricultural and Forest Meteorology*, *150*(7–8), 881–894. doi.10.1016/j.agrformet.2010.02.009

North, M., Oakley, B., Chen, J., Erickson, H., Gray, A., Izzo, A., … Schowalter, T. (2002). Vegetation and ecological characteristics of mixed-conifer and red fir forests at the Teakettle Experimental Forest. Retrieved from http://www.treesearch.fs.fed.us/pubs/6197

Oker-Blom, P., Pukkala, T., & Kuuluvainen, T. (1989). Relationship between radiation interception and photosynthesis in forest canopies: Effect of stand structure and latitude. *Ecological Modelling*, *49*(1–2), 73–87. doi.10.1016/0304-3800(89)90044-6

Oliver, C. D. (1980). Forest development in North America following major disturbances. *Forest Ecology and Management*, *3*, 153–168. doi.10.1016/0378-1127(80)90013-4

Parker, G. G., O'Neill, J. P., & Higman, D. (1989). Vertical profile and canopy organization in a mixed deciduous forest. *Vegetation*, *85*(1/2), 1–11.

Parker, G. G. (1995). Structure and microclimate of forest canopies. In M. D. Lowman, & N. M. Nadkarni (Eds.), Forest canopies (pp. 73–106).San Diego, CA: Academic Press.

Parker, G. G. (1997). Canopy structure and light environment of an old-growth Douglas-fir/Western Hemlock Forest. Retrieved from https://research.libraries.wsu.edu:8443/xmlui/handle/2376/1231.

Parker, G. G., Lefsky, M. A., & Harding, D. J. (2001). Light transmittance in forest canopies determined using airborne laser altimetry and in-canopy quantum measurements. *Remote Sensing of Environment*, *76*(3), 298–309. doi.10.1016/S0034-4257(00)00211-X

Parker, G. G., Harding, D. J., & Berger, M. L. (2004). A portable LIDAR system for rapid determination of forest canopy structure. *Journal of Applied Ecology*, *41*(4), 755–767. doi.10.1111/j.0021-8901.2004.00925.x

Parker, G. G., & Russ, M. E. (2004). The canopy surface and stand development: assessing forest canopy structure and complexity with near-surface altimetry. *Forest Ecology and Management*, *189*(1–3), 307–315. doi.10.1016/j.foreco.2003.09.001

Peng, S., Zhao, C., & Xu, Z. (2014). Modeling spatiotemporal patterns of understory light intensity using airborne laser scanner (LiDAR). ISPRS Journal of *Photogrammetry and Remote Sensing*, *97*, 195–203. doi.10.1016/j.isprsjprs.2014.09.003

Pickett, S. T. A. (1989). Space-for-time substitution as an alternative to long-term studies. In G. E. Likens (Ed.), *Long-term studies in ecology* (pp. 110–135). New York, NY: Springer. doi.10.1007/978-1-4615-7358-6_5

Pinty, B., Widlowski, J.-L., Taberner, M., Gobron, N., Verstraete, M. M., Disney, M., … Zang, H. (2004). Radiation Transfer Model Intercomparison (RAMI) exercise: Results from the second phase. *Journal of Geophysical Research*, *109*, 19 PP. doi. 200410.1029/2003JD004252

Pukkala, T., Becker, P., Kuuluvainen, T., & Oker-Blom, P. (1991). Predicting spatial distribution of direct radiation below forest canopies. *Agricultural and Forest Meteorology*, *55*(3–4), 295–307. doi.10.1016/0168-1923(91)90067-Z

Pomeroy, J. W., & Dion, K. (1996). Winter radiation extinction and reflection in a boreal pine canopy: measurements and modelling. Hydrological processes, 10(12), 1591-1608.

Pomeroy, J., Ellis, C., Rowlands, A., Essery, R., Hardy, J., Link, T., Marks, D., & Sicart, J. E. (2008). Spatial variability of shortwave irradiance for snowmelt in forests. *Journal of Hydrometeorology*, *9*, 1482–1490.

Quillet, A., Peng, C., & Garneau, M. (2010). Toward dynamic global vegetation models for simulating vegetation–climate interactions and feedbacks: recent developments, limitations, and future challenges. *Environmental Reviews*, *18*(NA), 333–353. doi.10.1139/A10-016

Rich, P. M. (1990). Characterizing plant canopies with hemispherical photographs. *Remote Sensing Reviews*, *5*(1), 13–29.

Rich, P. M., & Weiss, S. B. (1991). Spatial models of microclimate and habitat suitability: Lessons from threatened species. In *Proceedings of the Eleventh Annual ESRI User's Conference* (pp. 95–102). Redlands: ESRI, Inc.

Rich, P. M., Weiss, S. B., Debinski, D. A., & McLoughlin, J. F. (1992). Physiographic inventory of a tropical reserve. *Proceedings of the Twelfth Annual ESRI User Conference Palm Springs, CA* (pp. 197–208).

Rich, P. M., Hetrick, W. A., & Saving, S. C. (1995). Modelling topographic influences on solar radiation: A manual for SOLARFLUX model, LA-12989-Manual *Los Alamos National Laboratory, Los Alamos, New Mexico* (pp. 1–44).

Reuter, H. I., Kersebaum, K. C., & Wendroth, O. (2005). Modelling of solar radiation influenced by topographic shading—Evaluation and application for precision farming. *Physics and Chemistry of the Earth, Parts A/B/C, 30*(1–3), 143–149. ISSN 1474-7065, doi.10.1016/j.pce.2004.08.027.

Rosam, J. R. (2015). Assessment of light quality, variability, and seedling presence in Hawaiian lowland wet forests. USDA Forest Service. Retrieved from https://dspace.lib.hawaii.edu/handle/10790/2477

Ross, J. (1981). *The radiation regime and architecture of plant stands*. Boston: Dr. W. Junk Publishers.

Ross, M. S., Flanagan, L. B., & Roi, G. H. L. (1986). Seasonal and successional changes in light quality and quantity in the understory of boreal forest ecosystems. *Canadian Journal of Botany*, *64*(11), 2792–2799. doi.10.1139/b86-373

Russell, G., Marshall, B., & Jarvis, P. G. (1990). Plant canopies: Their growth, form and function. Cambridge, UK: Cambridge University Press.

Rutter, N., Essery, R., Pomeroy, J., Altimir, N., Andreadis, K., Baker, I., … Yamazaki, T. (2009). Evaluation of forest snow processes models (SnowMIP2). *Journal of Geophysical Research: Atmospheres*, *114*(D6), n/a–n/a. doi.10.1029/2008JD011063

Sakai, T., & Akiyama, T. (2005). Quantifying the spatio-temporal variability of net primary production of the understory species, Sasa senanensis, using multipoint measuring techniques. *Agricultural and Forest Meteorology*, *134*(1–4), 60–69. doi. 10.1016/j.agrformet.2005.11.004

Saatchi, S. S., Harris, N. L., Brown, S., Lefsky, M., Mitchard, E. T. A., Salas, W., … Morel, A. (2011). Benchmark map of forest carbon stocks in tropical regions across three continents. *Proceedings of the National Academy of Sciences*, *108*(24), 9899–9904. doi. 10.1073/pnas.1019576108

Spies, T., Franklin, J.F. and Klopsch, M. (1990). Canopy gaps in Douglas-fir forests of Cascade Mountains. *Canadian Journal of Forest Research, 20*, 649–658.

Stadt, K. J., Lieffers, V. J., Hall, R. J., & Messier, C. (2005). Spatially explicit modeling of PAR transmission and growth of Picea glauca and Abies balsamea in the boreal forests of Alberta and Quebec. *Canadian Journal of Forest Research*, *35*(1), 1–12. doi.10.1139/x04-141

Steemers, T. C. (1990). *1989 2nd European Conference on Architecture: science and technology at the service of architecture: proceedings of an international conference held at Paris, France, 4-8 December 1989*. Kluwer Academic Pub.

Stephens, P. R., Watt, P. J., Loubser, D., Haywood, A., & Kimberley, M. O. (2007). Estimation of carbon stocks in New Zealand planted forests using airborne scanning LiDAR. In *Proceedings: ISPRS Workshop International archives of photogrammetry, remote sensing and spatial information sciences* (Vol. 36, pp. 389–394).

Storck, P., Lettenmaier, D. P., & Bolton, S. M. (2002). Measurement of snow interception and canopy effects on snow accumulation and melt in a mountainous maritime climate, Oregon, United States. *Water Resources Research*, *38*(11), 1223. doi.10.1029/2002WR001281

Šúri, M., & Hofierka, J. (2004). A New GIS-based Solar Radiation Model and Its Application to Photovoltaic Assessments. *Transactions in GIS*, *8*(2), 175–190. doi.10.1111/j.1467-9671.2004.00174.x

Svenning, J.-C. (2000). Small canopy gaps influence plant distributions in the rain forest understory. *Biotropica*, *32*(2), 252–261.

Svenning, Jens-Christian. 2002. “Crown Illumination Limits the population Growth Rate of a Neotropical Understorey Palm (Geonoma Macrostachys, Arecaceae).” *Plant Ecology* 159 (2): 185–99. doi:10.1023/A:1015520116260.

Takahashi, T., Yamamoto, K., Miyachi, Y., Senda, Y., & Tsuzuku, M. (2006). The penetration rate of laser pulses transmitted from a small-footprint airborne LiDAR: A case study in closed canopy, middle-aged pure sugi (Cryptomeria japonica D. Don) and hinoki cypress (Chamaecyparis obtusa Sieb. et Zucc.) stands in Japan. *Journal of Forest Research*, *11*(2), 117–123. doi.10.1007/s10310-005-0189-0

Tang, H., Dubayah, R., Swatantran, A., Hofton, M., Sheldon, S., Clark, D. B., & Blair, B. (2012). Retrieval of vertical LAI profiles over tropical rain forests using waveform lidar at La Selva, Costa Rica. *Remote Sensing of Environment*, *124*, 242–250. doi.10.1016/j.rse.2012.05.005

Tang, H., Brolly, M., Zhao, F., Strahler, A. H., Schaaf, C. L., Ganguly, S., … Dubayah, R. (2014). Deriving and validating Leaf Area Index (LAI) at multiple spatial scales through lidar remote sensing: A case study in Sierra National Forest, CA. *Remote Sensing of Environment*, *143*, 131–141. doi.10.1016/j.rse.2013.12.007

Tang, H., Ganguly, S., Zhang, G., Hofton, M. A., Nelson, R. F., & Dubayah, R. (2016). Characterizing leaf area index (LAI) and vertical foliage

profile (VFP) over the United States. *Biogeosciences*, *13*(1), 239–252. doi.10.5194/bg-13-239-2016

Teller, J., & Azar, S. (2001). Townscope II—A computer system to support solar access decision-making. *Solar Energy*, *70*(3), 187–200. doi.10.1016/S0038-092X (00)00097-9

Thomas, V., Finch, D. A., McCaughey, J. H., Noland, T., Rich, L., & Treitz, P. (2006). Spatial modelling of the fraction of photosynthetically active radiation absorbed by a boreal mixedwood forest using a lidar-hyperspectral approach. *Agricultural and Forest Meteorology*, *140*(1–4), 287–307. doi.DOI: 10.1016/j.agrformet.2006.04.008

Todd, K. W., Csillag, F., & Atkinson, P. M. (2003). Three-dimensional mapping of light transmittance and foliage distribution using lidar. *Canadian Journal of Remote Sensing*, *29*(5), 544–555.

Turner, W., Spector, S., Gardiner, N., Fladeland, M., Sterling, E., & Steininger, M. (2003). Remote sensing for biodiversity science and conservation. *Trends in Ecology & Evolution*, *18*(6), 306–314. doi.10.1016/S0169-5347 (03)00070-3

van Leeuwen, M., Coops, N. C., Hilker, T., Wulder, M. A., Newnham, G. J., & Culvenor, D. S. (2013). Automated reconstruction of tree and canopy structure for modeling the internal canopy radiation regime. *Remote Sensing of Environment*, *136*, 286–300. doi.10.1016/j.rse.2013.04.019

Varhola, A., Coops, N. C., Weiler, M., & Moore, R. D. (2010). Forest canopy effects on snow accumulation and ablation: An integrative review of

empirical results. *Journal of Hydrology*, *392*(3–4), 219–233. doi.10.1016/j.jhydrol.2010.08.009

Varhola, A., & Coops, N. C. (2013). Estimation of watershed-level distributed forest structure metrics relevant to hydrologic modeling using LiDAR and Landsat. *Journal of Hydrology*, *487*, 70–86. doi.10.1016/j.jhydrol.2013.02.032

Verseghy, D. L., McFarlane, N. A., & Lazare, M. (1993). Class—A Canadian land surface scheme for GCMS, II. Vegetation model and coupled runs. *International Journal of Climatology*, *13*(4), 347–370. doi.10.1002/joc.3370130402

von Arx, G., Dobbertin, M., & Rebetez, M. (2012). Spatio-temporal effects of forest canopy on understory microclimate in a long-term experiment in Switzerland. A*gricultural and Forest Meteorology*, *166–167*, 144–155. doi.10.1016/j.agrformet.2012.07.018

Vose, J. M., Sullivan, N. H., Clinton, B. D., & Bolstad, P. (1995). Vertical leaf area distribution, light transmittance, and the application of the Beer–Lambert Law in four mature hardwood stands in the southern Appalachians. *Canadian Journal of Forest Research*, *25*, 1036–1043.

Weiss, S. B., Rich, P. M., Murphy, D. D., Calvert, W. H., & Ehrlich, P. R. (1991). Forest canopy structure at overwintering monarch butterfly sites: Measurements with hemispherical photography. *Conservation Biology*, *5*(2), 165–175.

Weiss, M., Baret, F., Smith, G. J., Jonckheere, I., & Coppin, P. (2004). Review of methods for in situ leaf area index (LAI) determination. *Agricultural and Forest Meteorology*, *121*(1–2), 37–53. doi.10.1016/j.agrformet.2003.08.001

Willmott, C. J. (1982). Some comments on the evaluation of model performance. *Bulletin of the American Meteorological Society*, *63*(11), 1309–1313. doi.10.1175/1520-0477(1982)063<1309:SCOTEO>2.0.CO;2

Yamada, T., Yoshioka, A., Hashim, M., Liang, N., & Okuda, T. (2014). Spatial and temporal variations in the light environment in a primary and selectively logged forest long after logging in Peninsular Malaysia. *Trees*, *28*(5), 1355–1365. doi.10.1007/s00468-014-1040-z

Yoda, K. (1974). Three-dimensional distribution of light intensity in a tropical rain forest of West Malaysia. *Japanese Journal of Ecology*. Retrieved from http://agris.fao.org/agris-search/search.do?recordID=JP19750026559

Yu, B., Liu, H., Wu, J., & Lin, W.-M. (2009). Investigating impacts of urban morphology on spatio-temporal variations of solar radiation with airborne LIDAR data and a solar flux model: A case study of downtown Houston. *International Journal of Remote Sensing*, *30*(17), 4359–4385. doi.10.1080/01431160802555846

Zavitkovski, J. (1981). Characterization of light climate under canopies of intensively-cultured hybrid poplar plantations. *Agricultural Meteorology*, *25*, 245–255. doi.10.1016/0002-1571 (81)90077-7

Zhao, F., Yang, X., Schull, M. A., Román-Colón, M. O., Yao, T., Wang, Z., … Strahler, A. H. (2011). Measuring effective leaf area index, foliage profile,

and stand height in New England forest stands using a full-waveform ground-based lidar. *Remote Sensing of Environment*, *115*, 2954–2964. doi. 10.1016/j.rse.2010.08.030